Open quantum systems beyond the weak-coupling regime

PhD Thesis

Mehwish Majeed

Advisor: Dr. Adam Zaman Chaudhry

School of Science and Engineering

Lahore University of Management Sciences

June 2021

Lahore University of Management Sciences

School of Science and Engineering

Author's Declaration

I ***Mehwish Majeed*** hereby state that my PhD thesis titled ***"Open quantum systems beyond the weak-coupling regime"*** is my own work and has not been submitted previously by me for taking any degree from LAHORE UNIVERSITY OF MANAGEMENT SCIENCES or anywhere else in the country/world. At any time if my statement is found to be incorrect, even after my graduation, the university has the right to withdraw my PhD degree.

Name of Student: Mehwish Majeed

Date: 14-06-2021

Lahore University of Management Sciences

School of Science and Engineering

CERTIFICATE

I hereby recommend that the proposal prepared under my supervision by ***Mehwish Majeed*** titled, ***"Open quantum systems beyond the weak-coupling regime"*** be accepted in partial fulfillment of the requirements for the degree of PhD.

Dr. Adam Zaman Chaudhry (Advisor) _____

SYED BABAR ALI SCHOOL OF SCIENCE AND ENGINEERING

Dissertation Approval

The members of the Committee approve the dissertation entitled Open quantum systems beyond the weak coupling regime by Mehwish Majeed, defended on June 4, 2021.

It is recommended that this dissertation be used in partial fulfillment of the requirements for the degree of Doctor of Philosophy from Department of Physics in Syed Babar Ali School of Science and Engineering.

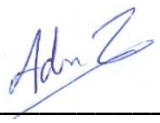

_____

(Advisor)

_____

(External Examiner)

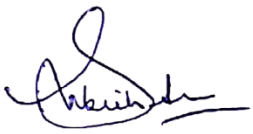

_____

(FDC Member)

_____

(FDC Member)

_____

(FDC Member)

_____

(FDC Member)

Dedicated to my parents

Acknowledgments

First of all, I would like to express my gratitude to my PhD supervisor, Prof. Adam Zaman Chaudhry for his continuous support and guidance throughout my PhD work. He not only took out time for discussion of results despite his busy routine, but also raised my spirits with constant encouragement on my progress. This work wouldn't exist without him. I am also highly obliged to Prof. Muhammad Sabieh Anwar and Prof. Muhammad Faryad for agreeing to serve as a member of my graduate committee. Besides that, I want to thank my family for their relentless support, particularly my elder brother who helped me a lot in completing my PhD task. Your assistance and faith in me has led me to achieve this goal. Thank You

List of Publications

- M. Majeed and A. Z. Chaudhry, *The quantum Zeno and anti-Zeno effects with non-selective projective measurements*, Sci. Rep. **8**, 14887 (2018).

- M. Majeed and A. Z. Chaudhry, *Effect of initial system–environment correlations with spin environments*, Eur. J. Phys. D **73**, 16 (2019).

- M. Majeed and A. Z. Chaudhry, *The quantum Zeno and anti-Zeno effects with driving fields in the weak and strong coupling regimes*, Sci. Rep. **11**, 1836 (2021).

- M. Majeed and A. Z. Chaudhry, *The quantum Zeno and anti-Zeno effects with composite environments*, in preparation.

Abstract

Isolated quantum systems are an idealization - realistic quantum systems interact with their environment. Due to these unavoidable interactions, such systems generally undergo decoherence and dissipation, which means that the quantum properties of the system are lost. Since upcoming powerful quantum technologies rely on the preservation of the quantum properties of systems, the study of this area of open quantum systems has acquired great importance. Unfortunately, this is generally a hard task, and various approximations have to be made to make the problem tractable. Most commonly, it is assumed that the system-environment coupling is weak, which may actually not be true in many different physical systems of interest. The central aim of the thesis is to look at open quantum systems beyond the usual weak coupling paradigm.

We first examine the role played by the initial system-environment correlations. This is done by examining an exactly solvable model of a central two-level system coupled to a spin environment. We show that if the system-environment coupling is strong, then the initial system-environment state cannot be considered to be a simple product state of the initial system state and the environment state. Rather, the correlations between the system and the environment that exist before the system state preparation procedure need to be taken into account. These correlations affect the environment state when the system state is prepared, and thus the subsequent dynamics of the system is also affected. We then look at what happens to an open quantum system in the presence of repeated projective measurements. In particular, we look start by looking at non-selective projective measurements, that is, projective measurements where we do not care about the measurement result. We derive a general formalism that allows us to find the effective decay rate of a quantum state when it is subjected to periodic projective measurements for an arbitrary system-environment model. Importantly, we show that the decay rate with non-selective measurements is in general only different from the usual selective projective measurements scenario when we go beyond

the weak system-environment coupling regime. Our formalism is applied to three exactly solvable models in order to illustrate our results.

We next analyze the effect of repeated measurements on open quantum systems which are subjected to coherent driving fields. We first assume that the system-environment coupling strength is weak; however, no such restriction is placed on the driving fields. We work out general expressions for the effective decay rate of a quantum system. Next, we use a polaron transformation to find the effective decay rate in the strong system-environment coupling regime as well. In general, one obtains an interplay between the driving fields and the repeated measurements. Finally, we also consider the effect of repeated measurements on a quantum system interacting with a composite environment. That is, the quantum system is directly interacting with a 'near' environment - this interaction strength can be strong - and this near environment in turn is interacting weakly with a 'far' environment.

Contents

Chapter 1

Introduction

Quantum mechanics is the most successful and far-reaching physical theory ever devised, with a myriad of different physical applications ranging from transistors to lasers and atomic clocks [1]. Yet, anyone who first encounters it is undoubtedly intimidated and perplexed by the very mathematical and abstract nature of the theory. For example, the 'state' of a quantum system is ideally described by a normalized vector living in an abstract Hilbert space. A linear combination, or, in other words, a superposition, of such vectors is another possible quantum state of the system; this is the superposition principle. Quantum states evolve unitarily and deterministically via the Schrodinger equation [2]. However, observed quantum systems often show irreversible behavior due to their interaction with the surrounding environment [3–6]. This irreversibility is actually omnipresent since no physical system in the real world is truly isolated [5, 6]. Every system is influenced, for example, by its neighboring atoms or surrounding electromagnetic field. Spontaneous emission - the process whereby an atom goes into a lower energy state even in the absence of any incident radiation - takes place precisely because the surrounding 'empty' electromagnetic field can nevertheless nudge the atom into emitting a photon [7].

The primary objective of this thesis is to look at such quantum systems that are interacting with their environment. Studies of these so-called open quantum systems have gained increasing interest in recent years for mainly two reasons. First, the study of open quantum

systems helps to understand the quantum-to-classical transition [8, 9]. After all, why do we not easily observe 'weird' superposition states, such as the superposition of different momentum states, for macroscopic objects around us? Such problems can be answered by observing that the environment is continuously monitoring the states of macroscopic systems. As a result of this interaction, the system and its environment become entangled, and coherence is then generally lost. Second, the study on open quantum systems is rather practical. Realistic implementations of futuristic quantum technologies such as quantum computation and quantum metrology [10, 11] need to account for the system-environment interactions. In fact, decoherence is the biggest enemy of quantum resources such as quantum entanglement, and various methods such as dynamical decoupling [12–16], the use of decoherent-free subspaces [17] and quantum error correction [18] have been devised to protect these quantum resources.

It is clear that the surrounding environment can have a very significant effect on the quantum system. For example, a hot body cools down by exchanging energy to its environment - this is known as dissipation [4]. Another process induced by the environment is known as decoherence, whereby knowledge of the relative phase between the states of the system is lost due to the creation of entanglement with the environment [8, 9]. Consequently, a superposition of states is destroyed and a 'pure' ideal state of a quantum system becomes a classical mixture. Both dissipation and decoherence lend a non-unitary character to the system evolution. However, if the word 'system' is extended to consider both the system its environment, then the system and its environment as a whole evolve in a unitary fashion. Thus, one approach to investigate the dynamics of open quantum systems is to consider the system and its environment jointly, perform unitary evolution, and to then remove the environment degrees of freedom to obtain the system dynamics only. Performing this in practice, however, is far from straightforward. Different approximations generally need to be made [3, 4]. For example, the system-environment interaction is assumed to be weak, and it is also common to consider environments without memory [19, 20]. Moreover, the initial system-environment correlations are also ignored. However, these assumptions are question-

able when the system-environment interaction are strongly coupled and the temperature of environment is low [21–53]. In such situations, if some process is carried out on the system - in particular, a projective measurement to prepare the quantum system in a desired state - the state of the environment is also affected, which then subsequently affects the system dynamics. In this thesis, we first study the effect of these initial system-environment correlations by investigating an exactly solvable model of a single two-level system interacting with a collection of two-level systems [54, 55]. We show that with strong system-environment coupling, the initial system-environment correlations can indeed affect the ensuing system dynamics significantly.

We then turn our attention to the effect of repeated measurements in open quantum systems [56–59]. It is well-known that a sequence of frequent projective measurements performed on a quantum system can freeze its evolution, an effect dubbed the quantum Zeno effect [60–81]. However, these rapid measurements may in fact also accelerate the decay process of quantum system; this is the quantum anti-Zeno effect [56, 59, 82–92]. This is because measurements can effectively change the manner in which the quantum system interacting with its environment. The quantum Zeno and the quantum anti-Zeno effects have gained considerable interest both theoretically and experimentally. This is not only due to their considerable importance in the foundations of quantum mechanics, but also due to their possible applications in quantum control technologies [93], quantum communication [94, 95], noise sensing [96–98] and quantum information processing [64, 65, 99, 100]. In this thesis, we first consider these effects when we perform non-selective projective measurements rather than the selective projective measurements usually considered [90]. In other words, we do not care about the intermediate measurement results; rather, we only want the final measurement result to give the initial quantum state. Thereafter, we consider the 'driven' case of the Zeno and anti-Zeno effects whereby coherent driving fields are applied to the system concurrently with the periodic projective measurements [101]. Finally, we look at the quantum Zeno and anti-Zeno effects for composite environments in which the environment consists of, for example, a two-level system and many harmonic oscillators rather than

simply harmonic oscillators.

1.1 Thesis outline

After this brief introduction, the remaining part of this thesis is arranged as follows.

- Chapter 2 is mainly a review chapter in which we briefly describe the basic concepts used in the study of open quantum systems. These include quantum entanglement, the density matrix formalism, the modeling of open quantum systems, and projective measurements.

- In chapter 3, we study the effects of the initial system-environment correlations on the central system dynamics [54]. For this, we analyze the dynamics of a quantum spin interacting with a spin environment. We show that the effects of the initial correlations can be significant when the system and its environment are strongly coupled. This is then extended to two spins to show that the initial correlations also affect the dynamics of the entanglement between the two central spins.

- In chapter 4, we consider the effect of repeated non-selective projective measurements [90, 102]. In this scheme, only the final measurement is required to correspond to the initial state; we do not care about the results of the intermediate measurements [90, 102]. We first present a general formalism to derive the effective decay rate of the initial quantum state with such non-selective measurements. Importantly, we show that there is a difference between using non-selective projective measurements and the usual approach of considering only selective measurements only if we go beyond the weak system-environment coupling regime in models other than the usual population decay models. As such, we then apply our formalism to investigate the quantum Zeno and anti-Zeno effects for three exactly solvable system-environment models: a single two-level system undergoing dephasing, a single two-level system interacting with an environment of two-level systems and a large spin undergoing dephasing. Our results

show that the quantum Zeno and anti-Zeno effects in the presence of non-selective projective measurements can differ very significantly as compared to the repeated selective measurement scenario.

- In chapter 5, we consider the effects of selective projective measurements on open quantum systems in the presence of coherent control fields [101, 103]. We present a general treatment of the quantum Zeno and anti-Zeno effects for arbitrary driven open quantum systems, assuming only that the system-environment coupling is weak. In particular, it is shown that decay rate of a quantum state that is subjected to repeated projective measurements as well as periodic measurements depends on the overlap integral of the spectral density of the environment and a generalized filter function [57, 101]. This filter function depends on the driving fields, the state of the environment, and the measurement being performed. We demonstrate that the driving fields change the decay rate for two-level system, and hence the quantum Zeno and anti-Zeno behavior, both qualitatively and quantitatively. We also extend our results to systems consisting of more than one two-level system, as well as a two-level system strongly coupled to an environment of harmonic oscillators, to further illustrate the non-trivial effect of the driving fields on the quantum Zeno and anti-Zeno effects.

- We consider the quantum Zeno and the quantum anti-Zeno effects for a two-level system coupled to a composite environment [5, 6] in Chapter 6. Here, the composite environment consists of a single harmonic oscillator which is in turn weakly coupled to a collection of harmonic oscillators. We find interesting effects by varying the coupling strengths between the parts of the composite environment.

- Finally, we conclude the thesis in Chapter 8 by briefly summarizing our main results. We also present our future work plan to proceed further into the details of open quantum system dynamics.

Chapter 2

Preliminaries

In this chapter, we briefly explain some overarching terms and ideas in the field of open quantum systems [3]. These include, in particular, quantum entanglement, the density matrix formalism, and the modeling of open quantum systems. With these basics dispensed with, we can move in the future chapters to the novel results we have derived.

2.1 Quantum entanglement

Suppose that there is a quantum system S composed of two sub-systems S_1 and S_2 [104]. These 'systems' may belong to different physical systems such as different atoms or molecules, or even to different degrees of freedom of the same physical system (for example, the translational and spin degrees of freedom of an atom). In any case, the Hilbert space of the composite system S is the direct product of the Hilbert spaces of the sub-systems S_1 and S_2. The composite system state[1] $|\Psi\rangle$ is entangled if this state vector cannot be written as a tensor product of vectors belonging to the Hilbert spaces for S_1 and S_2. That is, if we cannot write $|\Psi\rangle = |\psi_1\rangle \otimes |\psi_2\rangle$, with $|\psi_1\rangle$ and $|\psi_2\rangle$ some state vectors for the sub-systems S_1 and S_2 respectively, then we say that we are dealing with an entangled state of the composite system. The fact that entangled states exist is a consequence of the superposition princi-

[1]For simplicity, we will restrict ourselves here to the case where the composite state is pure.

ple extended to composite systems. For example, consider two spin-1/2 particles described by the mutually orthogonal eigenstates $|0_i\rangle$ and $|1_i\rangle$ (where $i = 1, 2$). States $|0_i\rangle$ and $|1_i\rangle$ correspond to particle i having its spin pointing up or down respectively. Eigenstates for composite Hilbert space are then the tensor products of the eigenstates for the sub-system Hilbert spaces [9]. It then follows that we can have states of the composite system such as

$$\left|\Phi^{\pm}\right\rangle = \frac{1}{\sqrt{2}}(|0_1\rangle\,|0_2\rangle \pm |1_1\rangle\,|1_2\rangle), \tag{2.1}$$

$$\left|\Psi^{\pm}\right\rangle = \frac{1}{\sqrt{2}}(|0_1\rangle\,|1_2\rangle \pm |1_1\rangle\,|0_2\rangle). \tag{2.2}$$

It can easily be checked that these states are impossible to write as a tensor product of states of the two spin-1/2 particles [9]. Entanglement actually indicates quantum correlations [9] between the two subsystems and these correlations lead to 'the sum being greater than the parts'. In other words, for entangled states, the sub-systems lose their individuality and the global properties of the total system S cannot be derived from the measurements on the individual sub-systems alone. On the other hand, when S_1 and S_2 are not entangled, each sub-system possesses its own complete description.

For us, entanglement is important mainly because a quantum system and its environment generally become entangled due to the system-environment interaction [3, 4, 9]. As a result, due to correlations between the system and the environment, some information about the system is invariably lost. This means that we cannot use vectors living in the system Hilbert space to describe the state of the quantum state - we can only do so if we know as much as we possibly could about the system, but due to system's interaction with its environment, the system has lost its individuality [5, 6]. Therefore, we need density matrix formalism [105], and this is what we now discuss.

2.2 The density matrix formalism

As discussed above, it is generally not possible to describe the state of a quantum system by a vector. Rather, we must consider the state to be a mixture, or ensemble, of different

state vectors $|\psi_i\rangle$. Such a state is said to be a mixed state. To describe both pure and mixed states with the same formalism, the density matrix is used. For a pure quantum state $|\psi\rangle$, the density matrix ρ is defined as [9]

$$\rho = |\psi\rangle \langle\psi| , \tag{2.3}$$

which is just a projection operator [2] onto the state vector $|\psi\rangle$. The expectation value for an arbitrary operator O is then

$$\langle O\rangle = \langle\psi|O|\psi\rangle = \mathrm{Tr}(\rho O), \tag{2.4}$$

where we have used the trace operation. For an ensemble of different pure states $|\psi_i\rangle$ with probabilities p_i, this expectation value is naturally

$$\langle O\rangle = \sum_i p_i \langle\psi_i| O |\psi_i\rangle . \tag{2.5}$$

We can write this again as $\mathrm{Tr}(\rho O)$, if we identify

$$\rho = \sum_i p_i |\psi_i\rangle \langle\psi_i| . \tag{2.6}$$

Since p_i are probabilities, we must have that $p_i \geqslant 0$ and $\sum_i p_i = 1$. It follows from this that the following three conditions must be met by the density matrix:

1. ρ is a positive semi-definite matrix, that is $\langle\psi| \rho |\psi\rangle \geq 0$, for any state vector $|\psi\rangle$. This is equal to requiring that all eigenvalues of the density matrix are positive, with some of its eigenvalues begin possibly equal to zero.

2. ρ is a Hermitian matrix, that is $\rho^\dagger = \rho$. Thus, eigenvalues of the density matrix are real.

3. ρ has unit trace, that is $\mathrm{Tr}[\rho] = \sum_i \langle\psi_i| \rho |\psi_i\rangle = \sum_i p_i = 1$. Consequently, the sum of the eigenvalues of the density matrix is one.

In fact, any operator that satisfies the above three conditions is a valid quantum state. To give one example of a mixed state, consider a two-level system in the state

$$\rho = p_1 |1\rangle \langle 1| + p_0 |0\rangle \langle 0| , \tag{2.7}$$

with $p_0 + p_1 = 1$, where p_1 or p_0 are the probabilities of measuring the system in the state $|1\rangle$ or $|0\rangle$ respectively, with $\langle 0|1\rangle = 0$. If $p_1 = p_0 = 1/2$, this will be a maximally mixed state - a state of maximum ignorance. We emphasize that this state is very different from the pure state described by the $\frac{1}{\sqrt{2}}|0\rangle + \frac{1}{\sqrt{2}}|1\rangle$, even though the probabilities of measuring the system in the state $|0\rangle$ or $|1\rangle$ are the same. The matrix representation of the mixed state density operator has, in the $|0\rangle$, $|1\rangle$ basis, zero off-diagonals, while the off-diagonal elements for the pure state are non-zero. This means that we perform a measurement in a basis other than $|0\rangle$ and $|1\rangle$, we will be able to, in general, clearly see a difference between the mixed state and the pure state. If either $p_1 = 1$ or $p_0 = 0$, then we have a pure state. We can quantify the 'purity' of any state ρ by finding $\mathrm{Tr}[\rho^2]$. Pure states satisfy $\mathrm{Tr}[\rho^2] = 1$, while for mixed states, we have $\mathrm{Tr}[\rho^2] < 1$[2].

Before moving on, let us also note that a mixed state for a composite system is said to be entangled if it cannot be expressed as a sum of product states, that is, if we cannot write the composite state ρ_{12} as $\rho_{12} = \sum_i p_i \rho_{1i} \otimes \rho_{2i}$, where ρ_{1i} and ρ_{2i} are the local density matrices pertaining to two systems S_1 and S_2, with $p_i \geqslant 0$ and $\sum_i p_i = 1$ [9].

We now briefly introduce reduced density matrices [9]. They play a crucial role for composite systems where a quantum system S is entangled with another system B and we are only interested in the state of S. For example, we can imagine that only the system S is in our control with measurements being performed only on S and not on B [9]. Then, everything which will be known about the state [3, 4] of composite system regarding only S are often extracted from the reduced density matrix describing the state of S alone. We obtain the reduced density matrix by 'tracing out' B, that is,

$$\rho_S = \mathrm{Tr}_B[\rho], \tag{2.8}$$

where ρ_S is the reduced density matrix that describes the state of S alone, ρ is the total state of the composite system, and Tr_B is the partial trace operation which eliminates the unobserved system B. As a simple example, consider the entangled state of a composite

[2]The von Neumann entropy, defined by $-\mathrm{Tr}[\rho \log_2 \rho]$, also tells us the 'mixedness' of a quantum state.

system consisting of two two-level systems given by [see Eq. (2.1)]

$$\left|\Phi^+\right\rangle\left\langle\Phi^+\right| = \frac{1}{2}(|0_1\rangle|0_2\rangle + |1_1\rangle|1_2\rangle)(\langle 0_1|\langle 0_2| + \langle 1_1|\langle 1_2|). \tag{2.9}$$

We can evaluate the state of the first two-level system only by tracing over the second two-level system, namely,

$$\rho_1 = \frac{1}{2}(|0_1\rangle\langle 0_1|\langle 0_2|0_2\rangle + |1_1\rangle|1_1\rangle\langle 1_2|1_2\rangle + |0_1\rangle\langle 1_1|\langle 1_2|0_2\rangle + |1_1\rangle\langle 0_1|\langle 0_2|1_2\rangle). \tag{2.10}$$

Since $\langle 0_2|1_2\rangle = 0$, we have

$$\rho_1 = \frac{1}{2}(|0_1\rangle\langle 0_1| + |1_1\rangle\langle 1_1|), \tag{2.11}$$

which is a maximally mixed state for the first two-level system! This is what we meant by saying that quantum systems lose their individuality by becoming entangled - by throwing away the second two-level system, we are completely ignorant about the state of the first two-level system [104].

2.3 Modeling open systems

We now discuss quantum systems interacting with another system possessing a large number of degrees of freedom (the 'environment' or 'reservoir'), and how such a situation can be modeled. There are numerous different types of physical systems interacting with their environment in the world. The task to study each system individually would appear rather hopeless. Fortunately, many (if not most) physical situations can get away by studying only a few 'canonical' models. This statement is indeed very powerful, which does not take into account details of system and its environment. However, the essential physics [106, 107] can be explained by one among few canonical models [5, 6, 9]. In such models, the central system is described by an effective 'two-level system' (TLS)[3] or as a 'harmonic oscillator' [5, 6]. Similarly, the environment is modeled by a set of two-level systems (TLSs) or harmonic oscillators [9].

[3]In this work, both qubit and TLS are often used to represent a two-level system. Sometimes, the term spin-1/2 or simply spin is also used for this purpose.

Mapping of the central system

In many physical situations, the relevant dynamics of a central system are often explained by only a very few coordinates of the system [9]. These relevant coordinates can be either discrete or continuous. If the coordinate of physical system is continuous [5, 6], we attempt to represent it as a harmonic oscillator. Such a harmonic oscillator model describes very accurately situation where the potential of the system is described accurately with a quadratic approximation. For instance, the vibrational modes of atoms bound in a molecule, the state of an atom confined to a cold atom trap [108], and a single mode of electromagnetic field in a cavity [109] can be represented by harmonic oscillators. On the other, physical systems involving discrete coordinates are effectively two-level systems [9]. One example is that of a particle restricted in a double-well potential with the particle being found only in the lowest-lying states of each well [110]. Similarly, a system consisting of multiple, discrete energy levels can be considered as a two-level system when only two energy levels of the system are important [7] or the total angular momentum of the system is spin-1/2 [111]. Other examples of two-level systems include solid state qubits based on electrons in quantum dot (QD) systems, polarization photon qubit, superconducting qubits (phase, charge, and flux qubits), diamond-based nitrogen-vacancy (NV) qubits, and cold trapped atomic and molecular qubits [112–117]. Two-level systems play an important role in quantum computation, where they physically correspond to qubits used to store quantum information.

Mapping of the environment

The modeling of the environment of a quantum system as a collection of harmonic oscillators is very common [9]. It is demonstrated in Refs. [118, 119] that if the interaction between system-environment is sufficiently weak, then any environment are often mapped onto a harmonic oscillator environment coupled linearly to the system [5, 6]. Physically, oscillator environments correspond to 'delocalized' bosonic field modes, such as magnons, phonons and photons, into which energy and coherence from the central system are transferred. By delocalized modes, we mean that the wave function of each oscillator mode is spread

out over a large spatial region. On the other hand, spin environments [106, 107] play an important role at low temperatures and represent 'localized' modes. This means that their wave functions are not spread out but are rather confined to a limited space. This is the case with defects, paramagnetic impurities, and nuclear spins in solids. The coupling to such a spin environment is often strong, which makes the dynamics of each spin of the environment also very much dependent on the state of the system. With strong coupling, we cannot map a spin environment to an oscillator environment - they constitute a different class of quantum environments.

Different choices of canonical open quantum system models

Having mapped the system as well as the environment, we now have four different possible ways during which choices for description of system and its environment are often arranged [9]. We thus get a total of four canonical models. The model which describes the interaction of a single spin with a harmonic oscillator environment is called spin-boson model [110]. Similarly, spin-spin models describe the physics of a two-level system in the presence of a spin environment [106, 107]. In this work, we shall deal with spin-boson model and spin-spin environment model as well as their extensions. We also note in passing that oscillator-oscillator environment model explains quantum version of Brownian motion [120] as well as describing a single mode of electromagnetic field in a lossy cavity [121], while the oscillator-spin environment model is used to describe quantum electromechanical systems [122]. In the next chapters, we will introduce these models and use them as needed. For now, we note that once the system and its environment has been modeled, the most commonly used approach to study the dynamics of the system is the following. The Hamiltonian of the system and its environment is written down, the initial system-environment is specified, and then total unitary operator of system and environment is used to generate time-evolution, with partial trace is taken over environment [3]. The end result is the system density matrix at an arbitrary time, or, equivalently, the differential equation in time for the system density matrix. This procedure, which may sound straightforward, is actually generally very complicated.

Only in particular situations can it be carried out exactly, and generally approximations have to be made. In future chapters, different examples of this procedure being carried out in practice will be seen.

2.4 Quantum projective measurements

Let us now move to briefly review effect of projective measurements on quantum systems since such measurements show up very prominently in this thesis. In conventional quantum theory, for every measurable quantity, there is a a Hermitian operator in the Hilbert space for the system. According to the projection (or collapse) postulate, a projective measurement instantaneously and irreversibly changes the state of the system into one among eigenstates of measured observable, with probability of every of those eigenstates [105] given by Born's rule. Generalizing further, suppose we describe all the possible measurement outcomes by a set of Hermitian and orthogonal projection operators $\{P_m\}$ corresponding to the eigenspaces of a measured observable. If the quantum system before the measurement is in a pure state $|\psi\rangle$, then, just after the measurement, the system state is projected onto one of the eigenspaces of the measured observable. The corresponding probability is

$$p_m = \langle\psi| P_m |\psi\rangle , \tag{2.12}$$

and the post-measurement state is

$$|\psi_m\rangle = \frac{P_m |\psi\rangle}{\sqrt{p_m}}. \tag{2.13}$$

Such measurements can be called 'selective' projective measurements because the measurement outcome is recorded or read. Note that the set of orthogonal projection operators P_m satisfy the following completeness relation

$$\sum_m P_m = 1, \tag{2.14}$$

which leads to

$$\sum_m \langle\psi| P_m |\psi\rangle = \sum_m p_m = 1. \tag{2.15}$$

The completeness relation thus guarantees that the probabilities sum up to one. These results can also be generalized to cases where measurements are carried out on mixed states. If the pre-measurement state is ρ, then the post-measurement state is

$$\rho_m = \frac{P_m \rho P_m}{\mathrm{Tr}[P_m \rho]}, \tag{2.16}$$

with the probability

$$p_m = \mathrm{Tr}[P_m \rho]. \tag{2.17}$$

Selective measurements, in general, lead to a reduction in the entropy of state ρ, because we have perfect information about state of system after measurement.

Now suppose that outcome of measurement is discarded. In this case, the final state of the system after the measurement is given by taking the average over all the possible outcomes of measurement. The post-measurement state is then

$$\rho' = \sum_m p_m \rho_m = \sum_m P_m \rho P_m. \tag{2.18}$$

Such a measurement is called a non-selective measurement.

Chapter 3

Effect of initial system-environment correlations with spin environments

This chapter is based on M. Majeed and A. Z. Chaudhry, Effect of initial system–environment correlations with spin environments, Eur. J. Phys. D ***73****, 16 (2019) [54, 55].*

As we have discussed, realistic quantum systems interact with their environment. This means that investigating the dynamics of these systems is a complicated endeavor [3]. Various techniques have been formulated for this task which generally employ a variety of approximations and assumptions in order to make the complicated dynamics computationally feasible [4]. For instance, the system-environment interaction strength is commonly assumed to be weak, paving the way for the use of perturbation theory [3]. Moreoever, the environment is also often assumed to have a very short correlation time; memory effects are then negligible [3, 9, 123]. The system and its environment are also assumed to be initially in a product state; the system and the environment states are independent, and the environment is in the thermal equilibrium state [54, 55, 124]. In other words, any initial system-environment correlations are completely neglected [5, 6, 124], the justification being that the system-environment correlations can be ignored if the system-environment coupling is weak [5, 6]. The environment quickly loses any information regarding the system when the environment is Markovian [3, 21, 123], thereby providing further justification for ignoring the

system-environment correlations. In the strong system-environment coupling regime, these approximations and assumptions are no longer expected to be applicable [3, 22, 23, 123].

With various quantum systems of practical interest such as superconducting qubits, quantum dots and light-harvesting complexes exhibiting strong interactions with the environment, various studies have been performed to critically analyze the effect of the system-environment correlations [24–53]. It should be kept in mind that any effects of the correlations are only expected to be observable in the strong system-environment coupling regime, which is unfortunately not directly accessible via perturbative methods [3, 54, 55, 124]. To counter this problem, one approach has been to study the effect of the initial correlations using exactly solvable models - see, for example, Refs. [40] and [43]. However, these exactly solvable models in turn have different limitations. In particular, the study of initial correlations performed in Refs. [40] and [43] use exactly solvable dephasing models where the system energy does not change. As another example, Ref. [35] studied the effect of initial correlations in Jaynes-Cummings model, where the diagonal elements of the central qubit do change, but the 'environment' is only a single harmonic oscillator.

Our objective in this chapter is to examine an exactly solvable model in which we can include the effects of initial system-environment correlations exactly and in which the diagonal as well as the off-diagonal elements of the density matrix change. In other words, our system undergoes dephasing and its energy changes. We believe that studying such a model will give useful insights into the role of the initial system-environment correlations [5, 6] just like previous works (see, for example, Refs. [35, 40, 43]) have done before. To this end, we examine an extension of a previously studied model of a single spin interacting with an environment consisting of a collection of spins [54, 55, 125]. The system spin Hamiltonian does not commute with the system-environment interaction, making the solution non-trivial. The system and environment are allowed to reach a joint equilibrium state [45], and then a projective measurement is performed on the central system in order to initialize it in a desired pure state [21, 54, 55]. The total equilibrium state is, in general, a correlated state that is different from the usually assumed uncorrelated product state of the system and

environment [5, 6, 39]. The state preparation influences the subsequent dynamics of central system spin via the system-environment correlations that existed before the state preparation [40, 43, 44, 52, 54, 55, 123]. The advantage of this model is that we obtain relatively simple expressions for evolution of Bloch vector of system spin for arbitrary temperature and arbitrary system-environment coupling strength with both initially uncorrelated and correlated system-environment states. The exact analytical solutions for the Bloch vector allow us to show that the state preparation can have a very significant influence on the system dynamics via system-environment correlations. As expected, we find that the initial correlations are not important for weak system-environment coupling. For lower temperatures and stronger system-environment coupling strengths, the initial correlations between system and environment can play a very significant role [5, 6, 54]. However, interestingly, this is not always the case - even with very low temperatures and strong coupling strength between the system and its environment, it is possible that the state preparation does not significantly affect the system dynamics. This is in contrast with the harmonic oscillator environments investigated previously [40, 43]. We then extend our model to two spins interacting with a common spin environment. We once again illustrate that initial correlations can play a very important role. In particular, the phenomena of entanglement sudden death [126] and birth [127] can differ significantly due to initial correlations [54, 123].

3.1 The model

Our model consists of a single spin-1/2 particle interacting with a spin bath consisting of N spin-1/2 particles. Our system-environment Hamiltonian is [124]

$$H = H_S + H_B + H_{SB}, \tag{3.1}$$

where H_S and H_B, the self-Hamiltonians of the central system and the environment, are defined to be (with $\hbar = 1$ throughout)

$$H_S = \frac{\varepsilon}{2}\sigma_z + \frac{\Delta}{2}\sigma_x, \tag{3.2}$$

and

$$H_B = \sum_{i=1}^{N} \frac{\varepsilon_i}{2}\sigma_z^{(i)} + \sum_{i=1}^{N} \sigma_z^{(i)}\sigma_z^{(i+1)}\chi_i, \tag{3.3}$$

while the system-environment interaction is

$$H_{SB} = \frac{1}{2}\sigma_z \otimes \sum_{i=1}^{N} g_i \sigma_z^{(i)}. \tag{3.4}$$

Here σ_k (with $k = x, y, z$) represent the usual Pauli spin matrices, and ε and Δ denote the energy-level spacing and tunneling amplitude of central TLS respectively. Similarly, ε_i denotes the energy level spacing for the i^{th} environmental spin. We have also allowed the environment spins to interact with each other [123] via $\sum_{i=1}^{N} \sigma_z^{(i)}\sigma_z^{(i+1)}\chi_i$, where χ_i characterizes the nearest-neighbor interaction strength between the environment spins. The central spin interacts with the environment spins through H_{SB}, where g_i is the interaction strength between central spin system and the i^{th} environment spin [123]. Note that, system energy is not constant since H_S does not commute with the total system-environment Hamiltonian.

Our objective is to solve the dynamics of the central spin with both correlated and uncorrelated initial states. As such, we try to find the combined system-environment unitary evolution operator. Let us first write

$$H_{\text{SB}} = \frac{1}{2}\sigma_z \otimes B, \tag{3.5}$$

where the environment operator B is $B = \sum_{i=1}^{N} g_i \sigma_z^{(i)}$. To proceed further, we follow a method similar to that in Ref. [125]. However, unlike Ref. [125], we do not consider the environment Hamiltonian H_B to be negligible and we will not in general assume the initial environment state to be a pure state. The eigenstates of B can be written as products of eigenstates $|0_i\rangle$ and $|1_i\rangle$ of i^{th} environment spin operator $\sigma_z^{(i)}$ [124, 125], where $|0\rangle$ denotes

the spin 'up' state and $|1\rangle$ the spin 'down' state. As such, we write the eigenstates of B as $|n\rangle \equiv |n_1\rangle\,|n_2\rangle \ldots |n_N\rangle$, with $n_i = 0, 1$. It is clear that

$$B\,|n\rangle = G_n\,|n\rangle\,, \tag{3.6}$$

with

$$G_n = \sum_{i=1}^{N} (-1)^{n_i} g_i. \tag{3.7}$$

Also, since B commutes with H_B, we expect that H_B also has the same eigenstates. Indeed,

$$\sum_{i=1}^{N} \frac{\varepsilon_i}{2} \sigma_z^{(i)}\,|n\rangle = \frac{1}{2}\epsilon_n\,|n\rangle\,, \tag{3.8}$$

with

$$\epsilon_n = \sum_{i=1}^{N} (-1)^{n_i} \varepsilon_i, \tag{3.9}$$

and

$$\sum_{i=1}^{N} \sigma_z^{(i)} \sigma_z^{(i+1)} \chi_i\,|n\rangle = \eta_n\,|n\rangle\,, \tag{3.10}$$

with

$$\eta_n = \sum_{i=1}^{N} (-1)^{n_i} (-1)^{n_{i+1}} \chi_i. \tag{3.11}$$

Using the completeness relation over the states $|n\rangle$, that is, over all the different configurations of the environment spins, we find that the combined time-evolution operator is

$$U(t) = \sum_n e^{-i\epsilon_n t/2} e^{-i\eta_n t} e^{-i(H_S + H_{SB})t}\,|n\rangle\,\langle n|\,. \tag{3.12}$$

This further simplifies since

$$e^{-i(H_S+H_{SB})t}\,|n\rangle = e^{-iH^{\rm eff}_{s,n}t}\,|n\rangle\,, \tag{3.13}$$

with $H^{\rm eff}_{s,n} = \frac{\zeta_n}{2}\sigma_z + \frac{\Delta}{2}\sigma_x$, and $\zeta_n = \varepsilon + G_n$. We then have

$$U(t) = \sum_{n=0}^{2^N-1} U_n(t)|n\rangle\langle n|, \tag{3.14}$$

with

$$U_n(t) = e^{-i\eta_n t}e^{-i\epsilon_n t/2}\left[\cos(\Omega_n t) - \frac{i}{\Omega_n}\sin(\Omega_n t)\left(\frac{\zeta_n}{2}\sigma_z + \frac{\Delta}{2}\sigma_x\right)\right], \tag{3.15}$$

and $\Omega_n^2 = \frac{1}{4}\left(\zeta_n^2 + \Delta^2\right)$. Eq. (3.14) has the physical interpretation that for every configuration of the environment spins $|n\rangle$, the effective dynamics of central spin system can be found using $U_n(t)$ [54, 55, 123].

To proceed further in finding the dynamics of central TLS, we have to [21] specify the initial system-environment state. The usual choice is to consider [3, 4] a simple product state of form $\rho(0) = \rho_S(0)\otimes\rho_B$, with $\rho_S(0)$ is the initial system state, and ρ_B is the thermal state $e^{-\beta H_B}/Z_B$, with $Z_B = {\rm Tr}_B[e^{-\beta H_B}]$ [3–6, 128]. However, this choice is not justified if system and environment are interacting strongly since then system-environment correlations can play a significant role. To take these correlations into account, we imagine that system and environment have been interacting strongly for a long time and have thus reached the joint equilibrium state proportional to $e^{-\beta H}$ [5, 6, 43, 44, 54, 55]. A projective measurement is subsequently performed on the system to obtain the desired initial system state $|\psi\rangle$. This then means that the initial system-environment state is now $\rho(0) = |\psi\rangle\,\langle\psi|\otimes\langle\psi|e^{-\beta H}|\psi\rangle/Z$ [5, 6, 40, 43–45, 52]. Although this is still a product state, but it contains system-environment correlations that existed before system state preparation. In fact, we can quantify these correlations via the quantum mutual information defined as $I_{S:B} = E(\rho_S) + E(\rho_B) - E(\rho)$, where the von-Neumann entropy $E(\rho) = -{\rm Tr}(\rho\log_2\rho)$ can be employed to quantify the ignorance regarding the state ρ [129]. Here, ρ is the total density matrix of system and

environment, and $\rho_S = \mathrm{Tr}_B\rho$ and $\rho_B = \mathrm{Tr}_S\rho$. If the system and the environment are uncorrelated, we find that $I_{S:B}$ is zero, whereas for a correlated system-environment state, it has a non-zero value. In our system-environment model, we can compute the mutual information for $\rho = e^{-\beta H}/Z_{\mathrm{tot}}$, with $Z_{\mathrm{tot}} = \mathrm{Tr}_{S,B}[e^{-\beta H}]$, just before a projective measurement prepares the initial state of central system. It is found that the mutual information in the strong system-environment coupling regime is significant if temperature is not too high, and due to these correlations, the system preparation affects the environment state. The correlations are then expected to be manifested in the subsequent system dynamics. For example, we find that $I_{S:B}$ is approximately 0.01 at relatively high temperatures ($\beta = 0.1$), whereas it is approximately 0.21 at lower temperatures corresponding to $\beta = 1$ (here the system-environment parameters are $\Delta = 1$, $\varepsilon = 2$, $g_i = 1$, $\varepsilon_i = 1$, and number of spins $N = 10$). We have also considered g_i and ε_i to be the same for every environment spin and the interactions between spins of environment are assumed to be negligible. On the other hand, the mutual information is much smaller if g_i is weak, even at relatively low temperatures. With these insights, we now analyze the system dynamics with two different initial states one by one.

3.1.1 Uncorrelated initial system-environment state

The first choice of initial conditions is

$$\rho(0) = |\psi\rangle\langle\psi| \otimes \frac{e^{-\beta H_B}}{Z_B}. \tag{3.16}$$

We refer to this state as the 'uncorrelated initial state' since system-environment interaction term before state preparation on central system is neglected. The time-evolved system density matrix is

$$\rho_S(t) = \mathrm{Tr}_B[e^{-iHt}\rho(0)e^{iHt}]. \tag{3.17}$$

Using Eq. (3.14), we find that [9]

$$\rho_S(t) = \frac{1}{Z_B} \sum_{n=0}^{2^N-1} c_n U_n(t) \left|\psi\right\rangle \left\langle\psi\right| U_n^\dagger, \tag{3.18}$$

where $c_n = e^{-\beta\eta_n} e^{-\beta\epsilon_n/2}$, and $Z_B = \sum_n c_n$. This makes sense - each environment state configuration $|n\rangle$ occurs with probability c_n/Z_B in the initial state, and for each configuration, the system dynamics is generated by $U_n(t)$. The total central system state is then obtained simply by taking all the possible environment configurations into account. To better capture the evolution of the central system, it is useful to express the system density matrix in terms of the Bloch vector components $p_k(t) = \mathrm{Tr}_S[\sigma_k \rho_S(t)]$ as

$$\rho_S(t) = \frac{1}{2}\left[1 + \sum_k \sigma_k p_k(t)\right]. \tag{3.19}$$

We find that the Bloch vector at time t $\mathbf{p}(t)$ is given by $\mathbf{p}(t) = \frac{1}{Z_B}\mathbf{S}^{uc}(t)\mathbf{p}(0)$[1], that is,

$$\begin{pmatrix} p_x(t) \\ p_y(t) \\ p_z(t) \end{pmatrix} = \frac{1}{Z_B} \begin{pmatrix} S_{xx}^{uc} & S_{xy}^{uc} & S_{xz}^{uc} \\ S_{yx}^{uc} & S_{yy}^{uc} & S_{yz}^{uc} \\ S_{zx}^{uc} & S_{zy}^{uc} & S_{zz}^{uc} \end{pmatrix} \begin{pmatrix} p_x(0) \\ p_y(0) \\ p_z(0) \end{pmatrix}, \tag{3.20}$$

with

$$\begin{aligned} S_{xx}^{uc}(t) &= \sum_n \frac{c_n}{4\Omega_n^2}\left[\zeta_n^2 \cos(2\Omega_n t) + \Delta^2\right], \\ S_{xy}^{uc}(t) &= -\sum_n \frac{c_n}{2\Omega_n}\zeta_n \sin(2\Omega_n t), \\ S_{xz}^{uc}(t) &= \sum_n \frac{c_n}{2\Omega_n^2}\Delta\zeta_n \sin^2(\Omega_n t), \\ S_{yx}^{uc}(t) &= \sum_n \frac{c_n}{2\Omega_n}\zeta_n \sin(2\Omega_n t), \end{aligned} \tag{3.21}$$

[1]Note that, dynamical map describing [45] the evolution of Bloch vector components is independent of state prepared $|\psi\rangle$. This will not be the case when the initial system-environment correlations are considered.

$$
\begin{aligned}
S_{yy}^{uc}(t) &= \sum_n c_n \cos(2\Omega_n t), \\
S_{yz}^{uc}(t) &= -\sum_n \frac{c_n}{2\Omega_n} \Delta \sin(2\Omega_n t), \\
S_{zx}^{uc}(t) &= \sum_n \frac{c_n}{2\Omega_n^2} \Delta\zeta_n \sin^2(\Omega_n t), \\
S_{zy}^{uc}(t) &= \sum_n \frac{c_n}{2\Omega_n} \Delta \sin(2\Omega_n t), \\
S_{zz}^{uc}(t) &= \sum_n \frac{c_n}{4\Omega_n^2} \left[\zeta_n^2 + \Delta^2 \cos(2\Omega_n t)\right]. \qquad (3.22)
\end{aligned}
$$

Knowing the system-environment parameters, to find all the elements in this matrix one simply needs to perform sums over all the 2^N different environment configurations. We emphasize that this is an exact solution which is also valid if the g_i are large. It is also obvious that the off-diagonal and diagonal elements of the system density matrix both generally evolve.

3.1.2 Correlated initial system-environment state

We now take the system-environment correlations (before state preparation of central system) into account [5, 6, 43, 44, 54, 55]. We start from the correlated system-environment state

$$\rho = \frac{e^{-\beta H}}{Z_{\text{tot}}}, \qquad (3.23)$$

with $Z_{\text{tot}} = \text{Tr}_{S,B}[e^{-\beta H}]$. The presence of the system-environment interaction means that this state cannot, in general, be expressed as a product state [5, 6, 40, 43, 44, 52] of the system and its environment. At $t = 0$, we then perform a projective measurement on the system to prepare it in a desired state $|\psi\rangle$, meaning that initial state of system and environment is now [5, 6, 54, 55]

$$\rho(0) = |\psi\rangle \langle\psi| \otimes \frac{\langle\psi|e^{-\beta H}|\psi\rangle}{Z}, \qquad (3.24)$$

where $Z = \mathrm{Tr}_{S,B}[|\psi\rangle\langle\psi| \otimes \langle\psi|e^{-\beta H}|\psi\rangle]$ is the partition function of central system and surrounding environment as a whole [123]. Note that, initial environment state[2] $\rho_B = \langle\psi|e^{-\beta H}|\psi\rangle/Z$ depends on H_{SB} interaction term, and initial state preparation $|\psi\rangle$ of system. Thus, this is not a canonical equilibrium state for environment [123]. It is obvious that if g_i is small, the initial system-environment state (after system state preparation) would be the same as that in Eq. (3.16). In other words, the effect of the initial correlations is negligible with weak system-environment coupling. Furthermore, the state preparation influences the initial environment state due to initial correlations. This means that environment affects the system dynamics differently depending on the initial state preparation [5, 6, 45, 54, 55] - the effect of initial correlations also depends on the system state prepared.

To now evaluate dynamics of system , we start by observing that

$$\sum_n e^{-\beta H}|n\rangle\langle n| = \sum_n U_n(t = -i\beta)\,|n\rangle\,\langle n|\,, \tag{3.25}$$

with $U_n(t)$ given in Eq. (3.14). This then allows us to write $Z = \sum_n c_n A_n$, with

$$A_n = \cosh(\beta\Omega_n) - \frac{\sinh(\beta\Omega_n)}{\Omega_n}\langle\psi|\left(\frac{\zeta_n}{2}\sigma_z + \frac{\Delta}{2}\sigma_x\right)|\psi\rangle. \tag{3.26}$$

The system density matrix at time t is again given by $\rho_S(t) = \mathrm{Tr}_B[e^{-iHt}\rho(0)e^{iHt}]$, but now with the initial state $\rho(0)$ given by Eq. (3.24). Using Eq. (3.14) for unitary time-evolution operator and simplifying, we find that Bloch vector at time t $\mathbf{p}(t)$ is now given by $\mathbf{p}(t) = \frac{1}{Z}\mathbf{S}^c(t)\mathbf{p}(0)$ [54, 55], with

[2]The projective measurement is usually assumed to take negligible time; consequently, the unnormalized state of the environment after the measurement is $\langle\psi|\,e^{-\beta H}\,|\psi\rangle$.

$$
\begin{aligned}
S^c_{xx}(t) &= \sum_n \frac{c_n A_n}{4\Omega_n^2}\left[\zeta_n^2\cos(2\Omega_n t) + \Delta^2\right], \\
S^c_{xy}(t) &= -\sum_n \frac{c_n A_n}{2\Omega_n}\zeta_n \sin(2\Omega_n t), \\
S^c_{xz}(t) &= \sum_n \frac{c_n A_n}{2\Omega_n^2}\Delta\zeta_n \sin^2(\Omega_n t), \\
S^c_{yx}(t) &= \sum_n \frac{c_n A_n}{2\Omega_n}\zeta_n \sin(2\Omega_n t), \\
S^c_{yy}(t) &= \sum_n c_n A_n \cos(2\Omega_n t), \\
S^c_{yz}(t) &= -\sum_n \frac{c_n A_n}{2\Omega_n}\Delta \sin(2\Omega_n t), \\
S^c_{zx}(t) &= \sum_n \frac{c_n A_n}{2\Omega_n^2}\Delta\zeta_n \sin^2(\Omega_n t), \\
S^c_{zy}(t) &= \sum_n \frac{c_n A_n}{2\Omega_n}\Delta \sin(2\Omega_n t), \\
S^c_{zz}(t) &= \sum_n \frac{c_n A_n}{4\Omega_n^2}\left[\zeta_n^2 + \Delta^2\cos(2\Omega_n t)\right].
\end{aligned}
\tag{3.27}
$$

Comparing with the uncorrelated case, we can see that the difference in the evolution is essentially because of the factor A_n that includes initial state preparation. It also depends on the temperature, the strength of the system-environment coupling, and the parameters ε and Δ. Once again, this makes sense. The difference with the usual uncorrelated case is due to the difference in the initial environment state. Each environment spin configuration now occurs with probability $c_n A_n/Z$, as compared to c_n/Z_B previously, and this is precisely what leads to the different Bloch vector evolution. We emphasize that with our model, we can investigate the effect of the initial correlations in an exact, non-perturbative manner, with both diagonals and off-diagonals of the two-level system changing.

We now start to quantitatively examine the difference in the evolution of the system state with and without initial system-environment correlations [54, 55, 123]. Some general comments are in order. First, with weak system-environment coupling, as mentioned before,

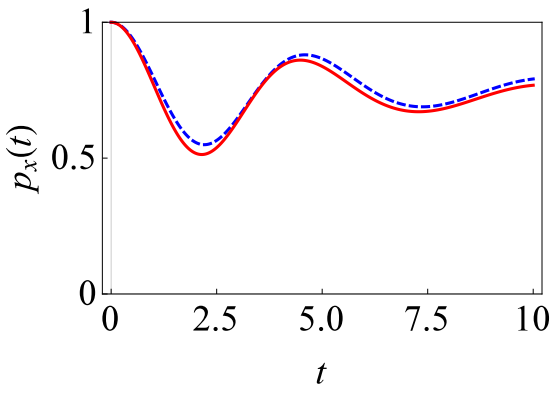

Figure 3.1: Graph of $p_x(t)$ versus time t for relatively weak system-environment coupling without initial correlations (dashed, blue line) and with initial correlations (solid, red line). We have set $\hbar = 1$ with $\Delta = 1$. For simplicity, we have chosen the coupling strength g_i and level spacing ε_i to be the same for every environment spin. Here we have $g_i = 0.1$, $\varepsilon = 2$, $\varepsilon_i = 1$, $\beta = 1$, $\chi_i = 0$, and $N = 50$. The initial system state is specified by $p_x(0) = 1$.

we expect that the system evolution in both cases will be very similar. Second, at high temperatures, we can again expect that effect of correlations to be negligible - in the very high temperature limit, the total state before the projective measurement on the system is a completely mixed state [49], meaning that there are no system-environment correlations. These two predictions are illustrated in Figs. 3.1 and 3.2 where we have plotted the Bloch vector component $p_x(t)$ starting from uncorrelated and correlated system-environment states. For simplicity of presentation, we will be presenting the evolution of Bloch vector component $p_x(t)$ only; however, all three components are generally changing. The figures clearly show a a very small difference in the system dynamics as the initial state is changed.

Let us consider now stronger coupling strengths g_i. As expected, if the temperature is not high, with stronger g_i, there is a more significant difference between system evolution starting from the uncorrelated initial state and correlated initial state [54, 55, 123]. This is illustrated in Fig. 3.3 where the coupling between the central spin and each of the environment spins has been set to $g_i = 0.5$ (the system parameters are $\varepsilon = 2$ and $\Delta = 1$). Note that, also system parameters such as Δ play a role in the dynamics of central system (compare Figs. 3.3

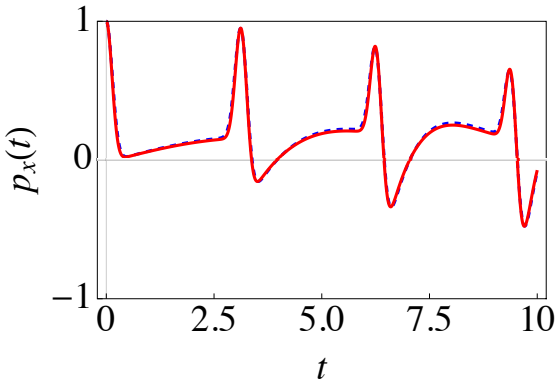

Figure 3.2: Same as Fig. 3.1, except that now we have $\beta = 0.1$ and $g_i = 1$.

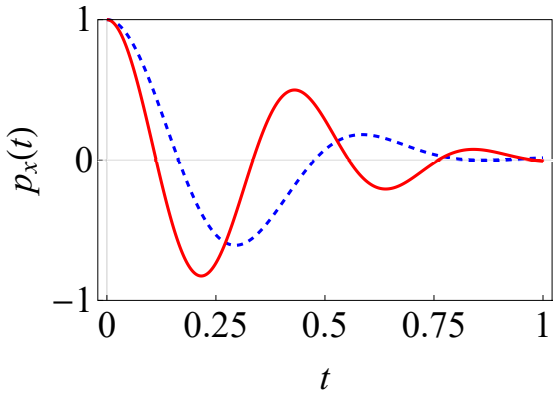

Figure 3.3: Same as Fig. 3.1, except that now we have $\beta = 1$ and $g_i = 0.5$.

and 3.4). If g_i is made even stronger, then there is an even bigger difference, as illustrated in Fig. 3.5 where we have set $g_i = 1$. Proceeding along these lines, it is interesting to investigate what happens at even lower temperatures. Surprisingly, as illustrated in Fig. 3.6, the difference in the dynamics due to state preparation disappears at lower temperatures, even for strong g_i. This is contrary to the expectation that strong coupling strengths and low temperatures imply a greater effect of initial system-environment correlations as is the case with harmonic oscillator environments [5, 6, 40, 43]. However, the explanation is simple. Consider first the 'uncorrelated' case $\rho(0) = \rho_S(0) \otimes e^{-\beta H_B}/Z_B$. At low temperatures, the environment will be (approximately) in its ground state. Considering all ε_i to be positive, this means that the initial environment state will be $|11\ldots1\rangle$, that is, all the environment spins

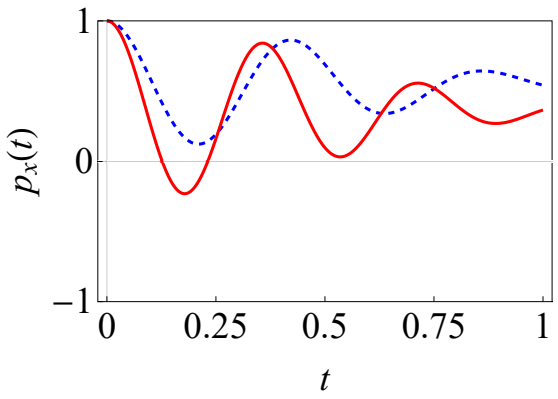

Figure 3.4: Same as Fig. 3.3, except that now we have $\Delta = 10$.

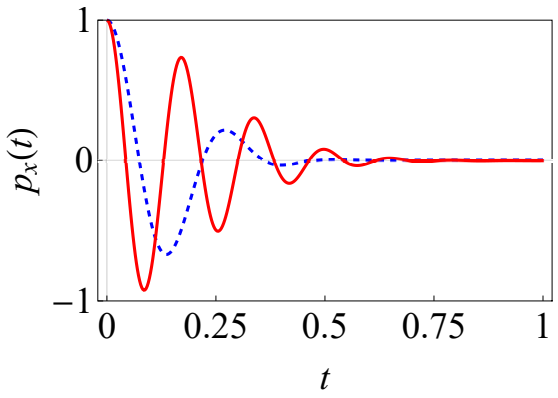

Figure 3.5: Same as Fig. 3.1, except that now we have $\beta = 1$ and $g_i = 1$.

will be in the spin 'down' state. The system state, on the other hand, is simply the state that we choose to prepare $|\psi\rangle$. Now, examine the total initial state $\rho(0) = \rho_S(0) \otimes \langle\psi|e^{-\beta H}|\psi\rangle/Z$. At low temperatures, the system-environment state just before the system state preparation will be (approximately) the ground state of total system-environment Hamiltonian H. If H_B contributes significantly towards the total Hamiltonian, then the ground state corresponds to (approximately) the environment being all spins down and the system is spin up (assuming g_i to be positive). Thus, the measurement on central spin system that prepares the initial state of central system does not affect the environment state, and the initial system-environment state is the same as before, meaning that the dynamics from the two initial states are the same. To test this prediction, let us instead consider the situation where H_B is relatively

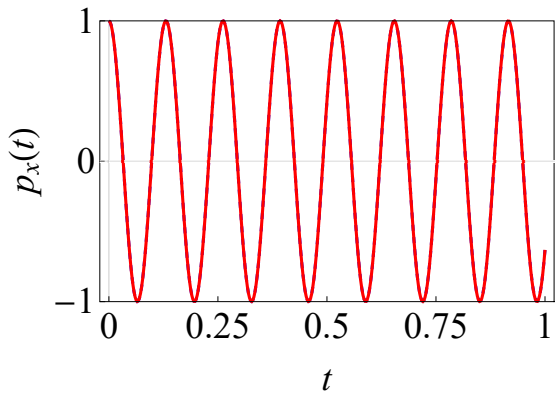

Figure 3.6: Same as Fig. 3.1, except that now we have $g_i = 1$ and $\beta = 10$.

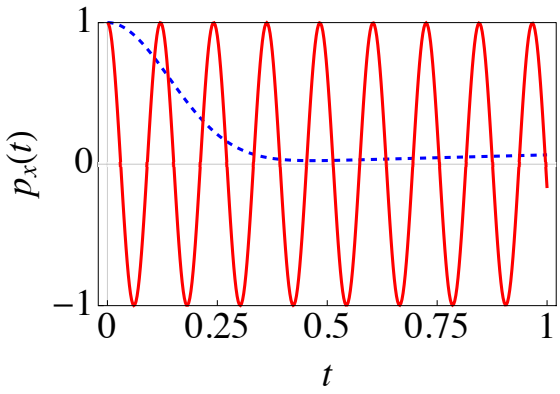

Figure 3.7: Same as Fig. 3.1, except that now we have $\varepsilon_i = 0.01$, $g_i = 1$ and $\beta = 10$.

small, which we can do by setting ε_i to be small. Then, with strong system-environment coupling, the ground state of the system-environment is not simply $|0\rangle \otimes |1 \ldots 1\rangle$, that is, the central spin system is in 'up' state and all environment spins are spin 'down'. Rather, the ground state is now a mixture of $|0\rangle \otimes |1 \ldots 1\rangle$ and $|1\rangle \otimes |0 \ldots 0\rangle$. On the other hand, initial state of environment with correlated system-environment state is the maximally mixed state. Clearly then, we expect a difference in the dynamics now. This is precisely what is illustrated in Fig. 3.7.

Next, we consider the environment spins to be interacting as well. As expected, for high temperatures and weak system-environment coupling, the initial correlations still have no effect on the system dynamics. In contrast, as before, for strong g_i (system-environment

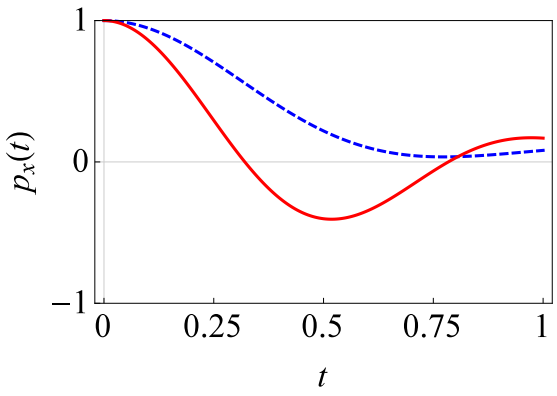

Figure 3.8: Graph of $p_x(t)$ versus time t for moderate system-environment coupling without initial correlations (dashed, blue line) and with initial correlations (solid, red line). Here we have considered the interactions between the spins of the environment and we have set $\Delta = 1$. For simplicity, we have chosen the coupling strength g_i, level spacing ε_i, and interactions between the spins of environment χ_i to be the same for every environment spin. Here we have $g_i = 1$, $\varepsilon = 2$, $\varepsilon_i = 1$, $\beta = 1$, $N = 10$ and $\chi_i = 0.1$. The initial system state is specified by $p_x(0) = 1$.

coupling strength) and moderate temperature, the initial correlations can play a significant role [see Fig. 3.8]. Furthermore, as before, at lower temperatures, the difference in the system evolution with the uncorrelated and uncorrelated states can disappear as illustrated in Figs. 3.9 and 3.10. However, the situation is more complicated in Fig. 3.11, since now the initial correlations can play a role for very low temperatures. Let us try to explain this. Consider the spin-spin interaction for the environment χ_i to be positive, that is, the interaction is anti-ferromagnetic. Then, there are three effects at play here. First, due to the energies ε_i, the environment spins would like to be aligned. Second, if g_i is positive, the environment spins would again like to be aligned. Third, due to the interaction between the spins, the environment spins would like to be anti-aligned. The different initial states can lead to different dynamics depending on which term is more dominant. If χ_i is small and ε_i is relatively large, then combined system-environment ground state is approximately $|0\rangle \otimes |1 \ldots 1\rangle$, that is, all the environment spins are aligned, which means that there is no difference in dynam-

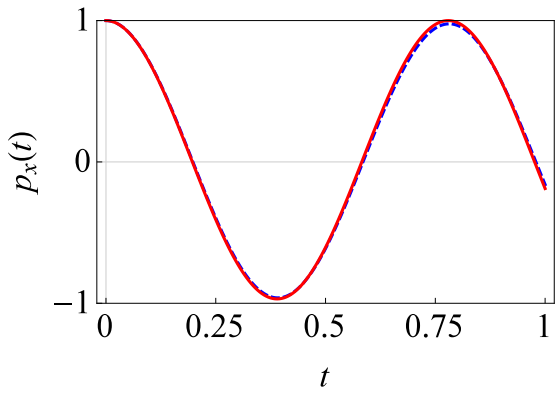

Figure 3.9: Same as Fig. 3.8, except that now we have $\beta = 10$ and $g_i = 1$.

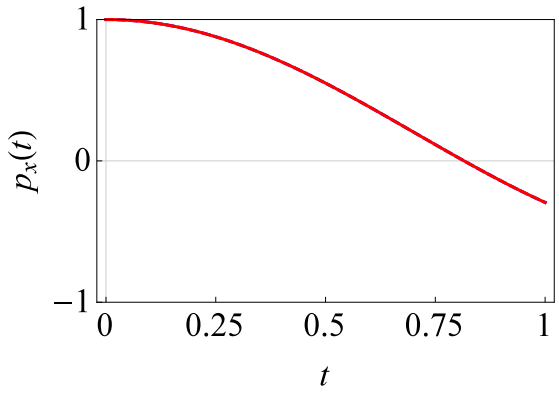

Figure 3.10: Same as Fig. 3.8, except that now we have $\beta = 10$, $\varepsilon_i = 0.01$, $\chi_i = 1$ and $g_i = 1$.

ics [see Fig. 3.9]. On the other hand, if ε_i is small and χ_i is large, the environment state consists of anti-aligned spins in the uncorrelated case. If the system-environment coupling is not completely dominant, then the environment state is the same for the correlated case. Once again, there is no difference in the dynamics [see Fig. 3.10]. Now consider the situation where ε_i and χ_i are comparable, while the system and the environment are strongly coupled. Then for the uncorrelated state, the environment state is 'confused' between being aligned or anti-aligned. However, for the correlated initial state, the environment state consists of all spins aligned. Clearly then, the system dynamics will be different as illustrated in Fig. 3.11.

Until now, the numerical results we have presented have assumed that, for instance, the

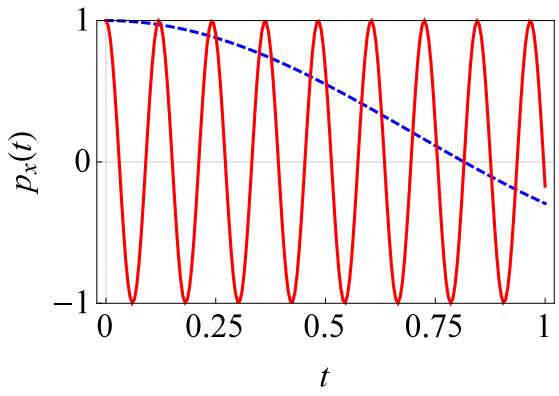

Figure 3.11: Same as Fig. 3.8, except that now we have $\beta = 10$, $\chi_i = 1$ and $g_i = 5$.

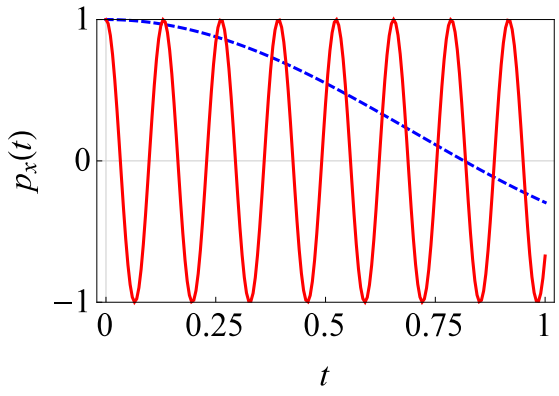

Figure 3.12: Graph of $p_x(t)$ versus time t for relatively strong system-environment coupling without initial correlations (dashed, blue line) and with initial correlations (solid, red line). We have set $\hbar = 1$, with $\Delta = 1$. The coupling strength g_i, level spacing ε_i and interactions between the environment spins are considered to be Gaussian random variables. Here we have mean value of coupling strength $g_i = 5$ (standard deviation = 0.01), $\varepsilon = 2$, mean value of level spacing $\varepsilon_i = 1$ (standard deviation = 0.001), $\beta = 10$, mean interactions between the spins $\chi_i = 1$ (standard deviation = 0.01) and $N = 10$. The initial state is specified by $p_x(0) = 1$.

coupling strength between central spin system and each spin of environment g_i is the same [124]. Of course, in reality, this is unlikely to be the case. To overcome this shortcoming, we now illustrate that even if the environment parameters and the central spin-environment

spin coupling strengths are randomly distributed, we obtain similar conclusions compared to what we have presented before. In Fig. 3.12, we have assumed that g_i is a Gaussian random variable with a small standard deviation; the environment level spacings ε_i and the inter-spin interactions χ_i are treated similarly. We find that the difference between the initially correlated case and the uncorrelated case persists. This difference persists even with larger standard deviations [see Fig. 3.13].

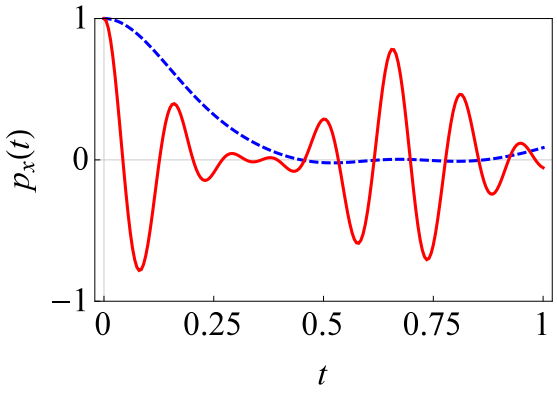

Figure 3.13: Same as Fig. 3.12, except that now the mean value of $g_i = 5$ (standard deviation = 1), mean value of level spacing $\varepsilon_i = 1$ (standard deviation = 0.2), $\beta = 10$, and mean interactions between the spins $\chi_i = 1$ (standard deviation = 0.2).

3.2 Extension to two two-level systems

To further illustrate the difference in the system evolution with and without initial correlations, let us extend our formalism to deal with two TLSs interacting with a common spin environment. It is well known that the dynamics of two qubits can display characteristics that are absent from the single qubit case. Particularly, we can look at the behavior of entanglement between the two qubits. If the initial two-qubit state is a fully entangled state, then due to the interaction with the environment, this entanglement can disappear in a finite amount of time interval, a phenomenon known as entanglement sudden death (ESD) [126]. The entanglement between the two qubits can also revive - this is referred to as entanglement

sudden birth (ESB) [127]. If the two qubits are not entangled to begin with, then we can investigate the dynamics of the generation of entanglement.

Our Hamiltonian is a straightforward extension of the previous Hamiltonian for a single qubit. Namely, we now have

$$H = H_S^{(1)} + H_S^{(2)} + H_{12} + H_B + H_{SB}^{(1)} + H_{SB}^{(2)}, \tag{3.28}$$

with

$$H_S^{(1)} = \frac{\varepsilon_1}{2}\sigma_{z1} + \frac{\Delta_1}{2}\sigma_{x1}, \tag{3.29}$$

$$H_S^{(2)} = \frac{\varepsilon_2}{2}\sigma_{z2} + \frac{\Delta_2}{2}\sigma_{x2}, \tag{3.30}$$

$$H_{12} = \lambda\sigma_{z1}\sigma_{z2}, \tag{3.31}$$

$$H_{SB}^{(1)} = \frac{1}{2}\sigma_{z1} \otimes \sum_{i=1}^{N} g_i\sigma_z^{(i)}, \tag{3.32}$$

$$H_{SB}^{(2)} = \frac{1}{2}\sigma_{z2} \otimes \sum_{i=1}^{N} g_i\sigma_z^{(i)}, \tag{3.33}$$

$$H_B = \sum_{i=1}^{N} \frac{\varepsilon_i}{2}\sigma_z^{(i)} + \sum_{i=1}^{N} \sigma_z^{(i)}\sigma_z^{(i+1)}\chi_i. \tag{3.34}$$

The qubits are labeled as 1 and 2 with two-level energies ε_1 and ε_2 and tunneling amplitudes Δ_1 and Δ_2 respectively, and are coupled by the interaction term H_{12}. σ_{j1} and σ_{j2} are the Pauli spin matrices for qubit 1 and 2 respectively. Our goal is to examine the dynamics of entanglement [126, 127] between the two qubits, starting from uncorrelated initial state and correlated initial state. The entanglement is quantified via the concurrence [130], defined as

$$C(t) = \max(0, \sqrt{M_1} - \sqrt{M_2} - \sqrt{M_3} - \sqrt{M_4}), \tag{3.35}$$

where M_i are eigenvalues of matrix M arranged in decreasing order of

$$M = \rho_S(t)\tilde{\rho}_S(t). \tag{3.36}$$

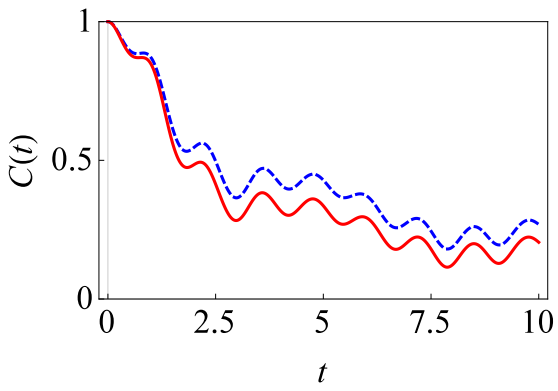

Figure 3.14: Graph of decay of entanglement of two qubits $C(t)$ versus time t for relatively weak system-environment coupling without initial correlations (dashed, blue line) and with initial correlations (solid, red line). We have set $\hbar = 1$, with $\lambda = 0$ and $\chi_i = 0$. For simplicity, we have chosen the coupling strength g_i and level spacing ε_i to be the same for every environment. Here we have $g_i = 0.1$, $\varepsilon_1 = 1$, $\varepsilon_2 = 2$, $\varepsilon_i = 1$, $\beta = 1$, $\Delta_1 = 4$, $\Delta_2 = 1$ and $N = 50$. The initial state of two qubits is the maximally correlated state $|\psi\rangle = \frac{1}{\sqrt{2}}(|0_1 0_2\rangle + |1_1 1_2\rangle)$.

Here $\tilde{\rho}(t) = (\sigma_{y1} \bigotimes \sigma_{y2})\rho_S^*(t)(\sigma_{y1} \bigotimes \sigma_{y2})$, and $\rho_S^*(t)$ is the complex conjugate of the two-qubit density matrix $\rho_S(t)$. The concurrence is one for maximum entanglement, and vanishes for separable states.

We now find the two-qubit system density matrix. To simplify the presentation, let us first deal with the case $\lambda = 0$, that is, the two qubits are not directly interacting. To find the unitary time-evolution operator, we use a similar approach as before - we insert a completeness relation over the eigenstates of the H_B. The total time-evolution operator is

$$U(t) = \sum_n e^{-i\epsilon_n t/2} e^{-i\eta_n t} e^{-i(H_S^{(1)} + H_{SB}^{(1)})t} e^{-i(H_S^{(2)} + H_{SB}^{(2)})t} |n\rangle \langle n| , \tag{3.37}$$

with ϵ_n and η_n as defined before. Now

,

$$e^{-i(H_S^{(1)} + H_{SB}^{(1)})t} e^{-i(H_S^{(2)} + H_{SB}^{(2)})t} |n\rangle = e^{-iH_{s,n}^{(1)\text{eff}} t} e^{-iH_{s,n}^{(2)\text{eff}} t} |n\rangle , \tag{3.38}$$

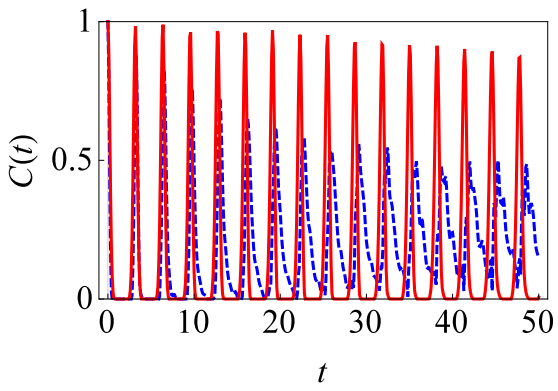

Figure 3.15: Same as Fig. 3.14, expect that now we have $\beta = 1$ and $g_i = 0.5$.

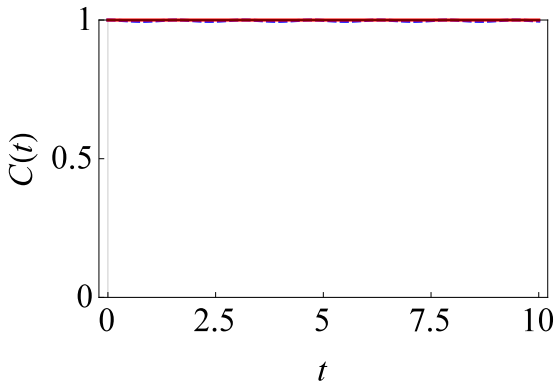

Figure 3.16: Same as Fig. 3.14, expect that now we have $\beta = 10$ and $g_i = 1$.

with $H_{s,n}^{(i)\text{eff}} = \frac{\zeta_{ni}}{2}\sigma_{zi} + \frac{\Delta_i}{2}\sigma_{xi}$, and $\zeta_{ni} = \varepsilon_i + G_n$ $(i = 1, 2)$. We then obtain

$$U(t) = \sum_{n=0}^{2^N-1} U_n^{(1)}(t) U_n^{(2)}(t) |n\rangle\langle n|, \tag{3.39}$$

where

$$U_n^{(i)}(t) = e^{-i\eta_n t/2} e^{-i\epsilon_n t/4} \left[\cos(\Omega_{ni} t) - \frac{i}{\Omega_{ni}} \sin(\Omega_{ni} t) \left(\frac{\zeta_{ni}}{2}\sigma_{zi} + \frac{\Delta_i}{2}\sigma_{xi} \right) \right], \tag{3.40}$$

and $\Omega_{ni}^2 = \frac{1}{4}(\zeta_{ni}^2 + \Delta_i^2)$. For the uncorrelated initial system-environment state [see Eq.

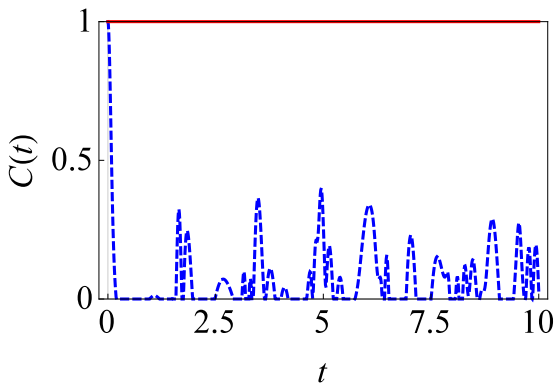

Figure 3.17: Same as Fig. 3.14, expect that now we have $\beta = 10$, $\varepsilon_i = 0.01$ and $g_i = 1$.

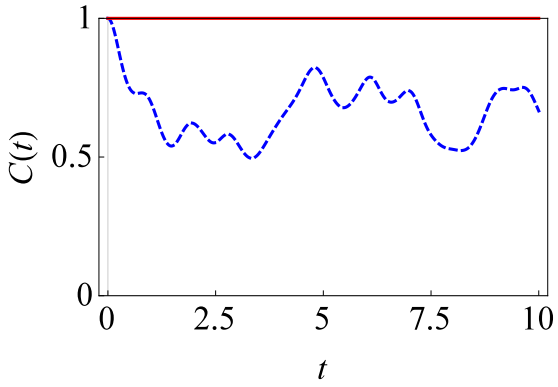

Figure 3.18: Same as Fig. 3.14, except that now we have $\varepsilon_i = 0.01$, $\chi_i = 0.1$, $g_i = 1$, $\beta = 10$ and $N = 10$.

(3.16)], it follows that

$$\rho_S(t) = \sum_{n=0}^{2^N-1} \frac{c_n}{Z_B} U_n^{(1)}(t) U_n^{(2)}(t) \left|\psi\right\rangle \left\langle\psi\right| U_n^{(2)\dagger} U_n^{(1)\dagger}, \tag{3.41}$$

with $Z_B = \sum_n c_n$. However, for correlated initial state of system and environment [see Eqs. (3.23) and (3.24)], we obtain

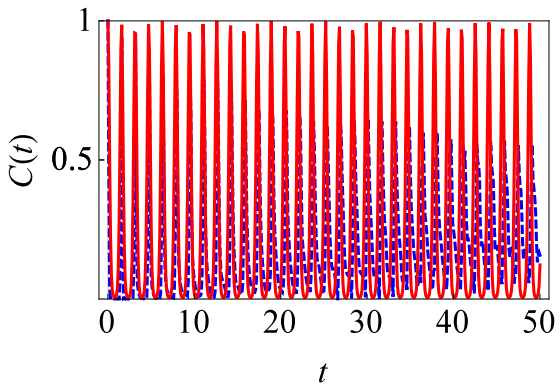

Figure 3.19: Same as Fig. 3.14, expect that now we have considered the interaction term λ between the two qubits of system with $\lambda = 3$, $\beta = 1$ and $g_i = 1$.

$$\rho_S(t) = \sum_{n=0}^{2^N-1} \frac{c_n A_n}{Z} U_n^{(1)}(t) U_n^{(2)}(t) \left|\psi\right\rangle \left\langle\psi\right| U_n^{(2)\dagger} U_n^{(1)\dagger}, \tag{3.42}$$

where $Z = \sum_n A_n c_n$, and $A_n = \langle\psi|A_n^{(1)} A_n^{(2)}|\psi\rangle$, with

$$A_n^{(i)} = \cosh(\beta\Omega_{ni}) - \frac{\sinh(\beta\Omega_{ni})}{\Omega_{ni}} \left[\frac{\zeta_{ni}}{2}\sigma_{zi} + \frac{\Delta_i}{2}\sigma_{xi}\right], \tag{3.43}$$

appearing due to the initial correlations.

With the two-qubit density matrix in hand, we can look at the behavior of entanglement with and without initial correlations and show that there can be considerable differences. Let us first look at weak coupling scenario. In this case, as expected, an initially entangled state largely loses its entanglement due to the interaction with the spin environment. As shown in Fig. 3.14, there is a small difference between the correlated and uncorrelated cases. However, with stronger coupling strength g_i, there can be a more significant difference in the entanglement dynamics due to initial correlations [see Fig. 3.15]. However, once again if we reduce the temperature further, the difference in the dynamics can disappear as shown

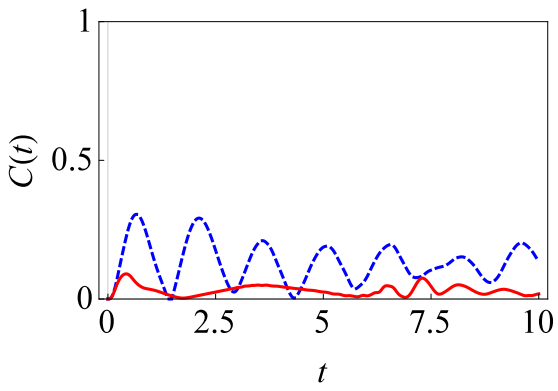

Figure 3.20: Graph of the birth of entanglement of two qubits $C(t)$ versus time t for relatively moderate system-environment coupling without initial correlations (dashed, blue line) and with initial correlations (solid, red line). We have set $\hbar = 1$, with $\lambda = 5$. Here we have $g_i = 0.5$, $\varepsilon_1 = 1$, $\varepsilon_2 = 2$, $\varepsilon_i = 1$, $\beta = 1$, $\Delta_1 = 4$, $\Delta_2 = 1$ and $N = 50$. The two qubits are initially in the product state $|\psi\rangle = |0_1 0_2\rangle$.

in Fig. 3.16. In fact, the concurrence is seen to remain very close to one. This is because the initial environment state in both scenarios is the same, namely, all spins down, and system-environment state remains (approximately) a product state. However, just like before, reducing the contribution of the environment Hamiltonian by decreasing the value of ε_i can restore this difference [see Fig. 3.17]. In fact, in this case, the uncorrelated initial state leads to repeated entanglement sudden death and birth, while with the correlated initial state, the entanglement remains largely intact. To further study evolution of central system, we can also consider interactions between environmental spins. For the uncorrelated initial state, the initial state of the environment at low temperatures will be all spins anti-aligned (assuming χ_i to be positive). For the correlated initial state, if g_i is dominant, then we expect that the environment state would be all spins aligned. Thus, we expect a difference in the entanglement dynamics in this regime. This is precisely what is illustrated in Fig. 3.18.

We now investigate the entanglement dynamics if the qubits are directly interacting with each other, that is, λ can now be non-zero. In this case, we have

$$U(t) = \sum_{n=0}^{2^N-1} U_n^{(12)}(t)|n\rangle\langle n|, \tag{3.44}$$

with

$$U_n^{(12)}(t) = e^{-i\eta_n t} e^{-i\epsilon_n t/2} e^{-i(H_{s,n}^{(1)\text{eff}} + H_{s,n}^{(2)\text{eff}} + H_{12})t}. \tag{3.45}$$

For the initially uncorrelated state [see Eq.(3.16)], the time-evolved reduced density matrix of the system is

$$\rho_S(t) = \frac{1}{Z_B} \sum_{n=0}^{2^N-1} c_n U_n^{(12)}(t) \, |\psi\rangle \, \langle\psi| \, U_n^{(12)\dagger}(t), \tag{3.46}$$

with $Z_B = \sum_n c_n$. For the initially correlated state, we get

$$\rho_S(t) = \frac{1}{Z} \sum_{n=0}^{2^N-1} c_n A_n U_n^{(12)}(t) \, |\psi\rangle \, \langle\psi| \, U_n^{(12)^\dagger}(t), \tag{3.47}$$

with

$$A_n = \langle\psi|e^{-\beta(H_{s,n}^{(1)\text{eff}} + H_{s,n}^{(2)\text{eff}} + H_{12})}|\psi\rangle, \tag{3.48}$$

and $Z = \sum_{n=0}^{2^N-1} c_n A_n$. For each n, we can calculate the 4×4 matrix $U_n^{(12)}$ numerically, and hence eventually the system density matrix. Once again, we can look at the entanglement dynamics due to initially uncorrelated and correlated system-environment states. Our central result - that there can be very significant differences between the dynamics due to the initial correlations - remains unchanged due to the presence of the qubit-qubit interaction [see Fig. 3.19]. For completeness, we also illustrate this difference in Fig. 3.20 for the case where initially two qubits are in a product state. In this case, it is clear that the generation of entanglement is also impacted by the initial correlations between central system and the surrounding environment.

3.3 Summary

In summary, we have solved the dynamics of a central two-level system interacting with a spin environment with and without initial system-environment correlations. For our model, both the diagonal and off-diagonal elements of the central spin density matrix evolve. We have found that as long as one remains in the high temperature and weak coupling regime, one can ignore any effect of initial correlations and system state preparation. On the contrary, for low temperatures and strong coupling strengths between central system and environment, the dynamics are substantially affected. However, surprisingly, this need not always be the case. We then extended our formalism to two spins, having interaction with a common spin environment to show that the entanglement dynamics can be affected by the initial correlations as well. Our results should lend very useful insights into the effect of the initial system-environment correlations.

Chapter 4

The quantum Zeno and anti-Zeno effects with non-selective projective measurements

This chapter is based on M. Majeed and A. Z. Chaudhry, The quantum Zeno and anti-Zeno effects with non-selective projective measurements, Sci. Rep. ***8****, 14887 (2018) [90, 102].*

The temporal evolution of a quantum system is slowed down when many repeated measurements are performed on a quantum system. This is known as quantum Zeno effect (QZE) [60]. On the other hand, a more ubiquitous phenomenon under realistic conditions is the opposite effect; this is the acceleration of the quantum state evolution via repeated measurements, and is known as quantum anti-Zeno effect (QAZE) [58, 82, 85]. Both the QZE and the QAZE have gained considerable attention [48, 56–59, 61–78, 80, 83, 84, 86, 87, 89–91, 102, 131–141] and studies have been performed by considering a variety of experimental setups such as trapped ions [131], cold atomic gas [83], nanomechanical oscillators [86], and superconducting qubits [141]. The general scenario - see, for example, Refs. [82–87, 132–136, 140] - is to prepare initially an excited state of the system. This excited state then decays [7] due to system's interaction with its surrounding environment. The idea is to repeatedly check via repeated projective measurements whether or not the system is still

in the excited state [60]. Each projective measurement prepares the initial state, and any other measurement result is rejected. This scenario can be generalized to go beyond such population decay models in the sense that dephasing can also be taken into account [56], and arbitrary system-environment models can be considered [57].

In this chapter [90, 102], we go beyond such selective projective measurements usually considered in the analysis of the QZE and the QAZE. First, we consider 'unsuccessful' measurements as well. In this case, we do read off the measurement results of the projective measurements, but we do not require the measurement results to correspond to the initial state for every measurement. Only the final measurement is required to do so. Second, rather than performing selective measurements, we can consider non-selective projective measurements where we do perform the measurements, but we do not read out the measurement results. Once again, only the final measurement is required to be a selective measurement corresponding to the initial state. A similar measurement strategy has been followed before to study the QZE and the QAZE for the case of a single harmonic oscillator interacting with an environment of harmonic oscillators [80] . For both of the above scenarios, the same final survival probability is obtained. In particular, we show that our expression for final survival probability reduces to expression obtained using the usual repeated selective projective measurement scheme if system-environment coupling is evaluated using only first-order time-dependent perturbation theory and higher-order terms are neglected. Our work is therefore a rare example of an investigation of QZE and QAZE beyond the weak system-environment coupling regime [58, 89]. As a consequence, the usual perturbative techniques cannot be used and we use exactly solvable models to analyze the effect of the non-selective projective measurements. We consider three such models. First, we consider a single two-level system undergoing dephasing via its interaction with an environment consisting of the harmonic oscillators [3, 124]. Second, we consider a single TLS [54, 55] interacting with many two-level systems. Third, we consider a large spin (or, equivalently, more than one TLS) interacting with harmonic oscillators environment [142] and undergoing dephasing. Using the final survival probability, we can define the effective decay rate in analogy with the usual studies of

QZE and QAZE [57, 58]. The behavior of effective decay rate allows us to examine the effect of non-selective measurements instead of the usual selective measurements [90, 102]. We show that the QZE and QAZE are considerably modified. In particular, the QZE and the QAZE effects now depend on the number of measurements performed. The effective decay rates are now reduced; moreover, the measurement rates corresponding to the crossover from the QZE regime to the QAZE regime and vice versa can also change.

4.1 Results

4.1.1 Background

Before presenting our results, it is useful to recap the basic theory [57]. The approach usually followed is that the system quantum state ρ_0 is prepared. The system then interacts with surrounding environment and evolves for time τ to state $\rho_0(\tau)$. A projective measurement is then performed at time τ in order to observe whether it is present in its initial state ρ_0. Let this probability be s_{00}. We also note that since we are concerned with the effect of the system-environment interaction only, the evolution due to free system Hamiltonian H_S is removed just before performing projective measurement by applying a suitable unitary operator on a very short timescale [56–59, 143]. The system state is then reset to ρ_0, and following another time interval τ, another measurement is performed. The probability that the system is still in the initial state ρ_0 is $S(M\tau) = s_{00}^M$ if system-environment correlation effects are neglected. We can then define an effective decay rate $\Gamma(\tau)$ via $S(M\tau) = e^{-\Gamma(\tau)M\tau}$ [57–59]. In this case, $\Gamma(\tau)$ is then found to be $-\frac{1}{\tau}\ln s_{00} = -\frac{1}{\tau}\ln(1 - s_{01})$, where s_{01} is the probability that the system, after a measurement, ends up in a state ρ_1 orthogonal to the initial state ρ_0. We emphasize that $\Gamma(\tau)$ is an effective decay rate which, in general, is not constant, thereby indicating non-exponential decay. For weak coupling strength between central system and environment, we expect transition probability s_{01} to be small, leading to $\Gamma(\tau) \approx s_{01}/\tau$. The probability s_{01} can then be calculated perturbatively to show that the effective decay rate is an overlap integral of spectral density of environment, and an

'effective' filter function that depends on measurements performed, measurement interval, and the system-environment model being considered [57, 58]. The effective decay rate $\Gamma(\tau)$ can then be plotted as a function of the measurement interval τ [144]. When $\Gamma(\tau)$ is an increasing function of τ, we are in the Zeno regime [56–59, 82, 133, 136], since in this case, shortening the measurement interval decreases effective decay rate; if the opposite is true, then we are in anti-Zeno regime.

4.1.2 The formalism

We now modify the scheme presented above to first take into account 'unsuccessful' measurement results as well. We no longer demand that every measurement result corresponds to the initial state. Intermediate measurement results can correspond to state(s) other than the initial state - these measurements are what we refer to as unsuccessful measurements. We keep track of the result of every measurement, and only the final measurement result should correspond to the initial state. For simplicity, we consider here the case of a two-level system - higher dimensional systems can be treated similarly as done later when we study large spin pure dephasing model. TLS is initially prepared in state ρ_0. We now perform repeated measurements on system with equal time interval τ, to check state of the quantum system. Just after each measurement, the state of the system could be ρ_0, or it could be the state ρ_1, which is orthogonal to ρ_0, due to the interaction of the system with its environment. Let s_{01} is transition probability that quantum system ends up in state ρ_1 if it started in state ρ_0. In a similar manner, we can define s_{10} (s_{11}) as the transition probability that the system ends up in state ρ_0 (ρ_1) if it started in state ρ_1. We are interested in what happens after M measurements; that is, what is probability that central system is still in state ρ_0 after M measurements? Calling this probability $S(M\tau)$, if we neglect any system-environment correlation effects, we can write

$$S(M\tau) = \sum_{i_1 i_2 \ldots i_{M-1}} s_{0 i_1} s_{i_1 i_2} s_{i_2 i_3} \ldots s_{i_{M-2} i_{M-1}} s_{i_{M-1} 0}. \tag{4.1}$$

This probability can be further evaluated using matrix multiplication (see the Methods subsection 4.3.1 at the end of this chapter). The final result is

$$S(M\tau) = \frac{s_{01}(1 - s_{01} - s_{10})^M + s_{10}}{s_{01} + s_{10}}. \tag{4.2}$$

This result is independent of the details of the system-environment model - the only assumption is that the system-environment coupling is not so strong that system-environment correlation effects become very significant [5, 6, 56]. This expression can also be cast in a more illuminating form. Noting that

$$(1 - s_{01} - s_{10})^M = 1 + \sum_{k=1}^{M} (-1)^k \binom{M}{k} (s_{01} + s_{10})^k, \tag{4.3}$$

we get

$$S(M\tau) = 1 - Ms_{01} + s_{01} \sum_{k=1}^{M-1} (-1)^{k+1} \binom{M}{k+1} (s_{01} + s_{10})^k. \tag{4.4}$$

We can perform simple checks on our results. We first set $s_{10} = 0$. Then it is obvious that $S(M\tau) = s_{00}^M$ in this case - once the system makes a transition to the state ρ_1, it cannot make a transition back to ρ_0. Eq. (4.2) reproduces this result, and, using

$$\sum_{k=1}^{M-1} (-1)^{k+1} \binom{M}{k+1} s_{01}^k = \frac{Ms_{01} + (1 - s_{01})^M - 1}{s_{01}}, \tag{4.5}$$

so does Eq. (4.4). Furthermore, for $M = 2$, it is obvious that we should get $S = s_{00}^2 + s_{01}s_{10} = 1 - 2s_{01} + s_{01}(s_{01} + s_{10})$. One can check that we get the same result using Eqs. (4.2) and (4.4). We should also point out that as $\tau \to 0$, we expect that the transition probability $s_{01} \to 0$, leading to $S(M\tau) \to 1$. This is the quantum Zeno effect beyond the simple repeated selective projective measurement case.

Let us now consider non-selective projective measurements where, after every time interval τ, we perform a projective measurement on the system as before, but now we do not

read the measurement results. We know from measurement theory that if the state just before the measurement is ρ, then the state just after the measurement is $\rho' = \sum_i P_i \rho P_i$, where P_i are the projection operators onto the eigenstates of the observable being measured [9, 105, 145]. It follows that if the initial state is ρ_0, the system state just after the first non-selective measurement is $\sum_{i_1} s_{0i_1}\rho_{i_1}$. The state just after the second non-selective measurement is $\sum_{i_1 i_2} s_{0i_1}s_{i_1 i_2}\rho_{i_2}$. Similarly, just after $M-1$ non-selective measurements, the state of the system is $\sum_{i_1 i_2 \ldots i_{M-1}} s_{0i_1}s_{i_1 i_2}s_{i_2 i_3}\ldots s_{i_{M-2}i_{M-1}}\rho_{i_{M-1}}$. The probability that a final selective measurement leads to ρ_0 is then

$$S(M\tau) = \sum_{i_1 i_2 \ldots i_{M-1}} s_{0i_1}s_{i_1 i_2}s_{i_2 i_3}\ldots s_{i_{M-2}i_{M-1}}s_{i_{M-1}0}, \tag{4.6}$$

which is the same as Eq. (4.1). Thus, if we do not read off the measurement results, we obtain exactly the same results as before for the effective decay rate. Whether or not we read the measurement results makes no difference. Let us also comment that the final survival probability as given in Eq. (4.1) can be considered as the sum over all possible 'histories' of going from the state ρ_0 to state ρ_0 [146, 147]. Moreover, if Eq. (4.1) is cast in terms of probability amplitudes instead of probabilities with only one non-selective projective measurement, then it essentially reduces to the Ersak equation that is used to explain non-exponential decay [148–150]. Variants of Eq. (4.1) have also been considered under the guise of quantum recurrence and the quantum first detection problem [151–154].

We now illustrate the effect of repeated non-selective projective measurements using our formalism. Before doing so, however, it is useful to note that Eq. (4.4) shows dependence of total survival probability on the coupling strength of system-environment in a very transparent manner. Suppose that coupling between system and its environment is very weak. Then s_{01} and s_{10} are very small and can be calculated using first order time-dependent perturbation theory. It follows that $S(M\tau) \approx 1 - Ms_{01}$, which corresponds to $\Gamma(\tau) = s_{01}/\tau$. This is the usual result for decay rate of central system in weak coupling regime [57]. Thus, non-selective projective measurements only influence the total survival probability $S(M\tau)$

if we go beyond simple first-order perturbation theory. Consequently, we now illustrate the effect of considering unsuccessful measurements using exactly solvable models where we can calculate s_{01} and s_{10} exactly in regimes beyond the applicability of first order perturbation theory.

4.1.3 Single spin pure dephasing model

We first study a single spin-1/2 particle interacting with a harmonic oscillator environment. The total Hamiltonian is (with $\hbar = 1$ throughout) [3, 5, 6]

$$H = H_S + H_B + H_{SB}, \tag{4.7}$$

where H_S and H_B are the self-Hamiltonians of the central system and the environment respectively

$$H_S = \frac{\omega_0}{2}\sigma_z, \tag{4.8}$$

$$H_B = \sum_k \omega_k b_k^\dagger b_k, \tag{4.9}$$

with H_{SB} is the interaction term between system and its environment [5, 6]

$$H_{SB} = \frac{\sigma_z}{2}\sum_k (g_k^* b_k + g_k b_k^\dagger). \tag{4.10}$$

Here ω_0 is the energy-level spacing of the two-level system, and ω_k denotes the frequency of k^{th} harmonic oscillator, while b_k ($b_k^\dagger$) are its annihilation(creation) operators, with g_k the coupling parameter between central spin system and environment oscillators. An important feature of this model is that only the off-diagonal elements of the system density matrix (in the σ_z eigenbasis) change in time [9].

Consider the initial state of TLS to be $|\psi_0\rangle = \cos\left(\frac{\theta}{2}\right)|e\rangle + e^{i\phi}\sin\left(\frac{\theta}{2}\right)|g\rangle$ with $\langle e|g\rangle = 0$. The states $|g\rangle$ (and $|e\rangle$) are ground (and excited) states of the spin-1/2 particle, and ϕ and θ are parameters characterizing the initial state $|\psi_0\rangle$. The state orthogonal to this state is $|\psi_1\rangle = \sin\left(\frac{\theta}{2}\right)|e\rangle - e^{i\phi}\cos\left(\frac{\theta}{2}\right)|g\rangle$. At time intervals τ, non-selective projective measurements in the basis $\{|\psi_0\rangle, |\psi_1\rangle\}$ are performed on the state of central system. If the state of system is $\rho_0 = |\psi_0\rangle\langle\psi_0|$, the probability that the system ends up in state $\rho_1 = |\psi_1\rangle\langle\psi_1|$ a time interval τ later (after removal of evolution due to H_S) is (see the Methods subsection 4.3.2 at the end of this chapter) [57]

$$s_{01} = \frac{1}{2}\sin^2\theta(1 - e^{-\gamma(\tau)}). \tag{4.11}$$

Here $\gamma(\tau) = 2\sum_k \frac{|g_k|^2}{\omega_k^2}\coth(\beta\omega_k/2)\sin^2(\omega_k\tau/2)$ describes environment-induced dephasing between the states $|e\rangle$ and $|g\rangle$ of σ_z operator. For an environment consisting of continuous modes, we replace the discrete sum ω_k with an integral via $\sum_k |g_k|^2(\ldots) \to \int_0^\infty d\omega\, J(\omega)(\ldots)$ [3, 90, 102]. Throughout, we will use an Ohmic spectral density $J(\omega) = G\omega e^{-\omega/\omega_c}$ with an exponential cutoff to illustrate our results, where ω_c is the cutoff frequency, and G is a measure of effective coupling strength between system and its environment [5, 6]. We have also assumed that the initial state of system and environment is $\rho_0 \otimes \rho_B$, with $\rho_B = e^{-\beta H_B}/Z_B$ and $Z_B = \mathrm{Tr}[e^{-\beta H_B}]$ [90, 102].

In a similar manner, we find that if system state is ρ_1, the probability that after τ time interval, system state is found to be ρ_0 is

$$s_{10} = \frac{1}{2}\sin^2\theta(1 - e^{-\gamma(\tau)}). \tag{4.12}$$

Thus, in this case, the transition probabilities are the same. Let us denote $s_{01} = s_{10} = s$. Using Eq. (4.2) gives the following form of survival probability

$$S(M\tau) = \frac{1}{2}\left[1 + (1 - 2s)^M\right]. \tag{4.13}$$

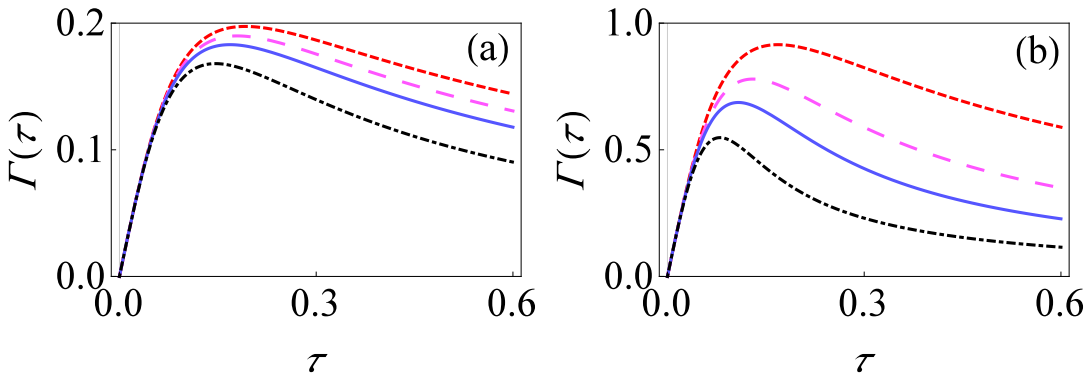

Figure 4.1: (a) Behavior of the effective decay rate $\Gamma(\tau)$ for the initial state of the central spin ψ_0 with only selective measurements (small-dashed, red curve), and with non-selective projective measurements with $M = 3$ (large-dashed, magenta curve), $M = 5$ (solid, blue curve) and $M = 10$ (dot-dashed, black curve) for single spin pure dephasing model. We use dimensionless units with $\hbar = 1$; the remaining parameters are set to $\phi = 0$, $\theta = \pi/2$, $\omega_0 = 1$, $\beta = 10$, $\omega_c = 10$ and $G = 0.1$. (b) Same as (a), except that now $G = 0.5$.

The corresponding effective decay rate of central TLS is

$$\Gamma(\tau) = -\frac{1}{M\tau} \ln \left\{ \frac{1}{2} \left[1 + [1 - \sin^2 \theta (1 - e^{-\gamma(\tau)})]^M \right] \right\}. \tag{4.14}$$

This expression should be compared with that obtained by performing only selective measurements. In the latter case, we simply have

$$\Gamma(\tau) = -\frac{1}{\tau} \ln[1 - \frac{1}{2} \sin^2 \theta (1 - e^{-\gamma(\tau)})]. \tag{4.15}$$

In Fig. 4.1, following Refs. [57, 58], we show the behavior of the effective decay rate $\Gamma(\tau)$ with weak [Fig. 4.1(a)] and relatively strong [Fig. 4.1(b)] system-environment coupling strength G at low temperatures. Similar to Refs. [57, 58, 155], it is clear that we the quantum Zeno and anti-Zeno regimes are both observed. For smaller values of τ, the effective decay rate de-

creases as the measurement interval is reduced, meaning that, shorter measurement intervals τ help to protect state of quantum system, thus indicating quantum Zeno regime. However, for larger values of measurement interval, the opposite situation takes place, namely, effective decay rate enhances as τ reduces, hence showing anti-Zeno regime for both selective and non-selective projective measurements. Furthermore, especially with relatively strong system-environment coupling, only three measurements can bring out a significant difference between performing non-selective measurements and performing only selective measurements (compare the small-dashed, red curve with the large-dashed, magenta curve). We notice that as we increase the number of non-selective measurements, $\Gamma(\tau)$ reduces. The value of τ for which we make a transition from the Zeno regime to the anti-Zeno regime also shifts to a lower value. These trends become more prominent with stronger system-environment coupling [compare Figs. 4.1(a) and (b)].

4.1.4 Spin interacting with spin environment

We now consider a single TLS interacting with an environment of N other spin-1/2 particles [9, 54]. Our total Hamiltonian is now written as[1]

$$H = H_S + H_B + H_{SB}, \tag{4.16}$$

where the first term is the central spin Hamiltonian is

$$H_S = \frac{\varepsilon}{2}\sigma_z + \frac{\Delta}{2}\sigma_x, \tag{4.17}$$

the second term is the environment Hamiltonian H_B is

$$H_B = \sum_{i=1}^{N} \frac{\varepsilon_i}{2}\sigma_z^{(i)}, \tag{4.18}$$

[1]Same form of total Hamiltonian was considered before in chapter 3 except that now interaction term χ_i is zero.

while the third term is the system-environment interaction Hamiltonian

$$H_{SB} = \frac{\sigma_z}{2} \otimes \sum_{i=1}^{N} g_i \sigma_z^{(i)}. \tag{4.19}$$

Here Δ and ε represent the tunneling amplitude and the energy spacing of the central spin system respectively, σ_k $(k = x, y, z)$ are usual Pauli spin operators as before, ε_i is energy spacing in case of i^{th} environmental spin, and g_i characterizes the interaction strength between the central spin system, and i^{th} environmental spin. In the previous chapter, we have already worked out the dynamics with this system-environment model. We then find the probability that, starting from the state $\rho_0 = \frac{1}{2}(1 + \sigma_x)$, after time τ we find the state $\rho_1 = \frac{1}{2}(1 - \sigma_x)$ is

$$s_{01}(\tau) = \frac{1}{2}\left[1 - p_x(\tau)n_x(\tau) - p_y(\tau)n_y(\tau) - p_z(\tau)n_z(\tau)\right], \tag{4.20}$$

where

$$\begin{aligned}
p_x(\tau) &= \frac{1}{Z_B} \sum_n \frac{c_n}{4\Omega_n^2} (\zeta_n^2 \cos(2\Omega_n t) + \Delta^2), \\
p_y(\tau) &= \frac{1}{Z_B} \sum_n \frac{c_n}{2\Omega_n} \zeta_n \sin(2\Omega_n t), \\
p_z(\tau) &= \frac{1}{Z_B} \sum_n \frac{c_n}{2\Omega_n^2} \Delta\zeta_n \sin^2(\Omega_n t),
\end{aligned} \tag{4.21}$$

and

$$\begin{aligned}
n_x(\tau) &= [\cos^2(\Omega\tau) + \frac{\sin^2(\Omega\tau)}{4\Omega^2}(\Delta^2 - \varepsilon^2)], \\
n_y(\tau) &= \frac{\varepsilon}{\Omega} \sin(\Omega\tau)\cos(\Omega\tau), \\
n_z(\tau) &= \frac{\varepsilon\Delta}{2} \frac{\sin^2(\Omega\tau)}{\Omega^2}.
\end{aligned} \tag{4.22}$$

Here $c_n = e^{-\beta\epsilon_n/2}$ with $\epsilon_n = \sum_{i=1}^{N}(-1)^{n_i}\varepsilon_i$, $Z_B = \sum_n c_n$, $\zeta_n = \varepsilon + G_n$ with $G_n = \sum_{i=1}^{N}(-1)^{n_i}g_i$, $\Omega_n^2 = \frac{1}{4}(\zeta_n^2 + \Delta^2)$ and $\Omega^2 = \frac{1}{4}(\varepsilon^2 + \Delta^2)$. We also find that $s_{01} = s_{10}$. Consequently, denoting $s_{01} = s$ and using Eq. (4.2), we get

$$S(M\tau) = \frac{1}{2}[1 + (1-2s)^M], \tag{4.23}$$

leading to following form of effective decay rate [90, 102]

$$\Gamma(\tau) = -\frac{1}{M\tau}\ln\left\{\frac{1}{2}[1 + (p_x(\tau)n_x(\tau) + p_y(\tau)n_y(\tau) + p_z(\tau)n_z(\tau))^M]\right\}. \tag{4.24}$$

This result should be compared with repeated selective measurements where $\Gamma(\tau)$ is independent of number of measurements and is written as

$$\Gamma(\tau) = -\frac{1}{\tau}\ln\{\frac{1}{2}[1 + (p_x(\tau)n_x(\tau) + p_y(\tau)n_y(\tau) + p_z(\tau)n_z(\tau))]\}. \tag{4.25}$$

In Fig. 4.2, the effective decay rate $\Gamma(\tau)$ has been plotted as a function of the measurement interval τ with different values of system and environment parameters, again at very low temperatures. The small-dashed red curve is decay rate of central system if we perform only selective measurements, while with non-selective projective measurements, the large-dashed magenta curve is the decay rate for $M = 3$, the solid blue curve is the decay rate for $M = 5$, and the dot-dashed black curve is the decay rate for $M = 10$. Let us first focus on the inset of Fig. 4.2. As mentioned before, for very weak system-environment coupling, s_{01} and s_{10} approach to zero; consequently, the decay rate of central system will be $\Gamma(\tau) \approx -\frac{1}{\tau}s_{10}$, independent of number of measurements. Thus, both selective and non-selective measurements lead to the same effective decay rate in such a case, independent of the number of measurements. This is precisely the case in the inset where the curves overlap. However,

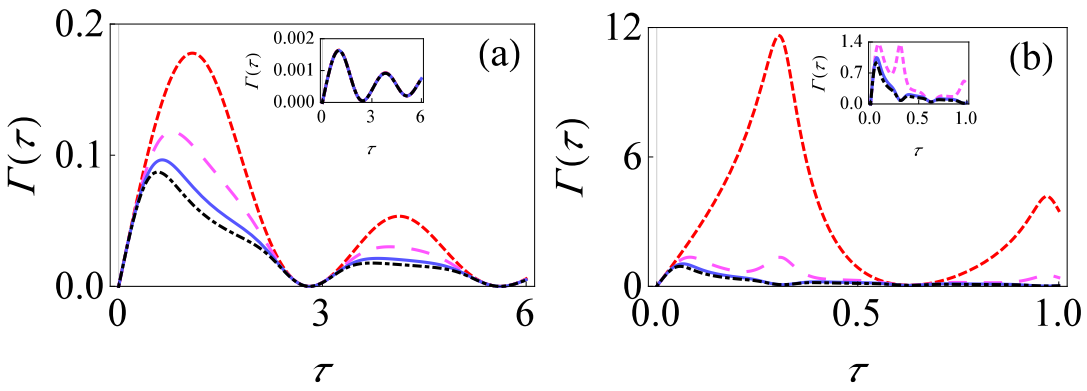

Figure 4.2: (a) Behavior of $\Gamma(\tau)$ versus τ for initial state of central system ψ_0 with $M = 1$ (small-dashed, red curve), $M = 3$ (large-dashed, magenta curve), $M = 5$ (solid, blue curve) and $M = 10$ (dot-dashed, black curve) for the spin environment. We use dimensionless units so that $\hbar = 1$. For simplicity, level spacing ε_i and coupling strength g_i are chosen to have the same value for every environment. Here, we have set $\phi = 0$, $\theta = \pi/2$, $\varepsilon = 1$, $\Delta = 2$, $\beta = 10$, $\varepsilon_i = 1$, $g_i = 0.01$ and the number of environmental spins is considered to be $N = 100$. The inset shows the effective decay rate with the same system-environment parameters, except that now $g_i = 0.001$). (b) Same as (a), except that now $g_i = 0.1$, with zoomed-up inset plot.

with stronger system-environment coupling strength, higher-order terms in Eq. (4.4) also contribute, making the effective decay rate different for the selective and the non-selective cases. This is illustrated in the main figure of Fig. 4.2(a). With both selective and non-selective projective measurements, there exist clear and well-defined multiple quantum Zeno and the anti-Zeno regimes, that is, sometimes decay rate decreases by decreasing the measurements interval τ (meaning that we are in quantum Zeno regime), while sometimes it enhanced by decreasing the τ (meaning that we are in anti-Zeno regime). For repeated non-selective projective measurements, we clearly see that once again $\Gamma(\tau)$ is lower compared to only selective measurements, and the decay rate further reduces as the number of measurements is increased. Moreover, as before in our study of the single spin pure dephasing model, the peak value of $\Gamma(\tau)$ is shifted to smaller values of the τ. With even stronger g_i,

these differences become even more pronounced, as illustrated in Fig. 4.2(b). Consequently, the differences in the effective decay rates translate to very significant differences in the final survival probabilities.

4.1.5 Large spin pure dephasing model

To further illustrate our formalism, we now consider a scenario beyond a simple two-level system. We consider in particular a spin $J = 1$ particle interacting with harmonic oscillator environment [56]. Such a model can describe the physics of two spin-1/2 particles which are interacting with a common environment of harmonic oscillators [90, 102]. The total Hamiltonian is now written as

$$H = H_S + H_B + H_{SB}, \tag{4.26}$$

with

$$H_S = \omega_0 J_z, \tag{4.27}$$

$$H_B = \sum_k \omega_k b_k^\dagger b_k, \tag{4.28}$$

$$H_{SB} = J_z \sum_k (g_k^* b_k + g_k b_k^\dagger), \tag{4.29}$$

where J_z is the usual angular momentum operator[2] and the remaining parameters are described as before. For the simplicity of presentation, let us suppose that we repeatedly measure the operator J_x. The initial system state that we prepare is the eigenstate of J_x, with eigenvalue +1. Written in the standard J_z eigenbasis, this state is

[2]This is equal to half of the sum of all the σ_z Pauli spin matrices.

$$\rho_0 = \frac{1}{4}\begin{pmatrix} 1 & \sqrt{2} & 1 \\ \sqrt{2} & 2 & \sqrt{2} \\ 1 & \sqrt{2} & 1 \end{pmatrix}. \tag{4.30}$$

The other two orthogonal eigenstates of J_x are

$$\rho_1 = \frac{1}{2}\begin{pmatrix} 1 & 0 & -1 \\ 0 & 0 & 0 \\ -1 & 0 & 1 \end{pmatrix}, \tag{4.31}$$

and

$$\rho_2 = \frac{1}{4}\begin{pmatrix} 1 & -\sqrt{2} & 1 \\ -\sqrt{2} & 2 & -\sqrt{2} \\ 1 & -\sqrt{2} & 1 \end{pmatrix}. \tag{4.32}$$

Knowing the Hamiltonian, we can work out density matrix of central system at any time exactly. Assuming that the initial system-environment state is $\rho_S(0) \otimes e^{-\beta H_B}/Z_B$ [5, 6], the result, written in the J_z eigenbasis after the removal of the evolution due to H_S, is (see the Methods subsection 4.3.2)

$$[\rho_S(\tau)]_{lm} = [\rho_S(0)]_{lm} e^{-i\delta(\tau)(l^2-m^2)} e^{-\gamma(\tau)(l-m)^2}.$$

Here $\gamma(\tau)$ is decoherence factor [3] defined before, and $\delta(\tau) = \sum_k \mid g_k \mid^2 (\sin(\omega_k\tau) - \omega_k\tau)/\omega_k^2$ describes indirect interaction [142] between two two-level systems due to the common environment. It is then simple to work out that[3]

$$s_{01} = \frac{1}{4}\left[1 - e^{-4\gamma(\tau)}\right] = s_{10} = s_{12} = s_{21}, \tag{4.33}$$

and

$$s_{02} = \frac{1}{8}\left[3 + e^{-4\gamma(\tau)} - 4\cos[\delta(\tau)]e^{-\gamma(\tau)}\right] = s_{20}. \tag{4.34}$$

[3]Here again, we consider continuum limit of oscillator modes, so summations over different k modes of the environment can be replaced by the integral via $|g_k|^2(...) \to \int_0^\infty d\omega J(\omega)(...)$. $J(\omega)$ is taken to be an Ohmic spectral density.

Our objective is to now evaluate Eq. (4.1) in this case. The result is

$$S(M\tau) = \frac{1}{6}\left[2 + (1 - 3s_{01})^M + 3(1 - s_{01} - 2s_{02})^M\right], \tag{4.35}$$

leading to the decay rate

$$\Gamma(\tau) = -\frac{1}{M\tau}\ln\left\{\frac{1}{6}\left[2 + \frac{1}{4^M}(1 + 3e^{-4\gamma(\tau)})^M + 3(\cos[\delta(\tau)]e^{-\gamma(\tau)})^M\right]\right\}. \tag{4.36}$$

In contrast, for selective measurements we have

$$\Gamma(\tau) = -\frac{1}{\tau}\ln\left[\frac{1}{8}(3 + 4e^{-4\gamma(\tau)} + 4\cos[\delta(\tau)]e^{-\gamma(\tau)})\right]. \tag{4.37}$$

The key difference now is the $\delta(\tau)$ term that describes the effect of the indirect interaction between the spins. The effective decay rate has been plotted in Fig. 4.3. If we perform selective measurements with relatively weak coupling strength G, it is clear that we observe distinct Zeno and anti-Zeno regimes [see Fig. 4.3(a)]. Comparing with the single spin case, we note that the indirect interaction between the spins is responsible for the multiple Zeno and the anti-Zeno transitions [90, 102]. However, with the non-selective projective measurements, we largely observe one Zeno regime and one anti-Zeno regime. This is because non-selective measurements lead to a lowering of the effective decay rate, and the measurement interval at which the peak effective decay rate occurs shifts to lower values as well. However, for smaller values of τ, the indirect interaction plays a relatively smaller role - we find that $\delta(\tau) \to 0$ as $\tau \to 0$. On the contrary, for stronger G as illustrated in Fig. 4.3(b), the decoherence factor $\gamma(\tau)$ plays a more dominant role as compared to the indirect interaction $\delta(\tau)$. Consequently, there are now less clear cut multiple Zeno and anti-Zeno regimes.

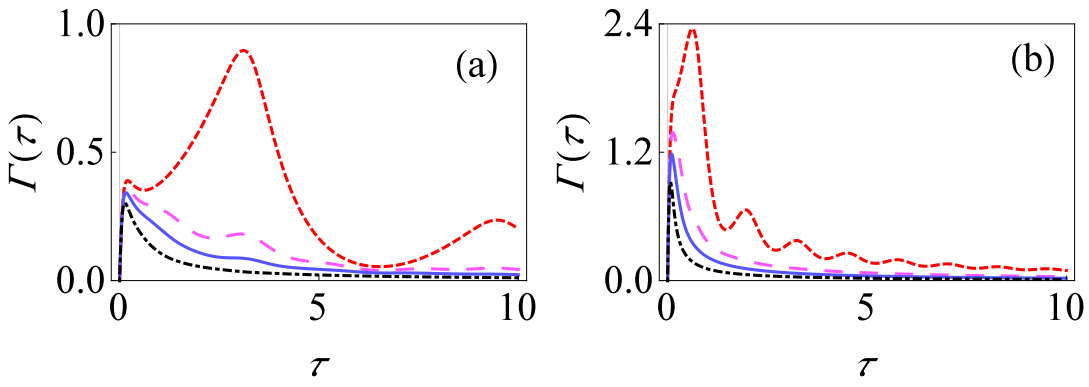

Figure 4.3: (a) Behavior of $\Gamma(\tau)$ versus τ starting from the state ρ_0 (spin up in the x direction) with only selective measurements (small-dashed, red curve), and using non-selective projective measurements with $M = 3$ (large-dashed, magenta curve), $M = 5$ (solid, blue curve) and $M = 10$ (dot-dashed, black curve) for the large spin pure dephasing model with $J = 1$. Here we have set $\omega_0 = 1$, $\beta = 10$, $\omega_c = 10$ and $G = 0.1$. (b) Same as (a), except that now $G = 0.5$.

4.2 Summary

In summary, we have generalized the treatment of QZE and QAZE by considering non-selective projective measurements. A general formalism for calculating the decay rate of a quantum state subjected to repeated non-selective measurements has been worked out. Importantly, we have shown that non-selective measurements lead to a different effective decay rate as compared to the usual strategy of using only selective measurements if we go beyond weak coupling regime between central system and environment [90, 102]. To illustrate our formalism, we also worked out the effective decay rate for the three exactly solvable system-environment models. These included a single spin interacting with a harmonic oscillator environment, a single spin interacting with a spin environment, and two spins interacting with a harmonic oscillator environment. Using these exactly solvable models, we found that non-selective projective measurements can qualitatively alter the analysis of the quantum Zeno and anti-Zeno effects [90, 102]. In particular, non-selective measurements considerably reduce the effective decay rate, and the transition from Zeno to anti-Zeno regimes (and vice

versa) is also altered. Our results should be important for a better understanding of the role played by repeated measurements when we go beyond the weak system-environment coupling regime.

4.3 Methods

4.3.1 Finding the final survival probability

To evaluate Eq. (4.1), we can employ matrix multiplication. Define the matrix $\mathcal{S}$ as

$$\mathcal{S} = \begin{pmatrix} 1 - s_{01} & s_{01} \\ s_{10} & 1 - s_{10} \end{pmatrix}. \tag{4.38}$$

Then it is straightforward to see that $S(M\tau) = [\mathcal{S}^M]_{00}$, that is, $S(M\tau)$ is simply the top-left element of the matrix $\mathcal{S}^M$. Our problem is then to $\mathcal{S}^M$. This can be done via diagonalization. Define $D = U^{-1}\mathcal{S}U$, where D is a diagonal matrix. Then,

$$D = \begin{pmatrix} 1 & 0 \\ 0 & 1 - s_{01} - s_{10} \end{pmatrix}, \tag{4.39}$$

$$U = \begin{pmatrix} 1 & -\frac{s_{01}}{s_{10}} \\ 1 & 1 \end{pmatrix}, \tag{4.40}$$

$$U^{-1} = \frac{1}{s_{01} + s_{10}} \begin{pmatrix} s_{10} & s_{01} \\ -s_{10} & s_{10} \end{pmatrix}, \tag{4.41}$$

and $\mathcal{S}^M = UD^MU^{-1}$ is

$$\mathcal{S}^M = \begin{pmatrix} \frac{s_{01}(1 - s_{01} - s_{10})^M + s_{10}}{s_{01} + s_{10}} & \frac{s_{01} - s_{01}(1 - s_{01} - s_{10})^M}{s_{01} + s_{01}} \\ \frac{s_{10} - s_{10}(1 - s_{01} - s_{10})^M}{s_{01} + s_{01}} & \frac{s_{01} + s_{10}(1 - s_{01} - s_{10})^M}{s_{01} + s_{01}} \end{pmatrix}. \tag{4.42}$$

Consequently, we can read off that $S(M\tau)$ is as given in Eq. (4.2).

A very similar method can be employed for a higher dimensional system. Consider, for example, a three-dimensional system as is the case for the large spin pure-dephasing model [5, 6, 44]. In this case, we construct

$$\mathcal{S} = \begin{pmatrix} 1 - s_{01} - s_{02} & s_{01} & s_{02} \\ s_{10} & 1 - s_{10} - s_{12} & s_{12} \\ s_{20} & s_{21} & 1 - s_{20} - s_{21} \end{pmatrix}. \tag{4.43}$$

Then, once again, $S(M\tau)$ is simply the top-left element of the matrix $\mathcal{S}^M$. Again, the task is to simply diagonalize $\mathcal{S}$. However, in this case, the algebra is much more cumbersome for the general case. Fortunately, for the pure dephasing model, $s_{01} = s_{10} = s_{12} = s_{21}$, and $s_{20} = s_{02}$, which leads to great simplifications. In this case, following the same method as above,

$$D = \begin{pmatrix} 1 & 0 & 0 \\ 0 & 1 - 3s_{01} & 0 \\ 0 & 0 & 1 - s_{01} - 2s_{02} \end{pmatrix}, \tag{4.44}$$

$$U = \begin{pmatrix} 1 & 1 & -1 \\ 1 & -2 & 0 \\ 1 & 1 & 1 \end{pmatrix}, \tag{4.45}$$

$$U^{-1} = \frac{1}{6} \begin{pmatrix} 2 & 2 & 2 \\ 1 & -1 & 2 \\ -3 & 0 & 3 \end{pmatrix}, \tag{4.46}$$

and the top-left element of $\mathcal{S}^M = UD^MU^{-1}$ is then given by Eq. (4.35).

4.3.2 Derivation of the spin density matrix with harmonic oscillator environment

Let us now explain how to find system density matrix with total system-environment Hamiltonian H given in Eq. (4.26). The single spin density matrix can then be found by simply setting the spin size to 1/2. Our first goal is to find the total unitary time-evolution operator $U(\tau)$ [5, 6, 124]. To this end, it is useful to first write $U(\tau) = U_F(\tau)U_I(\tau)$, where $U_F(\tau) = e^{-i(H_S+H_B)\tau}$ is free unitary time-evolution operator and $U_I(\tau)$ is the unitary operator due to system-environment interaction [2, 5, 6]. One can then show, using the Magnus expansion [156] that

$$U_I(\tau) = \exp\left[\sum_{j=1}^{\infty} A_j(\tau)\right], \tag{4.47}$$

The first term $A_1(\tau)$ of Magnus series is [5, 6, 124]

$$-i\int_0^\tau dt_1 H_I(t_1) = J_z\sum_k (a_k^\dagger \alpha_k(\tau) - a\alpha_k^*(\tau)), \tag{4.48}$$

where $H_I(t) = U_F^\dagger(t)H_{SB}U_F(t)$ is the interaction Hamiltonian in interaction frame and, similarly second term $A_2(\tau)$ is

$$-1/2\int_0^\tau dt_1 \int_0^{t_1} dt_2[H_I(t_1)H_I(t_2) - H_I(t_2)H_I(t_1)] = -iJ_z^2\delta(\tau), \tag{4.49}$$

where

$$\alpha_k(\tau) = g_k(1 - e^{i\omega_k\tau})/\omega_k, \tag{4.50}$$

and

$$\delta(\tau) = \sum_k |g_k|^2(\sin(\omega_k\tau) - \omega_k\tau)/\omega_k^2. \tag{4.51}$$

As this a constant number, so all other higher order terms are equal to zero in the Magnus

expansion, and the exact total unitary time-evolution operator is [5, 6]

$$U(\tau) = e^{-iH_B\tau}e^{-i\omega_0 J_z\tau}U_I(\tau), \tag{4.52}$$

where

$$U_I(\tau) = \exp[J_z\sum_k(b_k^\dagger\alpha_k(\tau) - b_k\alpha_k^*(\tau)) - iJ_z^2\delta(\tau)]. \tag{4.53}$$

$b_k^\dagger\alpha_k(\tau) - b_k\alpha_k^*(\tau)$ is the coherent state generator with $\alpha_k^*(\tau)$ is the coherent amplitude. The reduced density matrix of the central system $\rho_S(\tau)$ in terms of J_z eigenbasis is [5, 6]

$$[\rho_S(\tau)]_{lm} = \mathrm{Tr}_{S,B}[\rho_{\mathrm{tot}}(\tau)P_{lm}]. \tag{4.54}$$

Here $P_{lm} = |l\rangle\langle m|$, where $|l\rangle$ is the eigenstate of operator J_z with eigenvalue l. Assuming an initially uncorrelated system-environment state with the environment in thermal equilibrium, that is, $\rho_{\mathrm{tot}}(0) = \rho_S(0)\otimes\rho_B$ with $\rho_B = e^{-\beta H_B}/Z_B$ and $Z_B = \mathrm{Tr}[e^{-\beta H_B}]$, we obtain

$$[\rho_S(\tau)]_{lm} = [\rho_S(0)]_{lm}e^{-i\omega_0\tau(l-m)}e^{-i\delta(\tau)(l^2-m^2)}\left\langle e^{-R_{lm}(\tau)}\right\rangle, \tag{4.55}$$

with

$$R_{lm}(\tau) = (l-m)\sum_k[b_k^\dagger\alpha_k(\tau) - b_k\alpha_k^*(\tau)], \tag{4.56}$$

and $\mathrm{Tr}_B[e^{-R_{lm}(\tau)}\rho_B] = \left\langle e^{-R_{lm}(\tau)}\right\rangle$ is average over the thermal states of the bath in equilibrium [56]. For independent harmonic oscillator modes, we can write [5, 6, 56]

$$\left\langle e^{-R_{lm}(\tau)}\right\rangle = \prod_k\left\langle e^{-(l-m)\sum_k(a_k^\dagger\alpha_k(\tau) - a\alpha_k^*(\tau))}\right\rangle. \tag{4.57}$$

For an operator C, which is the linear combination of annihilation and creation operators, we have $\left\langle e^C\right\rangle = e^{\langle C\rangle^2/2}$. Using this identity and definition of $\alpha(\tau)$, this average is found to be

$$\mathrm{Tr}_B[e^{-R_{lm}(\tau)}\rho_B] = \exp[-\sum_k(l-m)^2|g_k|^2(1-\cos(\omega_k\tau))\coth(\beta\omega_k/2)/\omega_k^2]. \tag{4.58}$$

Consequently, all in all, we have

$$[\rho_S(\tau)]_{lm} = [\rho_S(0)]_{lm} e^{-i\omega_0 \tau (l-m)} e^{-i\delta(\tau)(l^2-m^2)} e^{-\gamma(\tau)(l-m)^2}, \tag{4.59}$$

where

$$\gamma(\tau) = 2 \sum_k |g_k|^2 \coth(\beta\omega_k/2) \sin^2(\omega_k \tau/2)/\omega_k^2. \tag{4.60}$$

We are really interested in finding the transition probabilities. Suppose that the initial system state is ρ_0. Then the probability that a measurement at time τ yields the state ρ_1 (after removal of the evolution due to H_S) is

$$s_{01} = \sum_{lm} e^{-i\delta(\tau)(l^2-m^2)} e^{-\gamma(\tau)(l-m)^2} [\rho_0]_{lm} [\rho_1]_{ml}. \tag{4.61}$$

Other survival probabilities can be calculated in an analogous manner.

Chapter 5

The quantum Zeno and anti-Zeno effects with driving fields in the weak and strong coupling regimes

This chapter is based on M. Majeed and A. Z. Chaudhry, The quantum Zeno and anti-Zeno effects with driving fields in the weak and strong coupling regimes, Sci. Rep. ***11****, 1836 (2021) [101, 103].*

As discussed in the previous chapter, the quantum Zeno and anti-Zeno effects have attracted widespread attention. What has been lacking, however, is a rigorous general study of QZE and QAZE in the presence of coherent driving fields [101]. The idea of controlling the coherent dynamics of a quantum system by an external time-dependent field has found widespread theoretical and experimental interest in many areas of physics and chemistry [111]. For example, driving fields are a commonly used tool to manipulate qubits as well as to control chemical reactions by external laser fields [157–160]. In quantum optics, it has been shown that a frequency-modulated excitation of a two-level atom significantly modifies the time evolution of the system [161]. In quantum tunneling systems, it has been demonstrated that tunneling can be brought to an almost complete standstill via an appropriately designed coherent driving field, an effect dubbed as the coherent destruction of tunneling

[162, 163]. Driving fields can even mitigate the system-environment interaction, which is precisely the idea behind dynamical decoupling [12–16, 164]. Driving fields have also been recently used in noise sensing [165].

It is then clear that driving fields, repeated measurements as well as the environment can all drastically influence the temporal evolution of a quantum system. Consequently, in this chapter, we study the QZE and the QAZE when driving fields are applied to the quantum system as well. We start by deriving a general expression of the effective decay rate for the driven quantum system, provided that the system-environment coupling is weak, thereby extending the formalism of Ref. [57]. We then consider in detail both the population decay model [7] and pure dephasing model [3] in the presence of different driving fields. For example, we show that decay rate for driven population decay model can no longer be obtained using usual sinc-squared function (as can be done in the absence of any driving fields [82]). Moreover, counter-rotating terms of system-environment interaction Hamiltonian can become important in the presence of the driving fields, in contrast with the undriven case. We then extend our formalism to more than one two-level system by modeling the multiple two-level systems as a single large spin [166]. We also demonstrate how our results are applicable in the strong system-environment coupling regime via the well-known polaron transformation [117, 167–172] along with perturbation theory. All in all, our results generally indicate that effective decay rate of central system is very significantly influenced by the driving fields.

5.1 Results

5.1.1 Effective rate of an arbitrary driven quantum system in the weak coupling regime

Let us start by writing total Hamiltonian of system, in the presence of driving fields, interacting with its environment as [101]

$$H(t) = H_S(t) + H_B + H_{SB}. \tag{5.1}$$

Here, the first term $H_S(t)$ describes Hamiltonian of central quantum system. This Hamiltonian carries explicit time-dependence, due to application of external driving fields on the system; consequently, we write it as the sum of a time-independent part H_S and a time-dependent part $H_c(t)$ describing the effect of the external fields. The second term H_B corresponds to the environment, whereas the last term H_{SB} is the coupling between them, which, for later convenience, we write in the diagonal form $H_{SB} = \sum_\mu F_\mu \otimes B_\mu$, with the F_μ operators belonging to the system Hilbert space and the B_μ operators living in the environment Hilbert space. As before, we are interested in the effective decay rate of the system when repeated projective measurements are performed on the central system with time interval τ [57, 58, 173]. To calculate the effective decay rate, we assume that the system is initially prepared in the pure state $|\psi\rangle$. We then find density matrix of central system at time τ, that is, $\rho_S(\tau)$, and then use this to find the survival probability $s(\tau)$ that the system is still in state $|\psi\rangle$ at time τ. Thereafter, we can find effective decay rate via $\Gamma(\tau) = -\ln s(\tau)/\tau$ [57, 58, 173]. The $\rho_S(\tau)$ is obtained via $\rho_S(\tau) = \mathrm{Tr}_B[U(\tau)\rho(0)U^\dagger(\tau)]$, where $\rho(0)$ is state of total system plus environment, Tr_B is the partial trace with respect to environment, and $U(\tau)$ is the total unitary time-evolution operator corresponding to the total Hamiltonian $H(t)$ [5, 6]. Generally speaking, for the time-dependent system-environment models considered here, it is usually impossible to calculate the time-evolution operator exactly. However, for weakly coupled system-environment models, we can find time-evolution operator $U(\tau)$ using time-dependent perturbation theory [2]. We assume that the system-environment state is initially of a simple product form, that is, $\rho(0) = |\psi\rangle\langle\psi| \otimes \rho_B$, where $\rho_B = e^{-\beta H_B}/Z_B$ is the thermal equilibrium state of the environment with $Z_B = \mathrm{Tr}_B[e^{-\beta H_B}]$. Extending the treatment of Ref. [57] to time-dependent Hamiltonians in a straightforward manner, we find that the decay rate of quantum state $|\psi\rangle$, in the presence of projective measurements and for weak system-environment coupling, is given by 'overlap integral' of two functions - the generalized filter function $Q(\omega, \tau)$ [57, 58, 173] and the spectral density of the environment $J(\omega)$ (see the Methods subsection 5.3.1), that is,

$$\Gamma(\tau) = \int_0^\infty d\omega\, Q(\omega, \tau) J(\omega). \tag{5.2}$$

Here, as before [57, 58, 173], the generalized filter function is defined as

$$Q(\omega,\tau)=\frac{2}{\tau}\mathrm{Re}\left(\sum_{\mu\nu}\int_0^\tau dt\int_0^t dt' f_{\mu\nu}(\omega,t')\mathrm{Tr}_S\left[P_\perp\widetilde{F}_\nu(t-t')\rho_S(0)\widetilde{F}_\mu(t)\right]\right), \tag{5.3}$$

where $F_\mu(t)=U_S^\dagger(t)H_S(t)U_S(t)$, with $U_S(t)$ being unitary time-evolution operators corresponding to $H_S(t)$ only, and $P_\perp$ is the projector onto the system subspace orthogonal to $|\psi\rangle\langle\psi|$. The environment correlation function is $C_{\mu\nu}(t)=\mathrm{Tr}_B[\rho_B e^{iH_Bt}B_\mu e^{-iH_Bt}B_\nu]$, which can generally be written as $C_{\mu\nu}(t)=\sum_k|g_k|^2 f_{\mu\nu}(\omega_k,t)$, where g_k is the coupling parameter between central system [4] and k^{th} mode of environment. The function $f_{\mu\nu}(\omega_k,t)$ then contains the remaining information about $C_{\mu\nu}(t)$. The sum over the modes for a continuous environment is typically replaced by an integral via the substitution $\sum_k|g_k|^2(\ldots)\rightarrow\int_0^\infty d\omega\, J(\omega)(\ldots)$, thereby introducing the spectral density function $J(\omega)$ of the environment [57, 58, 173]. It should be noted that $Q(\omega,\tau)$ depends not only on the frequency of the measurements, the way that central system is [57] coupled to its surrounding environment, the state of system which is repeatedly prepared, and part of environment correlation function $f_{\mu\nu}(\omega,t)$; most importantly for us, it also depends on the driving fields applied. Similar analytical expressions to account for the effect of driving fields have been considered before [157–160]. However, our expression takes into account the effect of both measurements as well as the concurrent application of driving fields for arbitrary system-environment models, and we do not make any assumptions regarding the driving fields such as the adiabatic approximation [174, 175]. We also note that there are different ways to define the survival probability of central system and, hence decay rate, as well as different ways of identifying the Zeno, and the anti-Zeno regimes [57, 58, 173]. For example, one can also look at history of measurements [146, 176] when calculating the survival probability [90]. Similarly, we identify the Zeno and anti-Zeno regimes by looking at when the decay rate $\Gamma(\tau)$ is an increasing function (the Zeno regime) or a decreasing function (the anti-Zeno regime) [57]; alternatively, one can compare the measurement modified decay rate with the decay rate without measurement [173, 177].

5.1.2 General expression of decay rate for a driven two-level system

To apply our formalism to a two-level system, we first note that, without loss of generality, we can assume the initial state to be $|e\rangle$, where $\sigma_z |e\rangle = |e\rangle$, since we can always choose our coordinate system in this manner. We then check with time τ [60], whether or not, central system is still in this state or not [57, 58, 173]. The projector onto the orthogonal subspace is $|g\rangle \langle g|$, where $\sigma_z |g\rangle = -|g\rangle$. Now comes a key insight. No matter what the external driving fields are, system unitary time-evolution operator $U_S(t)$ can always be expressed as

$$U_S(t) = e^{-i\alpha(t)\sigma_z/2} e^{-i\beta(t)\sigma_y/2} e^{-i\gamma(t)\sigma_z/2}, \tag{5.4}$$

where $\alpha(t)$, $\beta(t)$, and $\gamma(t)$ are time-dependent Euler angles. These are arbitrary functions of time with the constraint that $U_S(t=0) = \mathbb{1}$. The corresponding Hamiltonian $H_S(t)$ can be worked out from Schrodinger's equation. We find that

$$\begin{aligned} H_S(t) = {} & \frac{\sigma_z}{2}\frac{\partial\alpha(t)}{\partial t} + \frac{1}{2}\frac{\partial\beta(t)}{\partial t}\big(\cos[\alpha(t)]\sigma_y - \sin[\alpha(t)]\sigma_x\big) + \frac{1}{2}\frac{\partial\gamma(t)}{\partial t}\cos[\beta(t)]\sigma_z \\ & + \frac{1}{2}\frac{\partial\gamma(t)}{\partial t}\big(\sin[\beta(t)]\cos[\alpha(t)]\sigma_x + \sin[\beta(t)]\sin[\alpha(t)]\sigma_y\big). \end{aligned} \tag{5.5}$$

In other words, by choosing the functions $\alpha(t)$, $\beta(t)$, and $\gamma(t)$ appropriately [10, 101], we can work backward to find the corresponding system Hamiltonian.

With this form of $U_S(t)$, we can work out the effective decay rate. Using our previous general expression given in Eq. (5.3), we find that the filter function is

$$Q(\omega,\tau) = \frac{2}{\tau}\mathrm{Re}\left(\sum_{\mu\nu}\int_0^\tau dt \int_0^t dt' f_{\mu\nu}(\omega,t') G_\mu(t)\bar{G}_\nu(t-t')\right), \tag{5.6}$$

where

$$G_\mu(t) = e^{i(\alpha(t)+\gamma(t))}\cos^2\left[\frac{\beta(t)}{2}\right]F_{\mu eg} - e^{-i(\alpha(t)-\gamma(t))}\sin^2\left[\frac{\beta(t)}{2}\right]F_{\mu ge} + e^{i\gamma(t)}\frac{\sin[\beta(t)]}{2}(F_{\mu gg} - F_{\mu ee}), \tag{5.7}$$

and

$$\bar{G}_\nu(t) = e^{-i(\alpha(t)+\gamma(t))}\cos^2\left[\frac{\beta(t)}{2}\right]F_{\nu ge} - e^{i(\alpha(t)-\gamma(t))}\sin^2\left[\frac{\beta(t)}{2}\right]F_{\nu eg} + e^{-i\gamma(t)}\frac{\sin[\beta(t)]}{2}(F_{\nu gg} - F_{\nu ee}), \tag{5.8}$$

with $F_{\mu ij} = \langle i| F_\mu |j\rangle$. In the following sections, we use this form of the filter function with various $\alpha(t)$, $\beta(t)$, and $\gamma(t)$ to evaluate $\Gamma(\tau)$ for different system-environment models.

5.1.3 Application to driven population decay model in weak coupling regime

To illustrate our formalism, we first consider a single spin-1/2 particle, subjected to external driving fields, and interaction with a harmonic oscillator environment. The total Hamiltonian is now written as (with $\hbar = 1$ throughout) [101]

$$H(t) = H_S(t) + H_B + H_{SB}, \tag{5.9}$$

with

$$H_S(t) = \frac{\varepsilon_0}{2}\sigma_z + H_c(t), \tag{5.10}$$

$$H_B = \sum_k \omega_k b_k^\dagger b_k, \tag{5.11}$$

$$H_{SB} = \sum_k (g_k^* b_k \sigma_+ + g_k b_k^\dagger \sigma_-), \tag{5.12}$$

where $H_S(t)$ is the system Hamiltonian with ε_0 representing the energy spacing of the two-level system, while $H_c(t)$ is a time-dependent external driving field acting on central system. H_B is environment Hamiltonian with $b_k(b_k^\dagger)$ representing usual annihilation(creation) operators, and H_{SB} is system-environment interaction Hamiltonian with g_k denoting coupling strength between central two-level system and environment oscillators. As usual, σ_z is Pauli spin-1/2 matrix with σ_+(and σ_-) are the raising(and lowering) operators. Note that we have made the rotating-wave approximation (RWA) here for the system-environment interaction, which means that we have neglected those processes which do not conserve energy [50, 76, 178, 179][1].

[1]However, RWA tends to fail in ultra-strong system-environment coupling regime due to significant contribution of the non-conserving energy terms.

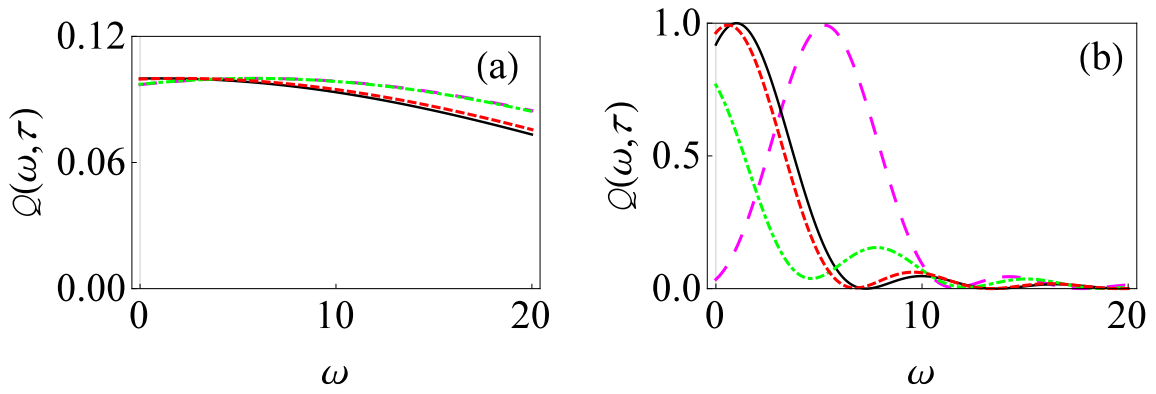

Figure 5.1: (a) Graph of filter function $Q(\omega,\tau)$ versus ω for driven population decay model with RWA: $\alpha(t) = \varepsilon_0 t + (V_0/\Omega)\sin(\Omega t)$, $\beta(t) = 0$ and $\gamma(t) = 0$ with $V_0 = 1$ and $\Omega = 5$ (dashed, red curve), $V_0 = 5$ and $\Omega = 1$ (large-dashed, magenta curve), and $V_0 = 5$ and $\Omega = 5$ (dot-dashed, green curve). $\alpha(\tau) = \varepsilon_0\tau$, $\beta(\tau) = 0$ and $\gamma(\tau) = 0$ for the solid, black curve. We have set $\varepsilon_0 = 1$ with $\hbar = 1$. Here we have used a relatively small measurement interval, that is, $\tau = 0.1$. (b) Same as (a), except that now $\tau = 1$.

With the model specified, we now move to find effective decay rate using the formalism described before. As is usually the case in studies of QZE and QAZE, we initially prepare our quantum system, that is, TLS in the excited state $|e\rangle$ such that $\sigma_z|e\rangle = |e\rangle$, and then we repeatedly check our quantum system in the excited state with time interval τ. To calculate $\Gamma(\tau)$ using our formalism, we note that $F_1 = \sigma_+$, $F_2 = \sigma_-$, $C_{\mu\nu}(t) = \mathrm{Tr}_B[\rho_B \widetilde{B}_\mu(t) B_\nu]$, $\widetilde{B}_\mu(t) = e^{iH_B t} B_\mu e^{-iH_B t}$, $B_1 = \sum_k g_k^* b_k$, and $B_2 = \sum_k g_k b_k^\dagger$. In the limit of zero temperature, we find that $f_{12}(\omega,t) = e^{-i\omega t}$, while $f_{11} = f_{22} = f_{21} = 0$. Moreover, we find $G_1(t) = e^{i(\alpha(t)+\gamma(t))}\cos^2[\beta(t)/2]$, and $\bar{G}_2(t-t') = e^{-i(\alpha(t-t')+\gamma(t-t'))}\cos^2[\beta(t-t')/2]$. Using these results, we obtain

$$Q(\omega,\tau) = \frac{2}{\tau}\int_0^\tau dt \int_0^t dt' \cos[\alpha(t)-\alpha(t-t')+\gamma(t)-\gamma(t-t')-\omega t'] \cos^2[\beta(t)/2]\cos^2[\beta(t-t')/2]. \tag{5.13}$$

In general, this can be a very complicated function. Therefore, we first consider the simplest case where $\alpha(t) = \varepsilon_0 t$, while $\beta(t) = \gamma(t) = 0$. This corresponds to [see Eq. (5.5)] $H = \frac{\varepsilon_0}{2}\sigma_z$,

that is, the usual population decay model with no driving field. After performing integration, we get $Q(\omega,\tau) = \tau \mathrm{sinc}^2[\frac{(\varepsilon_0-\omega)\tau}{2}]$, thereby reproducing the well-known [7] sinc-squared function for $Q(\omega,\tau)$. Our formalism, on the other hand, allows us to go much further. The next case that we can consider is $\alpha(t) = \varepsilon_0 t + (V_0/\Omega)\sin(\Omega t)$ with $\beta(t) = \gamma(t) = 0$, which corresponds to $H_S = \frac{\varepsilon_0}{2}\sigma_z$ and $H_c(t) = V_0\cos(\Omega t)\sigma_z/2$, with V_0 the amplitude of the applied sinusoidal field and Ω its frequency. Using the Jacobi-Auger identity $e^{ix\sin(\Omega t)} = \sum_{l=-\infty}^{\infty} J_l(x)e^{il\Omega t}$, with $J_l(x)$ being the Bessel functions of first kind [180], we find that now

$$Q(\omega,\tau) = \sum_{m,n=-\infty}^{\infty} \frac{\tau A_{mn}}{\varepsilon_0-\omega+m\Omega}\big(\mathrm{sinc}^2[\frac{(m-n)\Omega\tau}{2}](m-n)\Omega + \mathrm{sinc}^2[\frac{(\varepsilon_0-\omega+n\Omega)\tau}{2}](\varepsilon_0-\omega+n\Omega)\big), \tag{5.14}$$

with $A_{mn} = J_m(V_0/\Omega)J_n(V_0/\Omega)$. The filter function is no longer a simple sinc-squared function - although the average value of the sinusoidal applied field is zero, the filter function changes in a very non-trivial manner. In particular, it is clear that the filter function $Q(\omega,\tau)$ is no longer generally peaked at $\omega = \epsilon_0$, even for changing measurement interval τ. Rather, the second term in Eq. (5.14) makes it particularly clear that such a simple conclusion no longer holds in the driven case, and in fact the peak of the filter function changes as the measurement interval changes. Carrying on, we can also consider $\alpha(t) = \varepsilon_0 t$, with non-zero $\beta(t)$ (while $\gamma(t) = 0$). This corresponds to the driving field $H_c(t) = \frac{1}{2}\frac{\partial\beta(t)}{\partial t}\big(\cos[\varepsilon_0 t]\sigma_y - \sin[\varepsilon_0 t]\sigma_x\big)$. In these cases, $Q(\omega,\tau)$ needs to be calculated numerically, but the point is that in all such cases, the filter function, and hence the decay rate, changes in a very non-trivial manner. Similarly, we can also study non-zero values of $\gamma(t)$; the part of the Hamiltonian which contributes in $H_c(t)$ due to $\gamma(t)$ is of form $\frac{1}{2}\frac{\partial\gamma(t)}{\partial t}\cos[\beta(t)]\sigma_z + \frac{1}{2}\frac{\partial\gamma(t)}{\partial t}\big(\sin[\beta(t)]\cos[\alpha(t)]\sigma_x + \sin[\beta(t)]\sin[\alpha(t)]\sigma_y\big)$.

We now illustrate the change in the filter function as a result of these driving fields. Our results are shown in Fig. 5.1 where we demonstrate the behavior of filter function as a function of oscillator frequency for two different measurement intervals τ both with and without driving fields. Here, we have considered $\beta(t) = \gamma(t) = 0$, while $\alpha(t) = \varepsilon_0 t$ for the

solid, black curve (the undriven case) and $\alpha(t) = \varepsilon_0 t + (V_0/\Omega)\sin(\Omega t)$ for the other curves (the driven cases). For the small measurement interval case illustrated in Fig. 5.1(a), the different filter functions practically overlap - this is simply a manifestation of the convergence to the Zeno limit in the small measurement interval scenario even in the presence of time-dependent driving fields. However, for relatively large measurement interval τ, the filter function for population decay model (given by usual sinc-squared function) is qualitatively different from the cases where we place the central system in a time-dependent external field [see Fig. 5.1(b)]. It can be seen that for the solid, black curve (the no driving case), the filter function $Q(\omega, \tau)$ is sharply peaked at $\varepsilon_0 = \omega$ for $\tau = 1$, and changes very appreciably in the presence of strong driving fields (the dot-dashed green and long-dashed magenta curves). The long-dashed magenta curve corresponds to a relatively lower frequency ($V_0 = 5$ and $\Omega = 1$), and to a first approximation, this filter function can be obtained by considering that the peak of the usual sinc-squared filter function is now shifted to $\varepsilon_0 + V_0$. However, for strong driving fields with higher frequencies (the dot-dashed green curve), such a naive picture is no longer applicable. Looking at Eq. (5.14) and using the fact that for higher frequencies, the Bessel functions are rapidly decaying so that only a few terms in the sum are important, it is clear that not only is the frequency $\omega = \varepsilon_0$ important in the filter function, but also other frequencies such as $\omega = \varepsilon_0 + \Omega$, $\omega = \varepsilon_0 - \Omega$, and so on. This leads to a much richer and complicated filter function, whose peak in fact also changes as the measurement interval τ is varied. As a result, we can expect that the effective decay rate is non trivially modified.

Let us now consider more complicated driving fields such that we have non-zero values of $\beta(t)$ and $\gamma(t)$. As an example, we consider $\alpha(t) = \varepsilon_0 t$ and $\beta(t) = \upsilon t$, while $\gamma(t) = 0$. This introduces oscillatory fields in the system Hamiltonian [see Eq. (5.5)], and the filter function now changes as shown in Fig. 5.2(a). It is clear that adding in the control fields now greatly reduces the filter function (see the dot-dashed orange curve), and is thus expected to lead to a decrease in the effective decay rate. We can also consider what happens if these oscillating control fields are 'damped' - this is illustrated by the dashed blue curve. We have checked as that as the fields become more damped, the filter function starts to coincide with the

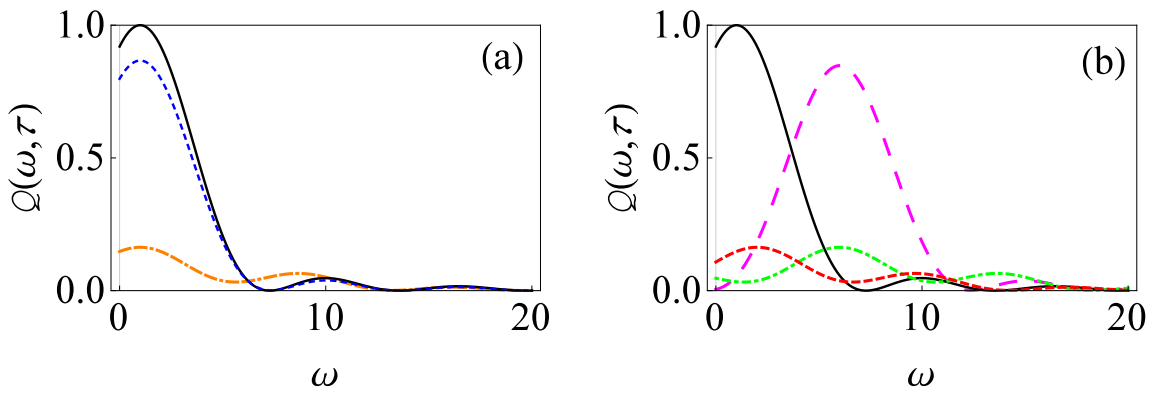

Figure 5.2: (a) Graph of filter function $Q(\omega,\tau)$ versus ω for driven population decay model with RWA: $\alpha(t)=\varepsilon_0 t$, $\beta(t)=-(e^{-\chi t}-1)/\chi$ and $\gamma(t)=0$ with $\chi=0.2$ (dashed, blue curve), $\alpha(t)=\varepsilon_0 t$, $\beta(t)=\upsilon t$ and $\gamma(t)=0$ with $\upsilon=5$ (dot-dashed, orange curve), $\alpha(t)=\varepsilon_0 t$, $\beta(t)=0$ and $\gamma(t)=0$ (solid, black curve). We have used large measurement interval $\tau=1$. (b) Here $\alpha(t)=\varepsilon_0 t$, $\beta(t)=\upsilon t$ and $\gamma(t)=\xi t$, with $\upsilon=5$ and $\xi=1$ (dashed, red curve), $\upsilon=1$ and $\xi=5$ (long-dashed, magenta curve), and $\upsilon=5$ and $\xi=5$ (dot-dashed, green curve). The solid black curve shows $\alpha(t)=\varepsilon_0 t$, $\beta(t)=0$ and $\gamma(t)=0$. We have again used $\tau=1$.

undriven scenario (the solid black curve). Proceeding along these lines, we can also work out the filter function when $\gamma(t)$ is also non-zero, further illustrating the drastic effect of the driving fields on the filter function [see Fig. 5.2(b)].

Having illustrated the effect of the driving fields on the filter function, we now demonstrate how this translates to a change in the effective decay rate $\Gamma(\tau)$ of two-level system and thereby quantum Zeno and the anti-Zeno behavior [57, 58, 101, 173]. The behavior $\Gamma(\tau)$ versus time τ for different driving fields is shown in Fig. 5.3. Let us note how the behavior of $\Gamma(\tau)$ helps us to identify the quantum Zeno and anti-Zeno regimes. If the effective decay rate $\Gamma(\tau)$ decreases by shortening the measurement interval τ, then the system shows the QZE; if the opposite is true, then we have the QAZE [57, 58, 101, 133, 136, 173]. Moreover, to actually compute $\Gamma(\tau)$, we need to specify the spectrum of environment [57, 58, 101, 173]. Throughout this work, we will use an Ohmic form of spectral density. As we have discussed

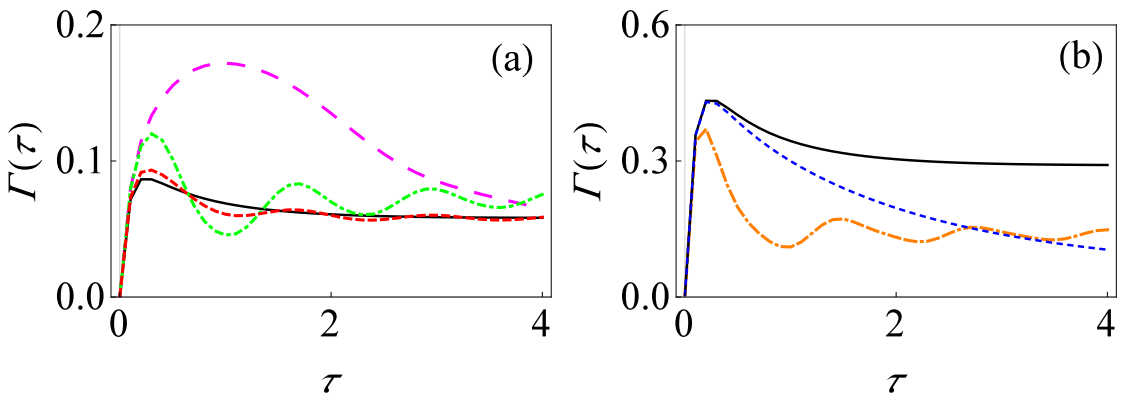

Figure 5.3: (a) Graph of effective decay rate $\Gamma(\tau)$ versus τ for driven population decay model with RWA: $\alpha(t) = \varepsilon_0 t + (V_0/\Omega)\sin(\Omega t)$, $\beta(t) = 0$ and $\gamma(t) = 0$ with $V_0 = 1$ and $\Omega = 5$ (dashed, red curve), $V_0 = 5$ and $\Omega = 1$ (long-dashed, magenta curve), and $V_0 = 5$ and $\Omega = 5$ (dot-dashed, green curve). The solid black curve shows $\alpha(t) = \varepsilon_0 t$, $\beta(t) = 0$ and $\gamma(t) = 0$. We remind the reader that we have set $\varepsilon_0 = 1$ with $\hbar = 1$. Here we have used $G = 0.01$ and $\omega_c = 10$. (b) We now have $\alpha(t) = \varepsilon_0 t$, $\beta(t) = -(e^{-\chi t} - 1)/\chi$ and $\gamma(t) = 0$ with $\chi = 0.2$ (dashed, blue curve), $\alpha(t) = \varepsilon_0 t$, $\beta(t) = \upsilon t$ and $\gamma(t) = 0$ with $\upsilon = 5$ (dot-dashed, orange curve), $\alpha(t) = \varepsilon_0 t$, $\beta(t) = 0$ and $\gamma(t) = 0$ (solid, black curve). We now have $G = 0.05$.

before, for weak coupling strength, the effective decay rate of the central system is the overlap integral of the environment spectral density $J(\omega)$ and the generalized filter function $Q(\omega, \tau)$ [57, 58, 101, 173]. If the peak value of the filter function is near the cutoff frequency of the spectrum of the environment, then there will be a significant overlap between $J(\omega)$ and the filter function $Q(\omega, \tau)$, leading to an enhanced decay rate. On the other hand, if the peak value of the generalized filter function is well beyond the cutoff frequency ω_c, then the overlap between $J(\omega)$ and $Q(\omega, \tau)$ is minimized, leading to a reduced decay rate [57, 58, 101, 173]. The dynamically modified filter function in the presence of driving fields [see Figs. 5.1 and 5.2] affects the overlap of $J(\omega)$ with $Q(\omega, \tau)$, and thus can either accelerate or inhibit the decay rate as compared to the undriven scenario. In particular, it is clear from Fig. 5.3(a) that for simple population decay case with no driving fields (the solid black curve), there is

a single local crossover between quantum Zeno and anti-Zeno regime, meaning that, for the short time regime, the $\Gamma(\tau)$ decreases by decreasing measurement interval τ while for large measurement interval, it increases by decreasing the measurement interval. In the presence of driving fields, not only is the effective decay rate greatly affected (see the long-dashed magenta curve) but also there are multiple Zeno and anti-Zeno regimes (see the dashed red curve and the dot-dashed green curve). For long-dashed magenta curve, the peak value of the filter function is at approximately $\omega = 5.6$ [see Fig. 5.1(b)] which is more near to the peak of the spectrum of the environment as compared to the solid black curve (for which the peak is at $\omega = 1$). As a result, this gives maximum overlap of $Q(\omega, \tau)$ with $J(\omega)$ for the magenta curve, which consequently enhances the effective decay rate compared to the undriven case. For the dot-dashed green curve, we observed previously that a large driving field frequency means that the peak of the filter function keeps changing as the measurement interval changes, and this leads to multiple Zeno and anti-Zeno regimes. However, at short time τ, all the curves agree. This is expected, since, as we have seen before, with very fast measurements, the filter function becomes the same, leading to the same decay rate. We have also looked at what happens with $\beta(t) \neq 0$. Having seen how the filter function is influenced by such driving fields in Fig. 5.2(a), we illustrate what happens to the corresponding decay rate in Fig. 5.3(b) for the same $\beta(t)$ as used in Fig. 5.2(a), where $\beta(t)$ is a damped function for the dashed blue curve, and it is a linear function of t for the dot-dashed orange curve. Since a linear function of t in the presence of non-zero ε_0 leads to a reduction in the peak value of the filter function [see Fig. 5.2(a)], the overlap between $Q(\omega, \tau)$ and $J(\omega)$ reduces for $\omega_c = 10$, leading to a reduction in the effective decay rate as compared to the solid black curve. On the other hand, if $\beta(t)$ is a damped function, effects of the oscillating fields are suppressed, meaning that decay rate is increased for the dashed blue curve as compared to dot-dashed orange curve. Once again, it is clear that driving fields greatly influence the decay rate both quantitatively, and qualitatively.

We next discuss the effect of the non-rotating terms of H_{SB} interaction Hamiltonian on the dynamics of central system subjected to a driving field. The total Hamiltonian is now

given by

$$H(t) = \frac{\varepsilon_0}{2}\sigma_z + H_c(t) + \sum_k \omega_k b_k^\dagger b_k + \sigma_x \sum_k (g_k^* b_k + g_k b_k^\dagger). \tag{5.15}$$

Notice the different form of the system-environment coupling as compared to before - the system-environment Hamiltonian now contains the 'non-rotating' terms $\sigma_+ b_k^\dagger$ and $\sigma_- b_k$. To calculate filter function $Q(\omega, \tau)$ now, we first evaluate correlation function of environment. With $F = \sigma_x$, we find $G(t) = -e^{-i(\alpha(t)-\gamma(t))}\sin^2[\beta(t)/2] + e^{i(\alpha(t)+\gamma(t))}\cos^2[\beta(t)/2]$ and $\bar{G}(t-t') = -e^{i(\alpha(t-t')-\gamma(t-t'))}\sin^2[\beta(t-t')/2] + e^{-i(\alpha(t-t')+\gamma(t-t'))}\cos^2[\beta(t-t')/2]$. Also, $f(\omega, t) = e^{-i\omega t}$ at zero temperature. Putting all this together,

$$Q(\omega, \tau) = \frac{2}{\tau}\int_0^\tau dt \int_0^t dt' \big(D_1(t,t') + D_2(t,t') + D_3(t,t') + D_4(t,t')\big), \tag{5.16}$$

where

$$D_1(t,t') = \cos[\gamma(t) - \gamma(t-t') - \omega t']\cos[\alpha(t)]\cos[\beta(t)]\cos[\alpha(t-t')]\cos[\beta(t-t')], \tag{5.17}$$

$$D_2(t,t') = -\sin[\gamma(t) - \gamma(t-t') - \omega t']\cos[\alpha(t-t')]\cos[\beta(t-t')]\sin[\alpha(t)], \tag{5.18}$$

$$D_3(t,t') = \sin[\gamma(t) - \gamma(t-t') - \omega t']\cos[\alpha(t)]\cos[\beta(t)]\sin[\alpha(t-t')], \tag{5.19}$$

$$D_4(t,t') = \cos[\gamma(t) - \gamma(t-t') - \omega t']\sin[\alpha(t)]\sin[\alpha(t-t')]. \tag{5.20}$$

Compared with Eq. (5.13), we can see that the two filter functions agree for $\beta(t) = 0$. This means that in the absence of driving fields (where $\alpha(t) = \varepsilon_0 t$ and $\beta(t) = 0$), the counter-rotating terms do not affect the decay rate. However, in the presence of driving fields with $\beta(t) \neq 0$, the counter-rotating terms become important, even in the weak system-environment coupling regime we are dealing with. The influence of the non-rotating terms is shown in Fig. 5.4, where the behavior of the filter function as a function of the frequency ω is shown in Fig. 5.4(a) and time-evolution of effective decay rate is illustrated in Fig. 5.4(b). Comparing Figs. 5.2(a) and Fig. 5.4(a), it is clear that when there are no driving fields, the filter function does not change since the solid, black curve is the same in both figures. However, as shown by dashed blue and dot-dashed orange curves, in the presence of driving

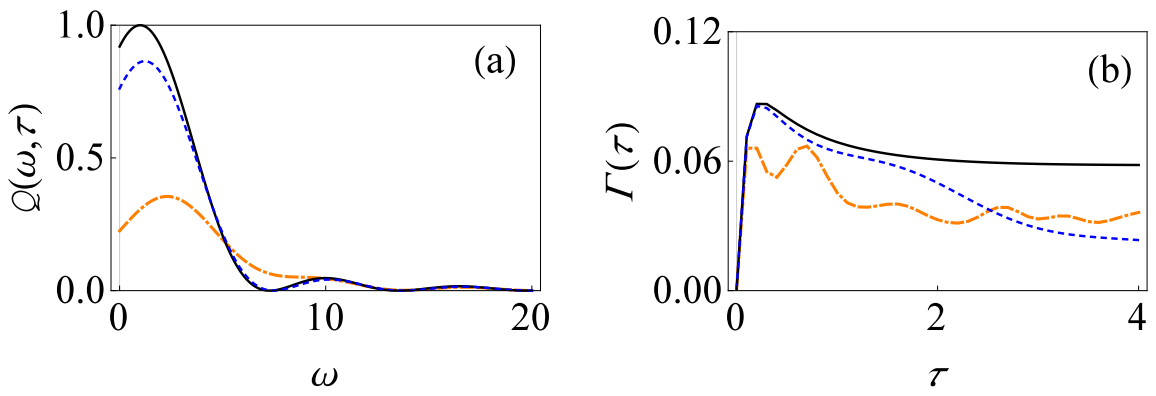

Figure 5.4: (a) Graph of filter function $Q(\omega, \tau)$ versus ω for driven population decay model without RWA: $\alpha(t) = \varepsilon_0 t$, $\beta(t) = -(e^{-\chi t} - 1)/\chi$ and $\gamma(t) = 0$ with $\chi = 0.2$ (dashed, blue curve); $\alpha(t) = \varepsilon_0 t$, $\beta(t) = \upsilon t$ and $\gamma(t) = 0$ with $\upsilon = 5$ (dot-dashed, orange curve); $\alpha(t) = \varepsilon_0 t$, $\beta(t) = 0$ and $\gamma(t) = 0$ (solid, black curve). Here we have used $\tau = 1$. (b) Similar to (a), except that now we have plotted effective decay rate $\Gamma(\tau)$ versus time τ with $G = 0.01$ and $\omega_c = 10$.

fields with $\beta(t) \neq 0$, the filter function does change. This correspondingly changes the effective decay rate by modifying the overlap of $J(\omega)$ with $Q(\omega, \tau)$ as can be seen by comparing Figs. 5.3(b) and 5.4(b). The counter-rotating terms help to enhance the peak value of the filter function, leading to an increase in the effective decay rate.

5.1.4 Application to the driven dephasing model with weak system-environment coupling

We now study pure dephasing model [3] given by total Hamiltonian [101]

$$H = H_S + H_B + H_{SB}, \tag{5.21}$$

with[2]

$$H_S = \frac{\varepsilon_0}{2}\sigma_z, \tag{5.22}$$

$$H_B = \sum_k \omega_k b_k^\dagger b_k, \tag{5.23}$$

$$H_{SB} = \sigma_z \sum_k (g_k^* b_k + g_k b_k^\dagger). \tag{5.24}$$

Notice the different form of interaction term between system and environment. With this model, the populations of the system energy eigenstates cannot change - only the off-diagonal coherences can change, which is why this is referred to as a pure dephasing model [56]. The initial state usually considered in this model is $|\psi\rangle = \frac{1}{\sqrt{2}}(|e\rangle + |g\rangle)$, with $\langle e|\, g\rangle = 0$. However, with the formalism we have developed, the initial state we considered was $|e\rangle$. To use our formalism, we consequently perform a unitary operation $U_R = e^{i\pi\sigma_y/4}$. The initial state then again becomes $|e\rangle$, while the Hamiltonian is transformed to

$$H^{(R)} = U^{(R)} H U^{(R)\dagger} = -\frac{\varepsilon_0}{2}\sigma_x + \sum_k \omega_k b_k^\dagger b_k - \sigma_x \sum_k (g_k^* b_k + g_k b_k^\dagger). \tag{5.25}$$

To find the filter function now, we look at Eq. (5.5) and find that $\alpha(t) = \pi/2$, $\beta(t) = \varepsilon_0 t$ and $\gamma(t) = -\pi/2$ gives the same Hamiltonian as Eq. (5.25). Then, using our developed formalism, we find that $G(t) = 1$ and $\bar{G}(t - t') = 1$. Consequently, assuming that the environment is at zero temperature, we get $Q(\omega, \tau) = \frac{2}{\tau}\frac{1-\cos(\omega\tau)}{\omega^2}$, which agrees with the filter function obtained using the exact solution [57]. Next, we add in the effect of the driving fields. To this end, we look at more complicated time-dependent functions $\alpha(t)$, $\beta(t)$, and $\gamma(t)$. We write the corresponding system-environment Hamiltonian as [101]

$$H(t) = -\frac{\varepsilon_0}{2}\sigma_x + H_c(t) + \sum_k \omega_k b_k^\dagger b_k - \sigma_x \sum_k (g_k^* b_k + + g_k b_k^\dagger). \tag{5.26}$$

To take into account the additional control fields given by $H_c(t)$, we write $\alpha(t) = \pi/2 + \widetilde{\alpha}(t)$ and $\gamma(t) = -\pi/2 + \widetilde{\gamma}(t)$, while $\beta(t)$ remains $\varepsilon_0 t$. Simple calculations then lead to the filter

[2]Note that, here we are are using coupling term $\sigma_z \sum_k (g_k^* b_k + g_k b_k^\dagger)$, instead of $\frac{\sigma_z}{2}\sum_k (g_k^* b_k + g_k b_k^\dagger)$ that was used in the previous chapter.

function

$$Q(\omega,\tau)=\frac{2}{\tau}\int_0^\tau dt\int_0^t dt'\big(D_1(t,t')+D_2(t,t')+D_3(t,t')+D_4(t,t')\big), \tag{5.27}$$

where now

$$D_1(t,t')=\cos[\widetilde{\gamma}(t)-\widetilde{\gamma}(t-t')-\omega t']\sin[\widetilde{\alpha}(t)]\cos[\beta(t)]\sin[\widetilde{\alpha}(t-t')]\cos[\beta(t-t')], \tag{5.28}$$

$$D_2(t,t')=\sin[\widetilde{\gamma}(t)-\widetilde{\gamma}(t-t')-\omega t']\sin[\widetilde{\alpha}(t-t')]\cos[\beta(t-t')]\cos[\widetilde{\alpha}(t)], \tag{5.29}$$

$$D_3(t,t')=-\sin[\widetilde{\gamma}(t)-\widetilde{\gamma}(t-t')-\omega t']\sin[\widetilde{\alpha}(t)]\cos[\beta(t)]\cos[\widetilde{\alpha}(t-t')], \tag{5.30}$$

$$D_4(t,t')=\cos[\widetilde{\gamma}(t)-\widetilde{\gamma}(t-t')-\omega t']\cos[\widetilde{\alpha}(t)]\cos[\widetilde{\alpha}(t-t')]. \tag{5.31}$$

Using these expressions, we have plotted the filter function (for $\tau=1$) in Fig. 5.5(a) for different control fields. Once again, it is clear that the driving fields greatly influence the filter function in general. For instance, with a sinusoidal driving field ($\widetilde{\alpha}(t)=(V_0/\Omega)\sin(\Omega t)$, $\beta(t)=\varepsilon_0 t$, and $\widetilde{\gamma}(t)=0$), the filter function is very different as compared with the undriven case (compare the solid black curve with the dot-dashed green and long-dashed magenta curves), with the difference becoming smaller as the driving field strength is reduced (see the dashed red curve). Consequently, the behavior of $\Gamma(\tau)$ and the corresponding quantum Zeno and the anti-Zeno phenomena is anticipated [101] to be greatly modified due to the different overlap of the filter function with the spectrum of the environment. That this is indeed the case as shown in Fig. 5.5(b). We see that there is a single peak in the case of the undriven pure dephasing model. On the other hand, due to external fields, the $\Gamma(\tau)$ increases with increasing V_0 and the effective decay rate shows multiple transitions of Zeno and the anti-Zeno regimes for fast oscillating external fields.

5.1.5 Application to driven large spin-boson model in weak coupling regime

We now briefly show how we can extend our formalism to more general systems in which a large spin greater than spin-1/2 particle is coupled to an oscillators environment. Such

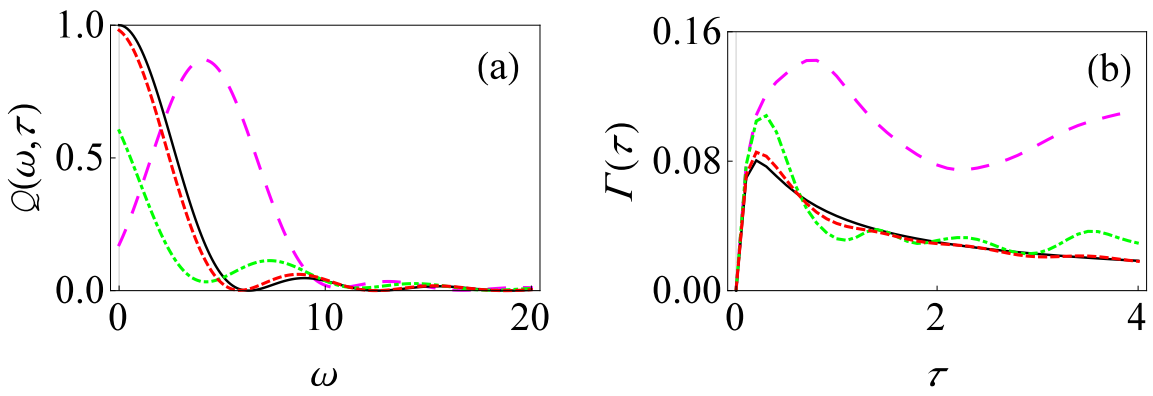

Figure 5.5: (a) Graph of filter function versus ω for driven dephasing model: $\widetilde{\alpha}(t) = (V_0/\Omega)\sin(\Omega t)$, $\beta(t) = \varepsilon_0 t$ and $\widetilde{\gamma}(t) = 0$ with $V_0 = 1$ and $\Omega = 5$ (dashed, red curve), $V_0 = 5$ and $\Omega = 1$ (large-dashed, magenta curve), and $V_0 = 5$ and $\Omega = 5$ (dot-dashed, green curve). The solid black curve is with $\widetilde{\alpha}(t) = 0$, $\beta(t) = \varepsilon_0 t$, and $\widetilde{\gamma}(t) = 0$. We have set $\varepsilon_0 = 1$ with $\hbar = 1$. Here we are have used $\tau = 1$. (b) Similar to (a), except that now we have plotted effective decay rate $\Gamma(\tau)$ versus τ with $G = 0.01$ and $\omega_c = 10$.

a model can describe, for instance, a set of N_S two-level systems coupled to a common harmonic oscillator environment[56, 142, 166]. We first define $J_k = \frac{1}{2}\sum_i \sigma_k^{(i)}$, where J_k $(k = x, y, z)$ are the large spin operators. As a concrete example, we consider the driven population decay model given by total Hamiltonian

$$H(t) = H_S(t) + H_c(t) + H_B + H_{SB}, \tag{5.32}$$

with

$$H_S(t) = \varepsilon_0 J_z + H_c(t), \tag{5.33}$$

$$H_B = \sum_k \omega_k b_k^\dagger b_k, \tag{5.34}$$

$$H_{SB} = 2J_x \sum_k (g_k^* b_k + g_k b_k^\dagger), \tag{5.35}$$

where ε_0 is the energy level spacing for each spin-1/2 particle, and $H_c(t)$ is the control field Hamiltonian. Analogous to what we did for the single spin-1/2 case, we consider the free system unitary time evolution operator to be $U_S(t) = e^{-i\alpha(t)J_z} e^{-i\beta(t)J_y} e^{-i\gamma(t)J_z}$. We take the

initial state to be $|j\rangle$ with $J_z|j\rangle = j|j\rangle$ and $j = N_S/2$. Performing the calculation for the filter function using our formalism, we find that the filter function is exactly the same as for the single spin-1/2 case [see Eq. (5.16)] except for an additional multiplicative factor of N_S (see the Methods subsection 5.3.2 for details). That is, the effective decay rate is now enhanced by a factor of N_S, reminiscent of the superradiance effect [181], which appears due to the common environment. A similar calculation shows that if the pure dephasing model is extended to the large spin case analogously, the effective rate is again enhanced by a factor of N_S.

5.1.6 Application to the driven spin-boson model with strong system-environment coupling

Finally, we extend our treatment of driven population decay model to strong coupling regime between system and environment. We start from the system-environment Hamiltonian

$$H(t) = H_S(t) + H_B + H_{SB}, \tag{5.36}$$

with

$$H_S(t) = \frac{\varepsilon(t)}{2}\sigma_z + \frac{\Delta}{2}\sigma_x, \tag{5.37}$$

$$H_B = \sum_k \omega_k b_k^\dagger b_k, \tag{5.38}$$

and

$$H_{SB} = \sigma_z \sum_k (g_k^* b_k + g_k b_k^\dagger). \tag{5.39}$$

The driving fields are contained in $\varepsilon(t)$. Now, if the system and the environment are interacting strongly, we cannot treat interaction strength between central system, and its environment perturbatively. Instead, we can consider performing a polaron transformation [58, 117, 168, 171, 172], which transforms our Hamiltonian to (see the Methods subsection 5.3.3)

$$H^{(P)}(t) = e^{\chi\sigma_z/2} H(t) e^{-\chi\sigma_z/2} = \frac{\varepsilon(t)}{2}\sigma_z + \sum_k \omega_k b_k^\dagger b_k + \frac{\Delta}{2}(\sigma_+ Y + \sigma_- Y^\dagger), \tag{5.40}$$

where symbol P is used for polaron frame[3], $\chi = \sum_k [\frac{2g_k}{\omega_k} b_k^\dagger - \frac{2g_k^*}{\omega_k} b_k]$, and $Y = e^\chi$.

We see that in rotated polaron frame, the form of system-environment interaction Hamiltonian is different. Now, if tunneling parameter Δ of central system is relatively small, we can apply perturbation theory [2, 58], treating system-environment coupling strength in polaron frame perturbatively. As before, at the initial time, our system is prepared in excited state $|e\rangle$, and then projective measurements are carried out on central system with time interval τ to observe whether it is still present in excited state $|e\rangle$, or not. It is also important to note that the initial state of system and environment in the untransformed frame cannot be written in the simple usual product form $\rho(0) = |e\rangle\langle e| \otimes e^{-\beta H_B}/Z_B$, with $\rho_B = e^{-\beta H_B}/Z_B$ and $Z_B = \mathrm{Tr}_B[e^{-\beta H_B}]$, since the system and its environment are interacting strongly in that frame and, consequently, the initial system-environment correlations are significant [43, 44, 54, 58, 124, 128]. However, since the system and its environment are effectively weakly interacting in the polaron frame, the initial state in the polaron frame can be taken as a simple product state [58, 101]. The rest of the calculation, performed in the polaron frame, proceeds in a similar way as the weak coupling case using perturbation theory. We eventually arrive at (see the Methods subsection 5.3.4)

$$\Gamma(\tau) = \frac{\Delta^2}{2\tau} \int_0^\tau dt \int_0^t dt' \cos[\zeta(t) - \zeta(t-t') - \Phi_I(t')] e^{-\Phi_R(t')}, \tag{5.41}$$

where $\Phi_I(t) = \int_0^\infty d\omega J(\omega) \coth(\frac{\beta\omega}{2}) \frac{\sin(\omega t)}{\omega^2}$, $\Phi_R(t) = \int_0^\infty d\omega J(\omega) \frac{1-\cos(\omega t)}{\omega^2}$, and $\zeta(t) = \int_0^t \varepsilon(t')\, dt'$. Assuming, as before, an Ohmic form of spectral density for oscillators environment, $\Phi_I(t)$ and $\Phi_R(t)$ are found to be (at zero temperature) $\Phi_I(t) = G \tan^{-1}(\omega_c t)$ and $\Phi_R(t) = \frac{G}{2} \ln(1 + \omega_c^2 t^2)$.

We now have everything we need to evaluate $\Gamma(\tau)$. It should be obvious from our expressions above that for the strong system-environment coupling strength G that we are considering here, $\Gamma(\tau)$ no longer depends on overlap of the generalized filter function with the spectrum of environment [58, 101]. Rather, $\Gamma(\tau)$ now shows a non-linear dependence on

[3]To avoid confusion, we use P to denote a projector, while (P) denotes the polaron frame.

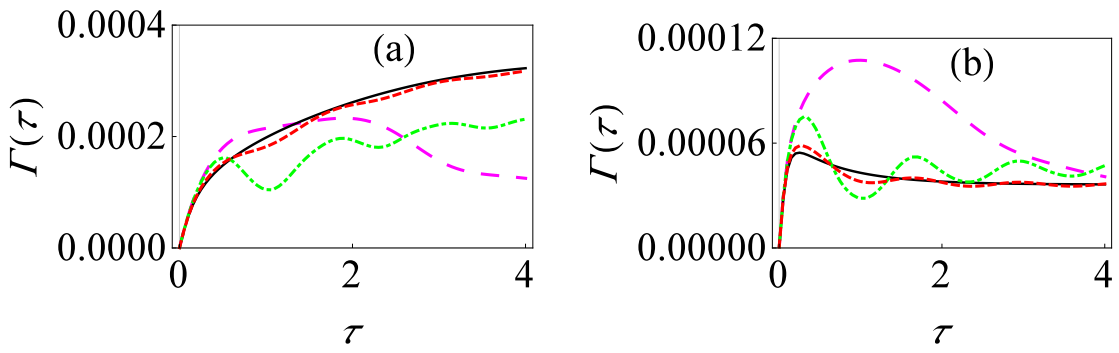

Figure 5.6: Graph of the effective decay rate $\Gamma(\tau)$ versus τ for strongly coupled driven spin-boson model: $\alpha(t) = \varepsilon_0 t + (V_0/\Omega)\sin(\Omega t)$, $\beta(t) = 0$ and $\gamma(t) = 0$ with $V_0 = 1$ and $\Omega = 5$ (dashed, red curve), $V_0 = 5$ and $\Omega = 1$ (large-dashed, magenta curve), and $V_0 = 5$ and $\Omega = 5$ (dot-dashed, green curve). The solid black curve shows $\alpha(t) = \varepsilon_0 t$, $\beta(t) = 0$ and $\gamma(t) = 0$. Here we have used $\Delta = 0.05$, $\omega_c = 10$ and $G = 1$. **(b)** Same as **(a)**, except that now $G = 2$.

$J(\omega)$ which then lead to very different qualitative behavior of $\Gamma(\tau)$, as compared with the usual weak coupling regime between system and its environment [58, 101]. For instance, as G increases, $e^{-\Phi_R(t)}$ decreases, and hence we anticipate $\Gamma(\tau)$ of central system to decrease. Most importantly for us, we expect that the driving fields have a drastic, non-trivial effect not only the value of $\Gamma(\tau)$ but also the quantum Zeno and the anti-Zeno behavior since the integrand in Eq. (5.41) obviously depends on the driving fields. To make these claims concrete, let us show behavior of $\Gamma(\tau)$. It is very clear from Fig. 5.6 that not only the driving fields affect the decay rate very significantly, but also that increasing G reduces the decay rate [compare Figs. 5.6(a) and (b)], in contrast with the weak coupling regime. Here again, we observe multiple oscillations in quantum Zeno to anti-Zeno regimes, as we increase Ω. Interestingly, Fig. 5.3(a) looks very similar to Fig. 5.6(b) despite having coupling strength G in different regimes. This similarity can be understood noting that in both cases, the pointer states are the eigenstates of the operator σ_z, and that in strong coupling regime of G, we have a population decay model in the polaron frame (see Eq. (5.40)). In both cases, the driving fields modulate the energy-level splitting. These similarities lead to the same

qualitative form of Fig. 5.3(a) and Fig. 5.6(b).

5.2 Summary

In this chapter, we started off by introducing a general formalism, to calculate decay rate of a system subjected to both periodic quantum projective measurements and driving fields, valid for weak coupling strength between system and environment [101]. We then applied this formalism to derive a general expression of decay rate for an arbitrary driven TLS. The decay rate is the overlap integral of spectrum of environment, and a filter function expressed using time-dependent Euler angles. These results were illustrated using population decay model, as well as, pure dephasing model. In both cases, the application of the driving fields very significantly changes the form of filter function of the central system, which then modifies (either enhances or minimizes) the effective decay rate and, consequently, quantum Zeno and the anti-Zeno regimes are altered. Interestingly, for population decay model, driving fields can lay bare the effect of non-rotating terms, even for weak system-environment coupling regime, that, we are dealing with. These results were then generalized to large spin systems to show a possible amplification of the decay rate. Finally, we also looked at driven two-level systems strongly coupled to harmonic oscillators environment, where the effective decay rate shows a non-linear dependence on $J(\omega)$ of environment. We showed once again that decay rate is modified by the application of driving fields. Our general expressions and insights should of interest in the broad areas of quantum control and quantum state engineering, such as quantum noise sensing, as well as in fundamental studies of the quantum Zeno and anti-Zeno effects. For example, a quantum system can be put into the Zeno regime, thereby protecting it from decoherence, by applying suitable control fields. On the other hand, the decay rate can be enhanced in the anti-Zeno regime via the applied control fields, and this can be useful for cooling the quantum system [182].

5.3 Methods

5.3.1 Effective decay rate using perturbation theory

We first discuss how to obtain effective decay rate of the system under frequent measurements [101], extending the treatment in Ref. [57] to time-dependent Hamiltonians. We first write total Hamiltonian as $H(t) = H_F(t) + H_{SB}$, where $H_F(t) = H_S(t) + H_B$ is sum of free system Hamiltonian and the environment Hamiltonian, and H_{SB} describes the system-environment interaction. Using standard perturbation approach, we set total unitary operator as $U(t) = U_F(t)U_I(t)$, where $U_F(t)$ describes the free time-evolution of the driven quantum system and its environment (this may be non-trivial and involve time-ordering due to the possible time dependence of H_S), and $U_I(t)$ is the leftover part that can be expanded perturbatively (assuming interaction strength between system and environment to be sufficiently weak) as $U_I(\tau) = \mathbb{1} + G_1 + G_2 + ...$, where G_1 and G_2 are the first and the second-order corrections respectively. Using this expansion, the reduced density matrix of system at time τ is

$$\rho_S(\tau) \approx \mathrm{Tr}_B\big[U_F(\tau)\big(\rho(0) + \rho(0)G_1^\dagger + G_1\rho(0) + \rho(0)G_2^\dagger + G_2\rho(0) + G_1\rho(0)G_1^\dagger\big)U_F^\dagger(\tau)\big]. \tag{5.42}$$

Perturbation theory tells us that

$$G_1 = -i\int_0^\tau dt_1 \widetilde{H}_{SB}(t_1), \tag{5.43}$$

and

$$G_2 = -\int_0^\tau dt_1 \int_0^{t_1} dt_2 \widetilde{H}_{SB}(t_1)\widetilde{H}_{SB}(t_2), \tag{5.44}$$

where $\widetilde{H}_{SB}(t) = U_F^\dagger(t)H_{SB}U_F(t) = \sum_\mu U_S^\dagger(t)F_\mu U_S(t) \otimes U_B^\dagger(t)B_\mu U_B(t) = \widetilde{F}_\mu(t)\widetilde{B}_\mu(t)$. Now we simplify Eq. (5.42), term by term, to get the reduced density matrix of the system at time τ. Firstly, we find the first term of Eq. (5.42)

$$\begin{aligned}\mathrm{Tr}_B[U_F(\tau)\rho(0)U_F^\dagger(\tau)] &= \mathrm{Tr}_B[U_B(\tau)\rho_B U_B^\dagger(\tau)]U_S(\tau)\rho_S(0)U_S^\dagger(\tau),\\ &= \widetilde{\rho}_S(\tau),\end{aligned} \tag{5.45}$$

with $\mathrm{Tr}_B[U_B(\tau)\rho_B U_B^\dagger(\tau)] = 1$, and $\rho(0) = \rho_S(0) \otimes \rho_B$. $\widetilde{\rho}_S(\tau) = U_S(\tau)\rho_S(0)U_S^\dagger(\tau)$ is the central system state, if system and environment are not interacting. The second term of Eq. (5.42) gives

$$\begin{aligned}\mathrm{Tr}_B[U_F(\tau)\rho(0)G_1^\dagger U_F^\dagger(\tau)] &= i\sum_\mu \int_0^\tau dt_1 \mathrm{Tr}_B[U_B(\tau)\rho_B \widetilde{B}_\mu(t_1)U_B^\dagger(\tau)]U_S(\tau)\rho_S(0)\widetilde{F}_\mu(t_1)U_S^\dagger(\tau), \\ &= i\sum_\mu \int_0^\tau dt_1 \langle \widetilde{B}_\mu(t_1)\rangle_F U_S(\tau)\rho_S(0)\widetilde{F}_\mu(t_1)U_S^\dagger(\tau), \end{aligned} \tag{5.46}$$

with $\mathrm{Tr}_B[\rho_B \tilde{B}_\mu(t)] = \langle \widetilde{B}_\mu(t_1)\rangle_B$. Similarly, the third term is

$$\mathrm{Tr}_B[U_F(\tau)G_1\rho(0)U_F^\dagger(\tau)] = -i\sum_\mu \int_0^\tau dt_1 \langle \widetilde{B}_\mu(t_1)\rangle_B U_S(\tau)\widetilde{F}_\mu(t_1)\rho_S(0)U_S^\dagger(\tau). \tag{5.47}$$

Now, $\langle \widetilde{B}_\mu(t_1)\rangle_B$ is zero[4] for system-environment assumptions generally considered in this chapter. Next, we find the fourth term of Eq. (5.42) to be

$$\mathrm{Tr}_B[U_F(\tau)\rho(0)G_2^\dagger U_F^\dagger(\tau)] \tag{5.48}$$

$$\begin{aligned} &= -\sum_{\mu\nu}\int_0^\tau dt_1 \int_0^{t_1} dt_2 \mathrm{Tr}_B[U_B(\tau)\rho_B \widetilde{B}_\nu(t_2)\widetilde{B}_\mu(t_1)U_B^\dagger(\tau)]U_S(\tau)\rho_S(0)\widetilde{F}_\nu(t_2)\widetilde{F}_\mu(t_1)U_S^\dagger(\tau), \\ &= -\sum_{\mu\nu}\int_0^\tau dt_1 \int_0^{t_1} dt_2 \langle \widetilde{B}_\nu(t_2)\widetilde{B}_\mu(t_1)\rangle_B U_S(\tau)\rho_S(0)\widetilde{F}_\nu(t_2)\widetilde{F}_\mu(t_1)U_S^\dagger(\tau), \\ &= -\sum_{\mu\nu}\int_0^\tau dt_1 \int_0^{t_1} dt_2 C_{\nu\mu}(t_2,t_1)U_S(\tau)\rho_S(0)\widetilde{F}_\nu(t_2)\widetilde{F}_\mu(t_1)U_S^\dagger(\tau), \end{aligned} \tag{5.49}$$

with $\mathrm{Tr}_B[\rho_B \widetilde{B}_\nu(t)\widetilde{B}_\mu(t')] = \langle \widetilde{B}_\nu(t)\widetilde{B}_\mu(t')\rangle_B = C_{\nu\mu}(t,t')$. Similarly, the fifth term is

[4]The interaction term contains $b_k^\dagger$ and b_k. These operators have zero diagonal elements in the eigenbasis of H_B.

$$\mathrm{Tr}_B[U_F(\tau)G_2\rho(0)U_F^\dagger(\tau)] \;=\; -\sum_{\mu\nu}\int_0^\tau dt_1\int_0^{t_1} dt_2 C_{\mu\nu}(t_1,t_2)U_S(\tau)\widetilde{F}_\mu(t_1)\widetilde{F}_\nu(t_2)\rho_S(0)U_S^\dagger(\tau). \tag{5.50}$$

Finally, the last term is

$$\mathrm{Tr}_B[U_F(\tau)G_1\rho(0)G_1^\dagger U_F^\dagger(\tau)] \;=\; \sum_{\mu\nu}\int_0^\tau dt_1\int_0^{\tau} dt_2 C_{\nu\mu}(t_2,t_1)U_S(\tau)\widetilde{F}_\mu(t_1)\rho_S(0)\widetilde{F}_\nu(t_2)U_S^\dagger(\tau). \tag{5.51}$$

Using the fact that $\int_0^\tau dt_2\int_0^{t_2} dt_1 + \int_0^\tau dt_1\int_0^{t_1} dt_2 = \int_0^\tau dt_1\int_0^\tau dt_2$ in Eq. (5.51), we have

$$\begin{aligned}\mathrm{Tr}_B[U_F(\tau)G_1\rho(0)G_1^\dagger U_F^\dagger(\tau)] = &\sum_{\mu\nu}\int_0^\tau dt_1\int_0^{t_1} dt_2 C_{\nu\mu}(t_2,t_1)U_S(\tau)\widetilde{F}_\mu(t_1)\rho_S(0)\widetilde{F}_\nu(t_2)U_S^\dagger(\tau)\\ &+\sum_{\mu\nu}\int_0^\tau dt_1\int_0^{t_1} dt_2 C_{\mu\nu}(t_1,t_2)U_S(\tau)\widetilde{F}_\nu(t_2)\rho_S(0)\widetilde{F}_\mu(t_1)U_S^\dagger(\tau).\end{aligned} \tag{5.52}$$

Putting all above terms of $\rho_S(\tau)$ back together, we find that

$$\rho_S(\tau) = U_S(\tau)\bigg(\rho_S(\tau)+\sum_{\mu\nu}\int_0^\tau dt_1\int_0^{t_1} dt_2 C_{\mu\nu}(t_1,t_2)[\widetilde{F}_\nu(t_2)\rho_S(0),\widetilde{F}_\mu(t_1)]+\mathrm{h.c.}\bigg)U_S^\dagger(\tau). \tag{5.53}$$

Here h.c. represents hermitian conjugate. Since, correlation function of environment $C_{\mu\nu}(t_1,t_2)$ depends on the time difference (t_1-t_2) only[5], we are motivated to introduce a new variable $t'=(t_1-t_2)$. In terms of t', the central system state is

$$\rho_S(\tau) = U_S(\tau)\bigg(\rho_S(0)+\sum_{\mu\nu}\int_0^\tau dt_1\int_0^{t_1} dt' C_{\mu\nu}(t')[\widetilde{F}_\nu(t_1-t')\rho_S(0),\widetilde{F}_\mu(t_1)]+\mathrm{h.c.}\bigg)U_S^\dagger(\tau). \tag{5.54}$$

[5]The environment is in thermal equilibrium state proportional to $e^{-\beta H_B}$.

Once we have expression for $\rho_S(\tau)$, we can evaluate survival probability of the system in the initial state. Since, we want to investigating system evolution due to H_{SB} only, we first apply the free driven system unitary operator on both sides of Eq. (5.54) to take away evolution of central system due to free driven system's Hamiltonian $H_S(t)$. Note that, this may not be necessary if $U_S(\tau)$ commutes with $\rho_S(0)$. We thereafter find probability that central system is still in initial state $|\psi\rangle$ after a projective measurement given by projector $|\psi\rangle\langle\psi|$ to be given by[6]

$$s(\tau) = 1 - \mathrm{Tr}_S\left[P_\perp\left(\rho_S(0) + \sum_{\mu\nu}\int_0^\tau dt_1 \int_0^{t_1} dt' C_{\mu\nu}(t')[\widetilde{F}_\nu(t_1 - t')\rho_S(0), \widetilde{F}_\mu(t_1)] + \text{h.c.}\right)\right], \quad (5.55)$$

where $P_\perp$ is the projector onto the subspace orthogonal to $|\psi\rangle\langle\psi|$. Using the fact that $\mathrm{Tr}_S[P_\perp\rho_S(0)] = 0$, $\mathrm{Tr}_S[P_\perp\widetilde{F}_\mu(t_1)\widetilde{F}_\nu(t_2)\rho_S(0)] = 0$ and $\mathrm{Tr}[R + R^\dagger] = 2\mathrm{Re}(\mathrm{Tr}[R])$, where Re stands for real part, we have

$$s(\tau) = 1 - 2\mathrm{Re}\left(\sum_{\mu\nu}\int_0^\tau dt \int_0^t dt' C_{\mu\nu}(t')\mathrm{Tr}_S\big[P_\perp\widetilde{F}_\nu(t - t')\rho_S(0)\widetilde{F}_\mu(t)\big]\right), \quad (5.56)$$

where we have also replaced the t_1 by t for notational simplicity. As usual, after performing a sequence of M repeated projective measurements, we find the survival probability that the system state is still present in the initial state is $S(M\tau) = [s(\tau)]^M$ if the system-environment correlations are ignored during the evolution. We can then find decay rate by $S(M\tau) = e^{-\Gamma(\tau)M\tau}$ which allows us to write $\Gamma(\tau) = -\ln s(\tau)/\tau$. In weak coupling between central system and environmet, we can further write[7]

$$\Gamma(\tau) = \frac{2}{\tau}\mathrm{Re}\left(\sum_{\mu\nu}\int_0^\tau dt \int_0^t dt' C_{\mu\nu}(t')\mathrm{Tr}_S\big[P_\perp\widetilde{F}_\nu(t - t')\rho_S(0)\widetilde{F}_\mu(t)\big]\right). \quad (5.57)$$

[6]Here Tr_S is the trace with respect to system.

[7]$\ln(1 - x) \approx x$, for $x \ll 1$.

This can be cast into the form

$$\Gamma(\tau) = \int_0^\infty d\omega\, Q(\omega,\tau) J(\omega),$$

with $Q(\omega,\tau)$ given in Eq. (5.3).

5.3.2 Finding the filter function for the driven large-spin population decay model

In this case, using the standard angular momentum relations $[J_i, J_j] = i\varepsilon_{ijk}J_k$, we evaluate

$$\widetilde{F}(t) = 2\big(J_x c_x(t) + J_y c_y(t) + J_z c_z(t)\big), \tag{5.58}$$

where

$$\begin{aligned} c_x(t) &= \cos[\alpha(t)]\cos[\beta(t)\cos[\gamma(t)] - \sin[\alpha(t)]\sin[\gamma(t)], \\ c_y(t) &= \cos[\alpha(t)]\cos[\beta(t)\sin[\gamma(t)] + \sin[\alpha(t)]\cos[\gamma(t)], \\ c_z(t) &= -\cos[\alpha(t)]\sin[\beta(t)]. \end{aligned} \tag{5.59}$$

For $\rho_S(0) = |j,j\rangle\langle j,j|$ and $P_\perp = \sum_{m=1}^{j-1} |j,m\rangle\langle j,m|$ with $J_z|j,m\rangle = m|j,m\rangle$, we have

$$\mathrm{Tr}_S\big[P_\perp \widetilde{F}(t-t')\rho_S(0)\widetilde{F}(t)\big] = \sum_{m=1}^{j-1} \langle j,m|\,\widetilde{F}(t-t')\,|j,j\rangle\,\langle j,j|\,\widetilde{F}(t)\,|j,m\rangle\,. \tag{5.60}$$

We next note that $\langle j,j|\,\widetilde{F}(t)\,|j,m\rangle = \sqrt{2j}\delta_{j-1,m}\big(c_x(t) - ic_y(t)\big)$. This leads to the generalized filter function

$$Q(\omega,t) = (2j)\frac{2}{\tau}\int_0^\tau dt \int_0^t dt' \big(D_1(t,t') + D_2(t,t') + D_3(t,t') + D_4(t,t')\big),$$

where expressions of $D_1(t,t')$, $D_2(t,t')$, $D_3(t,t')$ and $D_4(t,t')$ are defined in Eqs. (5.17)-(5.20).

5.3.3 Spin-boson Hamiltonian in polaron frame

To transform Hamiltonian of driven spin-boson model to polaron frame, we need to find

$$H^{(P)}(t) = e^{\chi\sigma_z/2} H(t) e^{-\chi\sigma_z/2}. \tag{5.61}$$

We use identity called Hadamard lemma

$$e^{A} O e^{-A} = O + [A, O] + \frac{1}{2!}[A, [A, O]] + ... \tag{5.62}$$

where $A = \chi\sigma_z/2$, with $\chi = \sum_k [\frac{2g_k}{\omega_k} b_k^\dagger - \frac{2g_k^*}{\omega_k} b_k]$ and $O = H(t) = \frac{\varepsilon(t)}{2}\sigma_z + \frac{\Delta}{2}\sigma_x + \sum_k \omega_k b_k^\dagger b_k + \sigma_z \sum_k (g_k^* b_k + g_k b^\dagger)$. We find that

$$e^{\chi\sigma_z/2} \sigma_z e^{-\chi\sigma_z/2} = \sigma_z,$$

and

$$e^{\chi\sigma_z/2} \sigma_x e^{-\chi\sigma_z/2} = \sigma_+ e^{\chi} + \sigma_- e^{-\chi}.$$

σ_- and σ_+ are the standard spin-1/2 lowering and raising operators. Carrying on further, we find

$$e^{\chi\sigma_z/2} (\sum_k \omega_k b_k^\dagger b_k) e^{-\chi\sigma_z/2} = \sum_k \omega_k b_k^\dagger b_k - \sigma_z \sum_k (g_k^* b_k + g_k b^\dagger) + \sum_k \frac{|g_k|^2}{\omega_k}.$$

Similarly

$$e^{\chi\sigma_z/2} \left(\sigma_z \sum_k (g_k^* b_k + g_k b^\dagger) \right) e^{-\chi\sigma_z/2} = \sigma_z \sum_k (g_k^* b_k + g_k b^\dagger) - 2 \sum_k \frac{|g_k|^2}{\omega_k}, \tag{5.63}$$

The third term of Eq. (5.62) in the above expression is a constant number, so higher-order commutators are zero. Now putting all these terms back together, the required driven Hamiltonian in rotated frame takes the following form

$$H^{(P)}(t) = \frac{\varepsilon(t)}{2}\sigma_z + \sum_k \omega_k b_k^\dagger b_k + \frac{\Delta}{2}(\sigma_+ Y + \sigma_- Y^\dagger) - \sum_k \frac{|g_k|^2}{\omega_k}, \tag{5.64}$$

with $Y = e^{\chi}$, and $\sum_k \frac{|g_k|^2}{\omega_k}$ is a constant number term that gives a constant shift in transformed Hamiltonian, and can thus be dropped.

5.3.4 Effective decay rate of driven spin-boson model in polaron frame

Since coupling between system and environment is weak in polaron frame therefore we can use expression [see Eq. (5.57)] to calculate effective decay rate. For $\rho_S(0) = |e\rangle\langle e|$ and $P_\perp = |g\rangle\langle g|$, use identity $F_1 = \frac{\Delta}{2}\sigma_+$, $F_2 = \frac{\Delta}{2}\sigma_-$, $B_1 = Y$, $B_2 = Y^\dagger$, $\widetilde{F}_1(t) = \frac{\Delta}{2}\sigma_+ e^{i\zeta(t)}$ and $\widetilde{F}_2(t) = \frac{\Delta}{2}\sigma_- e^{-i\zeta(t)}$ with $\zeta(t) = \int_0^t dt'\varepsilon(t')$ leading us to

$$\Gamma(\tau) = \frac{2}{\tau}\mathrm{Re}\bigg(\int_0^\tau dt \int_0^t dt' C_{12}(t') e^{i(\zeta(t)-\zeta(t-t'))}\bigg). \tag{5.65}$$

To get expression of effective decay rate, the environment correlation function $C_{12}(t)$ needs to be worked out. We now show the details how to find C_{12}. As we know $C_{12}(t) = \mathrm{Tr}_B[\rho_B \widetilde{B}_1(t) B_2]$, with $B1 = Y$, $B_2 = Y^\dagger$, $\widetilde{B}_1(t) = e^{iH_B^{(P)}t} Y e^{-iH_B^{(P)}t}$, $H_B^{(P)} = \sum_k \omega_k b_k^\dagger b_k$, $Y = e^{\chi}$ and $\chi = \sum_k [\frac{2g_k}{\omega_k} b_k^\dagger - \frac{2g_k^*}{\omega_k} b_k]$. Next, we calculate

$$\widetilde{B}_1(t) = e^{\sum_k \left(\frac{g_k}{\omega_k} b_k^\dagger e^{i\omega_k t} - \frac{g_k^*}{\omega_k} b_k e^{-i\omega_k t}\right)}, \tag{5.66}$$

using the fact $U^\dagger(t) e^A U(t) = e^{U^\dagger(t) A U(t)}$, and then find

$$\widetilde{B}_1(t) B_2 = e^{-i\sum_k \frac{|g_k|^2}{\omega_k^2}\sin(\omega_k t)} e^{\sum_k \left(\frac{g_k}{\omega_k} b_k^\dagger (e^{i\omega_k t}-1) + \frac{g_k^*}{\omega_k} b_k (e^{-i\omega_k t}-1)\right)}. \tag{5.67}$$

In order to convert double exponential in a single exponential to use useful fact $\mathrm{Tr}_B[\rho_B e^C] = e^{\langle C^2\rangle/2}$, where operator C is a linear combination [43] of the creation and the annihilation operators; we use the identity $e^X e^Y = e^{X+Y+\frac{1}{2}[X,Y]}$. Fortunately in this case, first commutator is a constant number, so higher order commutators are zero. Finally we have

$$C_{12}(t) = e^{-i\Phi_I(t)} e^{-\Phi_R(t)}. \tag{5.68}$$

where $\Phi_I(t)$ and $\Phi_R(t)$ have been defined before. Carrying on further,we have

$$\Gamma(\tau) = \frac{\Delta^2}{2\tau} \int_0^\tau dt \int_0^t dt' \cos[\zeta(t) - \zeta(t-t') - \Phi_I(t')] e^{-\Phi_R(t')}. \tag{5.69}$$

Chapter 6

The quantum Zeno and anti-Zeno effects with a composite environment

Until now, we have investigated the quantum Zeno and anti-Zeno effects for a quantum system directly coupled to an environment with a large number of degrees of freedom. The question then arises: what happens, if central system is indirectly coupled to environment [5, 6, 173]? In other words, we consider an environment that is not as simple as what we have analyzed in the previous chapters, yet still experimentally realizable [113, 183–191]. Namely, we can consider a situation where a central two-level system is coupled directly to only a single two-level system, or a single harmonic oscillator mode (the 'near environment'), which in turn is coupled to a large collection of two-level systems or harmonic oscillators (the 'far environment'). Such composite environments have been used before to study, for instance, non-Markovianity as well as pointer states [173]. In this chapter, we start by evaluating a general expression for finding effective decay rate of central system coupled to a composite environment, assuming only weak coupling between the near and the far environments. We then use this expression in a case where central system consisting of a single TLS is indirectly coupled to a harmonic oscillator environment at zero temperature via a single harmonic oscillator. Interestingly, we find that by increasing the coupling between near-far environment, the effective decay rate of the system can either decrease or increase.

6.1 The Model

We model the system and its environment as being made of three parts: the central system S, the 'near' environment N, and the 'far' environment F with Hilbert spaces $\mathcal{H}_{\mathcal{S}}$, $\mathcal{H}_{\mathcal{N}}$, and $\mathcal{H}_{\mathcal{F}}$ respectively. We assume that the central system is directly coupled only to the near environment; the system is only indirectly coupled to the far environment due to the interaction between the near environment and the far environment. To make the problem tractable, we suppose that this interaction between near and far environments is weak. For composite environment, the total Hamiltonian is written as

$$H = H_{S,N} + H_F + H_{NF}, \tag{6.1}$$

with

$$H_{S,N} = H_S + H_N + H_{SN}. \tag{6.2}$$

Here the Hamiltonians H_S, H_N and H_F are the Hamiltonians of central system, near environment and far environment respectively, with $H_{SN} = V_S \otimes V_N \otimes \mathbb{1}_F$ being the interaction Hamiltonian between the central system and the near environment, and $H_{NF} = \mathbb{1}_S \otimes V'_N \otimes V_F$ is the interaction between the near and far environment. Although, we work out a general framework for finding decay rate of central system (see the Methods section), here we consider the case, where a two-level system interacts with a single harmonic oscillator mode, which in turn interacts with a set of other harmonic oscillators [191–193]. For spin-1/2 central system, harmonic oscillator near environment and harmonic oscillators far environment, total Hamiltonian is written as

$$H = H_{S,N} + H_F + H_{NF}, \tag{6.3}$$

with

$$H_{S,N} = \frac{\varepsilon}{2}\sigma_z + \Omega a^\dagger a + \gamma(a\sigma_+ + a^\dagger\sigma_-), \tag{6.4}$$

$$H_F = \sum_k \omega_k b_k^\dagger b_k, \tag{6.5}$$

$$H_{NF} = \sum_k (g_k b_k a^\dagger + g_k^* b_k^\dagger a). \tag{6.6}$$

Here, $H_{S,N}$ in the total Hamiltonian which describes the central two-level system, the single harmonic oscillator near environment, as well as the interaction between them. The interaction between them has been taken to be of the Jaynes-Cummings form, with the rotating-wave approximation made [134, 194]. The parameter ε describes the energy-level spacing of the two-level system, and Ω and ω_k are used to represent the frequencies of single harmonic oscillator mode (the near environment) and the set of other harmonic oscillators (the far environment) respectively. Moreover, $\sigma_-(\sigma_+)$ are the standard lowering(raising) operators acting in the space of two-level system, while $a(a^\dagger)$ are the creation(annihilation) operators acting in the space of near environment. Also, $b_k(b_k^\dagger)$ are the annihilation(creation) operators acting solely in the space of far environment. Finally, parameter γ is the interaction strength between central system and the near environment, while g_k describes the coupling strength between the near and the far environment.

To proceed, it is very helpful to write the part of Hamiltonian corresponding to two-level system, and near environment as a sum of two commuting parts, that is,

$$H_{S,N} = H_1 + H_2, \tag{6.7}$$

with

$$H_1 = \frac{\Omega}{2}\sigma_z + \Omega a^\dagger a, \tag{6.8}$$

and

$$H_2 = \frac{\delta}{2}\sigma_z + \gamma(a\sigma^+ + a^\dagger\sigma^-), \tag{6.9}$$

where $\delta = \varepsilon - \Omega$ is the relative detuning of energy spacing ε from the frequency of single harmonic oscillator mode Ω. As usual, we consider initial state of central system to be the excited state $|e\rangle$ of the two-level system. The state orthogonal to the excited state is then $|g\rangle$, that is, $\langle e|\, g\rangle = 0$. At time intervals τ, we perform selective projective measurements on the central system in σ_z basis $\{|e\rangle, |g\rangle\}$ to compute effective decay rate that system ends up

in state $|e\rangle$ [56–59, 101]. We find that the effective decay rate of central TLS (after removal of evolution due to H_S Hamiltonian) is (For details, see Methods section 6.3)

$$\Gamma(\tau) = -\frac{1}{\tau}\ln\Bigg\{\frac{1}{X^2}\big(K^2+\gamma^2\cos^2(X\tau)\big) - 2\sum_k |g_k|^2 \int_0^\tau dt \int_0^t dt'\gamma^2 \left(\frac{\sin(X(t-t'))}{X^2}\right)\times$$
$$\Bigg[\cos[(\omega_k-\Omega-K)t']H_1(t,\tau) - K\sin[(\omega_k-\Omega-K)t']H_2(t,\tau)\Bigg]\Bigg\}, \tag{6.10}$$

with $X = \sqrt{\frac{\delta^2}{4}+\gamma^2}$, $K = \dfrac{\delta}{2}$, $H_1(t,\tau) = \sin(Xt) - \sin(X\tau)\cos[X(t-\tau)]$ and $H_2(t,\tau) = \dfrac{\sin(X\tau)}{X}\sin[X(t-\tau)]$. Notice that this expression is very different from the usual sinc-squared form [101] acquired from the usual population decay model [7]. Even though, environment is a set of harmonic oscillators in both cases, our model has a crucial difference: the two-level system in our case only couples to a single harmonic oscillator, and this single harmonic oscillator in turn couples to all the other harmonic oscillators. This differs from the commonly studied population decay model [7] where the central two-level system directly couples to all the harmonic oscillators comprising the environment.

With the analytical expression for the decay rate of the two-level system in hand, we now analyze the behavior the decay rate $\Gamma(\tau)$. For continuous environment, we replace sum over oscillator modes in far environment by an integral in the usual manner via $\sum_k |g_k|^2(\ldots) \to \int_0^\infty d\omega\, J(\omega)(\ldots)$ [3, 56, 58], thereby introducing the spectral density function $J(\omega)$. Throughout, we will use an Ohmic spectral density with an exponential cutoff to illustrate our results, that is, $J(\omega) = G\omega e^{-\omega/\omega_c}$, where G is the dimensionless system-environment coupling strength, and ω_c is the cutoff frequency. In Fig. (6.1), we have plotted the effective decay rate $\Gamma(\tau)$ as a function of the measurement interval τ for a fixed system-environment coupling γ and varying values of the near environment-far environment coupling. The solid green curve is the decay rate for coupling strength $G = 0$, the large-dashed black curve is the decay rate for $G = 0.05$, the small-dashed red curve is the decay rate for $G = 0.1$, and the dot-dashed magenta curve is the decay rate for $G = 0.2$. We observe that increasing the value of near-far environment coupling strength G shifts the value of Zeno time towards smaller values of τ. Therefore, in our plotted results, we can notice only the QZE for the weak coupling regime $G = 0$ and $G = 0.05$, while both QZE and QAZE

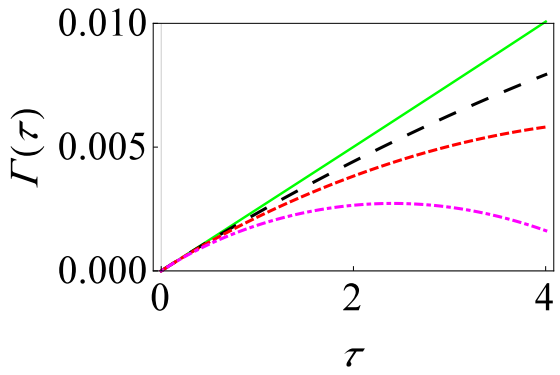

Figure 6.1: Behavior of $\Gamma(\tau)$ versus time τ with system-environment model defined in Eq. (6.3) for different values of the coupling strength between the near and the far environment. The curves show the behavior with $G = 0$ (solid, green curve), $G = 0.05$ (large-dashed, black curve), $G = 0.1$ (small-dashed, red curve) and $G = 0.2$ (dot-dashed, magenta curve) for a fixed value of $\gamma = 0.05$ at zero temperature. Here, we have set $\delta = 0$ with $\hbar = 1$. The initial state of the central system is prepared along excited state $|\psi\rangle = |e\rangle$, and $\Omega = 1$ and $\omega_c = 10$.

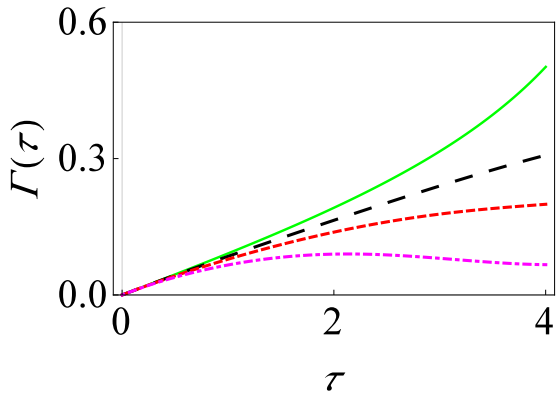

Figure 6.2: Same as Fig. 6.1, except that now $\gamma = 0.3$ and $\delta = 0.05$.

are observed for relatively stronger coupling strengths $G = 0.1$ and $G = 0.2$. Moreover, very surprisingly, for the sequence of increasing coupling strengths, the peak value of $\Gamma(\tau)$ decreases. This means that far environment neutralizes the near environment effect on the central system, and the system is protected from the presence of near environment by the

relatively strong coupling of near environment with the far environment. We also observe that increasing the value of γ from weak [Fig. 6.1] to relatively strong [Fig. 6.2] increases $\Gamma(\tau)$ of system, as central system has direct interaction with the near environment.

We now modify the form of interaction term between central system and near environment. Namely, we consider a dephasing interaction between central system and near environment. The total Hamiltonian is

$$H = H_{S,N} + H_F + H_{NF}, \tag{6.11}$$

with

$$H_{S,N} = \frac{\varepsilon}{2}\sigma_z + \Omega a^\dagger a + \frac{\lambda}{2}\sigma_z(a + a^\dagger), \tag{6.12}$$

and

$$H_F = \sum_k \omega_k b_k^\dagger b_k, \tag{6.13}$$

$$H_{NF} = \sum_k (g_k b_k a^\dagger + g_k^* b_k^\dagger a). \tag{6.14}$$

Here, λ stands for coupling between central system and near environment, and the remaining parameters are described as before. The initial central system state that we prepare at $t = 0$ is the linear superposition of the excited and ground states $\frac{1}{\sqrt{2}}(|e\rangle + |g\rangle)$, and the state orthogonal to this state is $\frac{1}{\sqrt{2}}(|e\rangle - |g\rangle)$. We now calculate the effective decay rate to be (for details, see Methods subsection 6.3)

$$\Gamma(\tau) =$$
$$-\frac{1}{\tau}\ln\Bigg\{\frac{1}{2}[1 + e^{-\gamma(\tau)}] - 2\sum_k |g_k|^2 \frac{\lambda^2}{\Omega^2}\sin\left(\frac{\Omega}{2}\tau\right) e^{-\gamma(\tau)} \int_0^\tau dt \int_0^t dt' \cos[\omega_k t' + \frac{\Omega}{2}(t-\tau)]\times$$
$$\sin\left[\frac{\Omega}{2}(t-t')\right] - 2\sum_k |g_k|^2 \frac{\lambda^2}{\Omega^2} e^{-\gamma(\tau)} \int_0^\tau dt \int_0^t dt' \cos\left[\omega_k t' - \frac{\Omega}{2}t'\right] \sin\left[\frac{\Omega}{2}(t-t')\right] \sin\left(\frac{\Omega}{2}t\right)\Bigg\}, \tag{6.15}$$

where $\gamma(\tau) = \frac{\lambda^2}{\Omega^2}[1 - \cos(\Omega\tau)]$. In Figs. 6.3 and 6.4, we show the effective decay rate $\Gamma(\tau)$ of central two-level system as a function of τ with weak and relatively strong coupling strength between the central system and the near environment for different values of G.

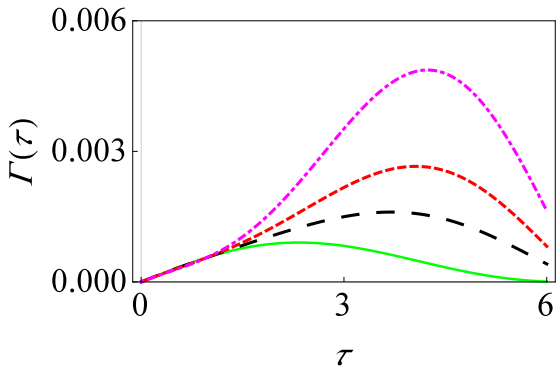

Figure 6.3: (a) Behavior of $\Gamma(\tau)$ versus time τ with system-environment model defined in Eq. (6.11). We have used different values of coupling strength between the near and the far environment, with $G = 0$ (solid, green curve), $G = 0.05$ (large-dashed, black curve), $G = 0.1$ (small-dashed, red curve) and $G = 0.2$ (dot-dashed, magenta curve), with a fixed value of $\lambda = 0.05$ at zero temperature. As usual, we have set $\hbar = 1$. The initial state of central system prepared is $|\psi\rangle = \frac{1}{\sqrt{2}}(|e\rangle + |g\rangle)$ with $\Omega = 1$ and $\omega_c = 10$.

It is noted that now, in contrast with the dissipative interaction between the system and the near-environment scenario discussed previously, the effective decay rate increases as we increase the coupling strength G between the near and the far environment. As we increase G, the influence of the far-environment on the system via the near-environment becomes more dominant, leading to a larger effective decay rate. It should be noted, however, that we cannot address the scenario where the near-environment and far-environment are interacting very strongly using our perturbative approach. It may be the case that in this strong regime, $\Gamma(\tau)$ shows different qualitative behavior.

6.2 Summary

We have used a simple model to explore the effect of a composite environment on the behavior of QZE and QAZE in a central system. The central system is coupled via a small intermediate system called the near environment; in turn, the near environment is coupled

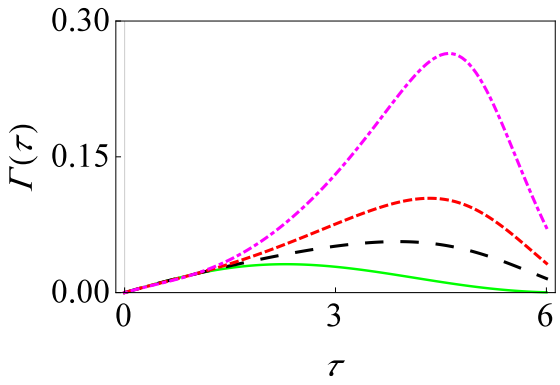

Figure 6.4: Same as Fig. 6.3, except that now $\lambda = 0.3$.

to a far environment having many or infinite degrees of freedom. In particular, we consider the central system to be a two-level system, the near environment to be a single harmonic oscillator, and the far environment to be a collection of harmonic oscillators. Assuming that the initial state of the total system is a product state of the central system plus the near and the far environment, we have obtained the effective decay rate. By applying these expressions, we have observed a highly non-trivial dependence of the decay rate on the coupling strengths as well as the nature of system-near environment coupling. Namely, we observe that increasing the near environment-far environment coupling can decrease the effective decay rate if the coupling is of dissipative form, while for a dephasing coupling, increasing coupling strengths enhances the effective decay rate.

6.3 Methods: The effective decay rate using perturbation theory

We are interested in studying the effect of the composite environment on the behavior of the quantum Zeno and anti-Zeno effects for the central system. For this purpose, we need to figure out effective decay rate [82] of central system. We first find density matrix of the central system by tracing out both the near and the far environment. If the total density

matrix is $\rho_{\rm tot}(\tau)$, then

$$\rho_S(\tau) = {\rm Tr}_{N,F}[\rho_{\rm tot}(\tau)]. \tag{6.16}$$

Since, the total density matrix evolves via a total unitary operator $U(\tau)$, until the first measurement is performed,

$$\rho_{\rm tot}(\tau) = U(\tau)\rho_{\rm tot}(0)U^\dagger(\tau). \tag{6.17}$$

Furthermore, we assume the absence of the initial correlations between the subsystems, that is the initial state of total system is in the product state

$$\rho_{\rm tot}(0) = \rho_S(0) \otimes \rho_N(0) \otimes \rho_F, \tag{6.18}$$

with $\rho_S(0)$ the initial state of the central system, and $\rho_N = e^{-\beta H_N}/Z_N$ and $\rho_F = e^{-\beta H_F}/Z_F$ the thermal equilibrium states of near and far environments respectively, with $Z_N = {\rm Tr}_N[e^{-\beta H_N}]$ and $Z_F = {\rm Tr}_F[e^{-\beta H_F}]$. As usual, it is generally not possible to calculate exact form of time-evolution operator $U(\tau)$. However, we can use perturbation theory if coupling between near-far environment is sufficiently weak. For weak coupling between near environment and far environment, the total time-evolution operator is $U(\tau) = U_0(\tau)U_I(\tau)$, where $U_0(\tau) = e^{-i(H_S+H_N+H_F+H_{SN})\tau}$ is the unitary operator due to H_{SN} Hamiltonian[1], and $U_I(\tau)$ is the unitary operator due to near-far environment interaction. Using perturbation theory, $U_I(\tau)$ can be written as $U_I(\tau) = \mathbb{1} + G_1 + G_2 + ...$, where G_1 and G_2 are the first and the second-order corrections respectively. Then we can write Eq. (6.16) as

$$\rho_S(\tau) = {\rm Tr}_{N,F}\big[U_0(\tau)\big(\rho_{\rm tot} + \rho_{\rm tot}G_1^\dagger + G_1\rho_{\rm tot} + \rho_{\rm tot}G_2^\dagger + G_2\rho_{\rm tot} + G_1\rho_{\rm tot}G_1^\dagger\big)U_0^\dagger(\tau)\big], \tag{6.19}$$

correct up to second order in coupling strength between near-far environments. Also

$$G_1 = -i\int_0^\tau dt_1 \widetilde{H}_{NF}(t_1), \tag{6.20}$$

and

$$G_2 = -\int_0^\tau dt_1 \int_0^{t_1} dt_2 \widetilde{H}_{NF}(t_1)\widetilde{H}_{NF}(t_2), \tag{6.21}$$

[1]Here, we will consider its exact form only.

where $\widetilde{H}_{NF}(\tau) = U_0^\dagger(\tau)H_{NF}U_0(\tau) = U_{S,N}^\dagger(\tau)V_N'U_{S,N}(\tau) \otimes U_F^\dagger(\tau)V_F U_F(\tau) = \widetilde{V}_N'(\tau)\widetilde{V}_F(\tau)$. Now, we simplify Eq. (6.19) term by term to find the reduced density matrix of the central system at time τ. First, we find the first term of Eq. (6.19).

$$\mathrm{Tr}_{N,F}[U_0(\tau)\rho_{\mathrm{tot}}(0)U_0^\dagger(\tau)] = \widetilde{\rho}_S(\tau), \tag{6.22}$$

with $\mathrm{Tr}_F[U_F(\tau)\rho_F U_F^\dagger(\tau)] = 1$ and $\rho_{SN}(0) = \rho_S(0) \otimes \rho_N(0)$. $\widetilde{\rho}_S(\tau)$ is the central system density matrix if near and the far environments are not interacting with each other. The second term of Eq. (6.19) gives

$$\mathrm{Tr}_{N,F}[U_0(\tau)\rho_{\mathrm{tot}}(0)G_1^\dagger U_0^\dagger(\tau)] = i\int_0^\tau dt_1 \langle\widetilde{V}_F(t_1)\rangle_F \mathrm{Tr}_N[U_{S,N}(\tau)\rho_{SN}(0)\widetilde{V}_N'(t_1)U_{S,N}^\dagger(\tau)], \tag{6.23}$$

with $\mathrm{Tr}_F[\rho_F\tilde{V}_F(t_1)] = \langle\widetilde{V}_F(t_1)\rangle_F$. Similarly, the third term is

$$\mathrm{Tr}_{N,F}[U(\tau)G_1\rho_{\mathrm{tot}}(0)U^\dagger(\tau)] = -i\int_0^\tau dt_1 \langle\widetilde{V}_F(t_1)\rangle_F \mathrm{Tr}_N[U_{S,N}(\tau)\widetilde{V}_N'(t_1)\rho_{SN}(0)U_{S,N}^\dagger(\tau)]. \tag{6.24}$$

$\tilde{V}_F(t)$ is zero for the far environment we have considered. Next, we find the fourth term of Eq. (6.19) to be

$$\begin{aligned}&\mathrm{Tr}_{N,F}[U_0(\tau)\rho_{\mathrm{tot}}(0)G_2^\dagger U_0^\dagger(\tau)] = \\ &-\int_0^\tau dt_1 \int_0^{t_1} dt_2 C(t_2,t_1)\mathrm{Tr}_N[U_{S,N}(\tau)\rho_{SN}(0)\widetilde{V}_N'(t_2)\widetilde{V}_N'(t_1)U_{S,N}^\dagger(\tau)],\end{aligned} \tag{6.25}$$

where $\mathrm{Tr}_F[\rho_F\widetilde{V}_F(t_2)\widetilde{V}_F(t_1)] = \langle\widetilde{V}_F(t_2)\widetilde{V}_F(t_1)\rangle_F = C(t_2,t_1)$ is the far environment correlation function. Similarly, the fifth term is

$$\begin{aligned}&\mathrm{Tr}_{N,F}[U_0(\tau)G_2\rho_{\mathrm{tot}}(0)U_0^\dagger(\tau)] = \\ &-\int_0^\tau dt_1 \int_0^{t_1} dt_2 C(t_1,t_2)\mathrm{Tr}_N[U_{S,N}(\tau)\widetilde{V}_N'(t_1)\widetilde{V}_N'(t_2)\rho_{SN}(0)U_{S,N}^\dagger(\tau)].\end{aligned} \tag{6.26}$$

Finally, the last term of Eq. (6.19) is found by using the identity $\int_0^\tau dt_1 \int_0^{t_1} dt_2 + \int_0^\tau dt_2 \int_0^{t_2} dt_1 = \int_0^\tau dt_1 \int_0^\tau dt_2$, namely

$$\begin{aligned}
&\mathrm{Tr}_{N,F}[U_0(\tau)G_1\rho_{\mathrm{tot}}(0)G_1^\dagger U_0^\dagger(\tau)] = \\
&\int_0^\tau dt_1 \int_0^{t_1} dt_2 \Big\{ C(t_2,t_1)\mathrm{Tr}_N[U_{S,N}(\tau)\widetilde{V}'_N(t_1)\rho_{SN}(0)\widetilde{V}'_N(t_2)U^\dagger_{S,N}(\tau)] + \\
&C(t_1,t_2)\mathrm{Tr}_N[U_{S,N}(\tau)\widetilde{V}'_N(t_2)\rho_{SN}(0)\widetilde{V}'_N(t_1)U^\dagger_{S,N}(\tau)] \Big\}.
\end{aligned} \tag{6.27}$$

Putting it all together, we then have the following form of reduced density matrix of central system at time τ

$$\rho_S(\tau) = \widetilde{\rho}_S(\tau) + \int_0^\tau dt_1 \int_0^{t_1} dt' \{ C(t')\mathrm{Tr}_N\big[U_{S,N}(\tau)[\widetilde{V}'_N(t_1-t')\rho_{SN}, \widetilde{V}'_N(t_1)]U^\dagger_{S,N}(\tau)\big] + \mathrm{h.c}\}, \tag{6.28}$$

where h c. denotes hermitian conjugate, and $t' = t_1 - t_2$ simplifies matters since the far environment correlation function $C(t_1,t_2)$ depends only on time difference $(t_1 - t_2)$. For more general near-far environments coupling $H_{NF} = \sum_\mu V'_{\mu N} \otimes V_{\mu F}$, Eq. (6.28) becomes

$$\begin{aligned}
&\rho_S(\tau) = \\
&\widetilde{\rho}_S(\tau) + \sum_{\mu\nu} \int_0^\tau dt \int_0^t dt' \{ C_{\mu\nu}(t')\mathrm{Tr}_N\big[U_{S,N}(\tau)[\widetilde{V}'_{\nu N}(t-t')\rho_{SN}, \widetilde{V}'_{\mu N}(t)]U^\dagger_{S,N}(\tau)\big] + \mathrm{h.c}\}.
\end{aligned} \tag{6.29}$$

For notational simplification, we have also replaced the t_1 by t. After getting the expression of the density matrix of the central system, we can evaluate the survival probability $s(\tau)$, and then decay rate of central system. To accomplish this task, as usual, M repeated projective measurements P parallel to the initial state of the central system are performed on it with time interval τ. The survival probability $s(\tau)$ of the central system after one measurement is simply one minus the probability of finding the system in some other state orthogonal to the initial state

$$s(\tau) = 1 - \mathrm{Tr}_S[P_\perp U_S^\dagger(\tau)\rho_S(\tau)U_S(\tau)], \tag{6.30}$$

where $P_\perp$ is the projection operator that projects the central system state at time τ onto the state which is orthogonal to the initial state of the system, and Tr_S is the trace over the system states only. Note that, we have removed the system evolution in Eq. (6.30) due to the free system evolution operator as we want to examine the QZE and the QAZE due to system-environment interaction only. Using Eq. (6.29), we can then write Eq. (6.30) as

$$s(\tau) = 1 - \mathrm{Tr}_{S,N}\big[P_\perp U_S^\dagger(\tau) U_{S,N}(\tau)\rho_{SN}(0)U_{S,N}^\dagger(\tau)U_S(\tau)\big] - 2\mathrm{Re}\bigg[\sum_{\mu\nu}\int_0^\tau dt\int_0^t dt'\times$$
$$C_{\mu\nu}(t')\mathrm{Tr}_{S,N}\big[P_\perp U_S^\dagger(\tau)U_{S,N}(\tau)[\widetilde{V}'_{\nu N}(t-t')\rho_{SN}(0),\widetilde{V}'_{\mu N}(t)]U_{S,N}^\dagger(\tau)U_S(\tau)\big]\bigg]. \quad (6.31)$$

We now use Eq. (6.31) to work out the effective decay rate [57] $\Gamma(\tau) = -\ln[s(\tau)]/\tau$ to identify existence of QZE and QAZE regimes for our composite environment model consisting a harmonic oscillator near environment and a far environment also consisting of harmonic oscillators. To evaluate the effective decay rate in Eq. (6.10), we first find the time-evolution operator of the system plus the near environment [see Eq. (6.4)],

$$U_{S,N}(t) = e^{-i\Omega\sigma_z t/2}e^{-i\Omega a^\dagger a t}\bigg[\cos(\varphi t) - \frac{i}{\varphi}\sin(\varphi t)\big(\frac{\delta}{2}\sigma_z + \gamma(a\sigma_+ + a^\dagger\sigma_-)\big)\bigg], \quad (6.32)$$

with $\varphi = \sqrt{\frac{\delta^2}{4} + \frac{\gamma^2}{2}(2a^\dagger a + \sigma_z + 1)}$. Now, we move to find the survival probability [see Eq. (6.31)] by using the following identities

$$\begin{aligned}
\frac{\sin(\vartheta t)}{\vartheta}a^\dagger &= a^\dagger\frac{\sin(\varkappa t)}{\varkappa}\,,\\
\frac{\sin(\vartheta t)}{\vartheta}a &= a\frac{\sin(\Lambda t)}{\Lambda}\,,\\
a^\dagger\frac{\sin(\vartheta t)}{\vartheta} &= \frac{\sin(\Lambda t)}{\Lambda}a^\dagger\,,\\
a\frac{\sin(\vartheta t)}{\vartheta} &= \frac{\sin(\varkappa t)}{\varkappa}a\,,
\end{aligned} \quad (6.33)$$

with $\Lambda = \sqrt{\frac{\delta^2}{4} + \gamma^2(a^\dagger a - 1)}$, $\vartheta = \sqrt{\frac{\delta^2}{4} + \gamma^2 a^\dagger a}$, and $\varkappa = \sqrt{\frac{\delta^2}{4} + \gamma^2(a^\dagger a + 1)}$. From the second term of Eq. (6.31), we have

$$\mathrm{Tr}_{S,N}[P_\perp U_S^\dagger(\tau)U_{S,N}(\tau)\rho_S(0)\rho_N(0)U_{S,N}^\dagger(\tau)U_S(\tau)] = \gamma^2\frac{\sin^2(X\tau)}{X^2}, \tag{6.34}$$

with $X = \sqrt{\frac{\delta^2}{4}+\gamma^2}$, $P_\perp = |g\rangle\langle g|$, $\rho_S(0) = |e\rangle\langle e|$ and $\rho_N(0) = e^{-\beta H_N}/Z_N$ with $Z_N = \mathrm{Tr}_N[e^{-\beta H_N}]$. Similarly, the third term at zero temperature corresponds to

$$\mathrm{Tr}_S\bigg[P_\perp U_S^\dagger(\tau)\int_0^\tau dt\int_0^t dt' C_{12}(t')\mathrm{Tr}_N\bigg[U_{S,N}(\tau)[\widetilde{V}'_{2N}(t-t')\rho_{SN}(0),\widetilde{V}'_{1N}(t)]U_{S,N}^\dagger(\tau)\bigg]U_S(\tau)\bigg].$$

We write this as $D_1(\tau) - D_2(\tau)$ with

$$D_1(\tau) = \\ \mathrm{Tr}_{S,N}\bigg[P_\perp U_S^\dagger(\tau)\bigg(\int_0^\tau dt\int_0^t dt' C_{12}(t')U_{S,N}(\tau)\widetilde{V}'_{2N}(t-t')\rho_S(0)\rho_N(0)\widetilde{V}'_{1N}(t)U_{S,N}^\dagger(\tau)\bigg)U_S(\tau)\bigg], \tag{6.35}$$

and

$$D_2(\tau) = \\ \mathrm{Tr}_{S,N}\bigg[P_\perp U_S^\dagger(\tau)\bigg(\int_0^\tau dt\int_0^t dt' C_{12}(t')U_{S,N}(\tau)\widetilde{V}'_{1N}(t_1)\widetilde{V}'_{2N}(t-t')\rho_S(0)\rho_N(0)U_{S,N}^\dagger(\tau)\bigg)U_S(\tau)\bigg]. \tag{6.36}$$

Now, at zero temperature $C_{12}(t) = \mathrm{Tr}_F[\rho_F\widetilde{V}_{1F}(t)V_{2F}] = \sum_k |g_k|^2 e^{-i\omega_k t}$ and $C_{21}(t) = C_{11}(t) = C_{22}(t) = 0$, with $\widetilde{V}_{1F}(t) = e^{iH_B t}V_{1F}e^{-iH_B t}$, $V_{1F} = \sum_k g_k^* b_k$ and $V_{2F} = \sum_k g_k b_k^\dagger$. Moreover, $\rho_F = e^{-\beta H_F}/Z_F$ with $Z_F = \mathrm{Tr}_F[\rho_F]$ and Tr_F is the average over the far environment states. For $\widetilde{V}'_{2N}(t) = U_{S,N}^\dagger(t)aU_{S,N}(t)$ and $\widetilde{V}'_{2N}(t) = U_{S,N}^\dagger(t)a^\dagger U_{S,N}(t)$. We then find that $D_1(\tau)$ is

$$D_1(\tau) = \int_0^\tau dt\int_0^t dt' C_{12}(t')e^{i\Omega t'}e^{iKt'}\gamma^2\bigg(\frac{\sin(Xt)\sin(X(t-t')}{X^2}\bigg), \tag{6.37}$$

with $K = \dfrac{\delta}{2}$. Similarly

$$D_2(\tau) = \int_0^\tau dt \int_0^t dt' C_{12}(t') \left(\frac{\sin(X\tau)\sin(X(t-t'))}{X^3} \right) e^{i\Omega t'} e^{iKt'} \gamma^2 \left(X\cos(X(t-\tau)) - iK\sin(X(t-\tau)) \right). \tag{6.38}$$

By using these expressions, the survival probability of central system in excited state at time τ is

$$s(\tau) = \frac{1}{X^2}\left(K^2 + \gamma^2\cos^2(X\tau) \right) - 2\sum_k |g_k|^2 \int_0^\tau dt \int_0^t dt' \gamma^2 \left(\frac{\sin(X(t-t'))}{X^2} \right) \Bigg[\cos((\omega_k - \Omega - K)t') \times \left(\sin(Xt) - \sin(X\tau)\cos(X(t-\tau)) \right) - K\sin((\omega_k - \Omega - K)t') \frac{\sin(X\tau)}{X} \sin(X(t-\tau)) \Bigg]. \tag{6.39}$$

This allows us [57] to work out effective decay rate.

Let us now outline the calculation of the survival probability when there is a dephasing-type interaction between the central two-level system and the harmonic oscillator near-environment. The corresponding unitary time-evolution operator has the following form

$$U_{S,N}(\tau) = e^{-i\varepsilon\sigma_z\tau/2} e^{-i\Omega a^\dagger a\tau} e^{\sigma_z(a^\dagger\alpha(\tau) - a\alpha^*(\tau))/2}, \tag{6.40}$$

with $\alpha(\tau) = \dfrac{\lambda}{\Omega}(1 - e^{i\Omega\tau})$. Now, the second term of Eq. (6.31) with $P_\perp = \frac{1}{2}(|e\rangle - |g\rangle)(\langle e| - \langle g|)$, $\rho_S(0) = \frac{1}{2}(|e\rangle + |g\rangle)(\langle e| + \langle g|)$ and $\rho_N(0) = e^{-\beta H_N}/Z_N$ becomes

$$\mathrm{Tr}_{S,N}[P_\perp U_S^\dagger(\tau) U_{S,N}(\tau) \rho_S(0) \rho_N(0) U_{S,N}^\dagger(\tau) U_S(\tau)] = \frac{1}{2}(1 - e^{-\gamma(\tau)}). \tag{6.41}$$

Here, we have used the fact that $\mathrm{Tr}_N[\rho_N(0)e^C] = \langle e^C \rangle = e^{\langle C^2 \rangle/2}$, with C is a linear com-

bination [43] of the creation and the annihilation operators, and $\gamma(\tau) = \frac{\lambda^2}{\Omega^2}[1 - \cos(\Omega\tau)]$. The third term is simplified by noting that, for zero temperature environment, $C_{12}(t) = \sum_k |g_k|^2 e^{-i\omega_k t}$, and $C_{21}(t) = C_{11}(t) = C_{22}(t) = 0$. Putting it all together, we obtain the effective decay rate given in Eq. (6.15).

Chapter 7

Conclusion

In this thesis, after briefly reviewing the basic concepts required to understand open quantum system dynamics, we studied the effects of the initial system-environment correlations on the system dynamics via an exactly solvable model [54] consisting of a single two-level system interacting with a collection of two-level systems. We found that, in general, for strong system-environment coupling strength, the initial system-environment correlations play a significant role in the system dynamics and need to be accounted for [5, 6]. The same behavior is also observed for the entanglement between the two two-level systems coupled to a common spin environment. We then moved on to study the effects of repeated measurements. Unlike classical measurements, quantum measurements in general disturb the state of the quantum system. Therefore repeated measurements in quantum mechanics can freeze (the quantum Zeno effect) or enhance the time-evolution (the quantum anti-Zeno effect) of a quantum system. We first observed that if the repeated measurements are non-selective [90], then the effective decay rate can change significantly if the system-environment coupling strength is not weak. We then showed that the application of time-dependent driving fields dynamically modifies the effective decay rate which consequently modifies the quantum Zeno and anti-Zeno effects both in the weak and relatively strong coupling system-environment coupling regimes [101]. Finally, we studied the effects of a composite environment [5, 6] on the decay rate of the central system. We showed that the effective decay rate is qualitatively and

quantitatively different as compared to the standard harmonic oscillator environment. In fact, as we increase the coupling strength between the near and far environments comprising the composite environment, the effective decay rate can decrease.

We would also like to use this opportunity to discuss briefly a couple of interesting questions which may be asked as extensions of the results of our work presented in this thesis:

- In chapter 3, we studied exactly the effects of initial system-environment correlations on the dynamics of a two-level system coupled to a spin environment. However, we considered a time-independent system Hamiltonian. The role of initial system-environment correlations in the case where driving fields are applied to the system is still a very much unexplored area. Also, we can extend our results by preparing the initial system state in a different way - rather than performing a projective measurement, we can use a unitary operation, applied to the system, to prepare at least approximately a desired initial system state. Moreover, how do the system-environment correlations evolve in time? Usually initial system-environment correlations lead to non-Markovian system dynamics.

- In our treatment of the quantum Zeno and anti-Zeno effects with non-selective projective measurements, we ignored the buildup of correlations between the system and its environment. When the system-environment interaction is not weak, these should be taken into account as well.

- When considering the quantum Zeno and anti-Zeno effects in the presence of driving fields, we focused on harmonic oscillator environments. What happens with spin environments or collision model?

- The effect of a composite environment on the quantum Zeno and anti-Zeno effects can easily be explored further. For example, what happens if the near environment is a harmonic oscillator, while the far environment is comprised of two-level systems?

Bibliography

[1] S. Haroche and J.-M. Raimond, *Exploring the quantum: atoms, cavities, and photons* (Oxford University Press, Oxford, 2006).

[2] J. J. Sakurai, *Modern Quantum Mechanics* (Addison Wesley, Reading, Mass., 1993).

[3] H.-P. Breuer and F. Petruccione, *The Theory of Open Quantum Systems* (Oxford University Press, Oxford, 2007).

[4] U. Weiss, *Quantum dissipative systems* (World Scientific, Singapore, 2008).

[5] A. Z. Chaudhry, *Understanding and controlling open quantum dynamics*, Ph.D. thesis, National University of Singapore (2013).

[6] A. Z. Chaudhry, "Understanding and controlling open quantum dynamics," (2013).

[7] M. O. Scully and M. S. Zubairy, *Quantum optics* (Cambridge University Press, Cambridge, 1997).

[8] E. Joos, *Decoherence and the appearance of a classical world in quantum theory* (Springer, Berlin, 2003).

[9] M. Schlosshauer, *Decoherence and the quantum-to-classical transition* (Springer Nature, Berlin, 2007).

[10] M. A. Nielsen and I. L. Chuang, *Quantum computation and quantum information* (Cambridge University Press, Cambridge, 2000).

[11] D. Bruss and G. Leuchs, *Lectures on quantum information* (Wiley-VCH, Berlin, 2006).

[12] L. Viola, E. Knill, and S. Lloyd, Phys. Rev. Lett. **82**, 2417 (1999).

[13] F. F. Fanchini, J. E. M. Hornos, and R. d. J. Napolitano, Phys. Rev. A **75**, 022329 (2007).

[14] A. Z. Chaudhry and J. Gong, Phys. Rev. A **85**, 012315 (2012).

[15] A. Z. Chaudhry and J. Gong, Phys. Rev. A **86**, 012311 (2012).

[16] S. Austin, M. Q. Khan, M. Mudassar, and A. Z. Chaudhry, Phys. Rev. A **100**, 022102 (2019).

[17] D. Bacon, D. A. Lidar, and K. B. Whaley, Phys. Rev. A **60**, 1944 (1999).

[18] A. M. Steane, Phys. Rev. Lett. **77**, 793 (1996).

[19] V. Gorini, A. Kossakowski, and E. C. G. Sudarshan, J. Math. Phys. (N.Y.) **17**, 821 (1976).

[20] G. Lindblad, Commun. Math. Phys. **48**, 119 (1976).

[21] K. Modi, Open Syst. Inf. Dyn. **18**, 253 (2011).

[22] V. Hakim and V. Ambegaokar, Phys. Rev. A **32**, 423 (1985).

[23] F. Haake and R. Reibold, Phys. Rev. A **32**, 2462 (1985).

[24] H. Grabert, P. Schramm, and G.-L. Ingold, Phys. Rep. **168**, 115 (1988).

[25] C. M. Smith and A. O. Caldeira, Phys. Rev. A **41**, 3103 (1990).

[26] R. Karrlein and H. Grabert, Phys. Rev. E **55**, 153 (1997).

[27] L. Dávila Romero and J. Pablo Paz, Phys. Rev. A **55**, 4070 (1997).

[28] E. Lutz, Phys. Rev. A **67**, 022109 (2003).

[29] S. Banerjee and R. Ghosh, Phys. Rev. E **67**, 056120 (2003).

[30] N. G. van Kampen, J. Stat. Phys. **115**, 1057 (2004).

[31] M. Ban, Phys. Rev. A **80**, 064103 (2009).

[32] M. Campisi, P. Talkner, and P. Hänggi, Phys. Rev. Lett. **102**, 210401 (2009).

[33] C. Uchiyama and M. Aihara, Phys. Rev. A **82**, 044104 (2010).

[34] A. G. Dijkstra and Y. Tanimura, Phys. Rev. Lett. **104**, 250401 (2010).

[35] A. Smirne, H.-P. Breuer, J. Piilo, and B. Vacchini, Phys. Rev. A **82**, 062114 (2010).

[36] J. Dajka and J. Łuczka, Phys. Rev. A **82**, 012341 (2010).

[37] Y.-J. Zhang, X.-B. Zou, Y.-J. Xia, and G.-C. Guo, Phys. Rev. A **82**, 022108 (2010).

[38] H.-T. Tan and W.-M. Zhang, Phys. Rev. A **83**, 032102 (2011).

[39] C. K. Lee, J. Cao, and J. Gong, Phys. Rev. E **86**, 021109 (2012).

[40] V. G. Morozov, S. Mathey, and G. Röpke, Phys. Rev. A **85**, 022101 (2012).

[41] V. Semin, I. Sinayskiy, and F. Petruccione, Phys. Rev. A **86**, 062114 (2012).

[42] E.-M. Laine, H.-P. Breuer, J. Piilo, C.-F. Li, and G.-C. Guo, Phys. Rev. Lett. **108**, 210402 (2012).

[43] A. Z. Chaudhry and J. Gong, Phys. Rev. A **87**, 012129 (2013).

[44] A. Z. Chaudhry and J. Gong, Phys. Rev. A **88**, 052107 (2013).

[45] A. Z. Chaudhry and J. Gong, Can. J. Chem. **92**, 119 (2013).

[46] J. Reina, C. Susa, and F. Fanchini, Sci. Rep. **4**, 7443 (2014).

[47] F. Buscemi, Phys. Rev. Lett. **113**, 140502 (2014).

[48] Y.-R. Zhang and H. Fan, Sci. Rep. **5**, 11509 (2015).

[49] C.-C. Chen and H.-S. Goan, Phys. Rev. A **93**, 032113 (2016).

[50] I. de Vega and D. Alonso, Rev. Mod. Phys. **89**, 015001 (2017).

[51] J. C. Halimeh and I. de Vega, Phys. Rev. A **95**, 052108 (2017).

[52] S. Kitajima, M. Ban, and F. Shibata, J. Phys. A: Math. Theor **50**, 125303 (2017).

[53] M. Buser, J. Cerrillo, G. Schaller, and J. Cao, Phys. Rev. A **96**, 062122 (2017).

[54] M. Majeed and A. Z. Chaudhry, Eur. J. Phys. D **73**, 1 (2019).

[55] M. Majeed and A. Z. Chaudhry, e-print arXiv , 1808.04988 (2018).

[56] A. Z. Chaudhry and J. Gong, Phys. Rev. A **90**, 012101 (2014).

[57] A. Z. Chaudhry, Sci. Rep. **6**, 29497 (2016).

[58] A. Z. Chaudhry, Sci. Rep. **7**, 1741 (2017).

[59] M. J. Aftab and A. Z. Chaudhry, Sci. Rep. **7**, 11766 (2017).

[60] B. Misra and E. C. G. Sudarshan, J. Math. Phys. (N. Y.) **18**, 756 (1977).

[61] P. Facchi, V. Gorini, G. Marmo, S. Pascazio, and E. Sudarshan, Phys. Lett. A **275**, 12 (2000).

[62] P. Facchi and S. Pascazio, Phys. Rev. Lett. **89**, 080401 (2002).

[63] P. Facchi and S. Pascazio, J. Phys. A: Math. Theor. **41**, 493001 (2008).

[64] X.-B. Wang, J. Q. You, and F. Nori, Phys. Rev. A **77**, 062339 (2008).

[65] S. Maniscalco, F. Francica, R. L. Zaffino, N. Lo Gullo, and F. Plastina, Phys. Rev. Lett. **100**, 090503 (2008).

[66] P. Facchi and M. Ligabò, J. Phys. A: Math. Theor. **51**, 022103 (2010).

[67] B. Militello, M. Scala, and A. Messina, Phys. Rev. A **84**, 022106 (2011).

[68] J. M. Raimond, P. Facchi, B. Peaudecerf, S. Pascazio, C. Sayrin, I. Dotsenko, S. Gleyzes, M. Brune, and S. Haroche, Phys. Rev. A **86**, 032120 (2012).

[69] A. Smerzi, Phys. Rev. Lett. **109**, 150410 (2012).

[70] S.-C. Wang, Y. Li, X.-B. Wang, and L. C. Kwek, Phys. Rev. Lett. **110**, 100505 (2013).

[71] K. T. McCusker, Y.-P. Huang, A. S. Kowligy, and P. Kumar, Phys. Rev. Lett. **110**, 240403 (2013).

[72] K. Stannigel, P. Hauke, D. Marcos, M. Hafezi, S. Diehl, M. Dalmonte, and P. Zoller, Phys. Rev. Lett. **112**, 120406 (2014).

[73] B. Zhu, B. Gadway, M. Foss-Feig, J. Schachenmayer, M. L. Wall, K. R. A. Hazzard, B. Yan, S. A. Moses, J. P. Covey, D. S. Jin, J. Ye, M. Holland, and A. M. Rey, Phys. Rev. Lett. **112**, 070404 (2014).

[74] F. Schäffer, I. Herrera, S. Cherukattil, C. Lovecchio, F. S. Cataliotti, F. Caruso, and A. Smerzi, Nat. Commun. **5**, 3194 (2014).

[75] A. Signoles, A. Facon, D. Grosso, I. Dotsenko, S. Haroche, J.-M. Raimond, M. Brune, and S. Gleyzes, Nat. Phys. **10**, 715 (2014).

[76] V. Debierre, I. Goessens, E. Brainis, and T. Durt, Phys. Rev. A **92**, 023825 (2015).

[77] A. H. Kiilerich and K. Mølmer, Phys. Rev. A **92**, 032124 (2015).

[78] J. Qiu, Y.-Y. Wang, Z.-Q. Yin, M. Zhang, Q. Ai, and F.-G. Deng, Sci. Rep. **5**, 17615 (2015).

[79] S. He, C. Wang, L.-W. Duan, and Q.-H. Chen, Phys. Rev. A **97**, 022108 (2018).

[80] L. Magazzu, P. Talkner, and P. Hanggi, New J. Phys. **20**, 033001 (2018).

[81] S. He, L.-W. Duan, C. Wang, and Q.-H. Chen, Phys. Rev. A **99**, 052101 (2019).

[82] A. G. Kofman and G. Kurizki, Nature (London) **405**, 546 (2000).

[83] M. C. Fischer, B. Gutiérrez-Medina, and M. G. Raizen, Phys. Rev. Lett. **87**, 040402 (2001).

[84] A. Barone, G. Kurizki, and A. G. Kofman, Phys. Rev. Lett. **92**, 200403 (2004).

[85] K. Koshino and A. Shimizu, Phys. Rep. **412**, 191 (2005).

[86] P.-W. Chen, D.-B. Tsai, and P. Bennett, Phys. Rev. B **81**, 115307 (2010).

[87] K. Fujii and K. Yamamoto, Phys. Rev. A **82**, 042109 (2010).

[88] S. He, Q.-H. Chen, and H. Zheng, Phys. Rev. A **95**, 062109 (2017).

[89] W. Wu and H.-Q. Lin, Phys. Rev. A **95**, 042132 (2017).

[90] M. Majeed and A. Z. Chaudhry, Sci. Rep. **8**, 14887 (2018).

[91] W. Wu, Ann. Phys. **396**, 147 (2018).

[92] B. Khalid and A. Z. Chaudhry, Eur. J. Phys. D **73**, 134 (2019).

[93] C. Sanz-Sanz, A. Sanz, T. González-Lezana, O. Roncero, and S. Miret-Artés, "Communication: Quantum Zeno-based control mechanism for molecular fragmentation," (2012).

[94] A. Tavakoli, H. Anwer, A. Hameedi, and M. Bourennane, Phys. Rev. A **92**, 012303 (2015).

[95] M. Smania, A. M. Elhassan, A. Tavakoli, and M. Bourennane, Npj Quantum Information **2**, 16010 (2016).

[96] F. Sakuldee and Ł. Cywiński, Phys. Rev. A **101**, 012314 (2020).

[97] M. M. Müller, S. Gherardini, N. Dalla Pozza, and F. Caruso, Phys. Lett. A **384**, 126244 (2020).

[98] F. Sakuldee and Ł. Cywiński, Phys. Rev. A **101**, 042329 (2020).

[99] G. Barontini, L. Hohmann, F. Haas, J. Estève, and J. Reichel, Science **349**, 1317 (2015).

[100] Y. Lin, J. P. Gaebler, F. Reiter, T. R. Tan, R. Bowler, Y. Wan, A. Keith, E. Knill, S. Glancy, K. Coakley, *et al.*, Phys. Rev. Lett **117**, 140502 (2016).

[101] M. Majeed and A. Z. Chaudhry, Sci. Rep. **11**, 1836 (2021).

[102] M. Majeed and A. Z. Chaudhry, e-print arXiv , 1808.08012 (2018).

[103] M. Majeed and A. Z. Chaudhry, e-print arXiv , 2012.15040 (2020).

[104] G. M. Paule, *Thermodynamics and synchronization in open quantum systems* (Springer Science and Business Media LLC, 2018).

[105] J. von Neumann, *Mathematical Foundations of Quantum Mechanics* (Princeton University Press, Princeton, NJ, 1955).

[106] N. V. Prokof'ev and P. C. E. Stamp, Rep. Prog. Phys. **63**, 669 (2000).

[107] P. Stamp, in *Tunneling in complex systems* (World Scientific, 1998) pp. 101–197.

[108] H. J. Metcalf and P. van der Straten, *Laser cooling and trapping* (Springer, New York, 1999).

[109] S. M. Dutra, *Cavity quantum electrodynamics* (Wiley, Hoboken, N.J., 2004).

[110] A. J. Leggett, S. Chakravarty, A. T. Dorsey, M. P. A. Fisher, A. Garg, and W. Zwerger, Rev. Mod. Phys. **59**, 1 (1987).

[111] M. Grifoni and P. Hänggi, Phys. Rep. **304**, 229 (1998).

[112] A. Lupaşcu, S. Saito, T. Picot, P. De Groot, C. Harmans, and J. Mooij, nature physics **3**, 119 (2007).

[113] J. Clarke and F. Wilhelm, Nature (London) **453**, 1031 (2008).

[114] I. Buluta, S. Ashhab, and F. Nori, Rep. Prog. Phys. **74**, 104401 (2011).

[115] J. You and F. Nori, Nature (London) **474**, 589 (2011).

[116] K. Le Hur, Phys. Rev. B **85**, 140506 (2012).

[117] T. Vorrath, *Dissipation-Induced Collective Effects in Two-Level Systems*, Ph.D. thesis (2003).

[118] R. P. Feynman and F. L. Vernon, Ann. Phys. (N. Y.) **24**, 118 (1963).

[119] A. O. Caldeira and A. J. Leggett, Annals of Physics **149**, 374 (1983).

[120] J. P. Paz, S. Habib, and W. H. Zurek, Phys. Rev. D **47**, 488 (1993).

[121] C. W. Gardiner and P. Zoller, *Quantum noise* (Springer, Berlin, 2004).

[122] M. Schlosshauer, A. P. Hines, and G. J. Milburn, Phys. Rev. A **77**, 022111 (2008).

[123] A. Dehghani, B. Mojaveri, and M. Vaez, Int. J. Theor. Phys. **59**, 3107 (2020).

[124] S. Austin, S. Zahid, and A. Z. Chaudhry, Phys. Rev. A **101**, 022114 (2020).

[125] F. M. Cucchietti, J. P. Paz, and W. H. Zurek, Phys. Rev. A **72**, 052113 (2005).

[126] T. Yu and J. H. Eberly, Phys. Rev. Lett. **93**, 140404 (2004).

[127] T. Yu and J. H. Eberly, Science **323**, 598 (2009).

[128] E. Pollak, J. Shao, and D. H. Zhang, Phys. Rev. E **77**, 021107 (2008).

[129] N. J. Cerf and C. Adami, Phys. Rev. Lett. **79**, 5194 (1997).

[130] W. K. Wootters, Phys. Rev. Lett. **80**, 2245 (1998).

[131] W. M. Itano, D. J. Heinzen, J. J. Bollinger, and D. J. Wineland, Phys. Rev. A **41**, 2295 (1990).

[132] S. Maniscalco, J. Piilo, and K.-A. Suominen, Phys. Rev. Lett. **97**, 130402 (2006).

[133] D. Segal and D. R. Reichman, Phys. Rev. A **76**, 012109 (2007).

[134] H. Zheng, S. Y. Zhu, and M. S. Zubairy, Phys. Rev. Lett. **101**, 200404 (2008).

[135] Q. Ai, Y. Li, H. Zheng, and C. P. Sun, Phys. Rev. A **81**, 042116 (2010).

[136] A. Thilagam, J. Phys. A: Math. Theor. **43**, 155301 (2010).

[137] D. Z. Xu, Q. Ai, and C. P. Sun, Phys. Rev. A **83**, 022107 (2011).

[138] Z.-T. Zhang and Z.-Y. Xue, JETP Letters **93**, 349 (2011).

[139] X. Cao, Q. Ai, C.-P. Sun, and F. Nori, Phys. Lett. A **376**, 349 (2012).

[140] A. Thilagam, J. Chem. Phys. **138**, 175102 (2013).

[141] D. H. Slichter, C. Müller, R. Vijay, S. J. Weber, A. Blais, and I. Siddiqi, New. J. Phys. **18**, 053031 (2016).

[142] N. Bar-Gill, D. D. B. Rao, and G. Kurizki, Phys. Rev. Lett. **107**, 010404 (2011).

[143] Y. Matsuzaki, S. Saito, K. Kakuyanagi, and K. Semba, Phys. Rev. B **82**, 180518 (2010).

[144] J.-M. Zhang, J. Jing, L.-G. Wang, and S.-Y. Zhu, Phys. Rev. A **98**, 012135 (2018).

[145] H. M. Wiseman and G. J. Milburn, *Quantum measurement and control* (Cambridge University Press, Cambridge, 2014).

[146] J. Halliwell, Annals N.Y. Acad. Sci. **755**, 726 (1995).

[147] D. Bedingham and J. J. Halliwell, Phys. Rev. A **89**, 042116 (2014).

[148] J. G. Muga, F. Delgado, A. del Campo, and G. García-Calderón, Phys. Rev. A **73**, 052112 (2006).

[149] A. del Campo, New. J. Phys. **18**, 015014 (2016).

[150] M. Beau, J. Kiukas, I. L. Egusquiza, and A. del Campo, Phys. Rev. Lett. **119**, 130401 (2017).

[151] F. A. Grunbaum, L. Velazquez, A. H. Werner, and R. F. Werner, Commun. Math. Phys. **320**, 543 (2013).

[152] S. Dhar, S. Dasgupta, A. Dhar, and D. Sen, Phys. Rev. A **91**, 062115 (2015).

[153] F. Thiel, E. Barkai, and D. A. Kessler, Phys. Rev. Lett. **120**, 040502 (2018).

[154] F. Thiel, D. A. Kessler, and E. Barkai, Phys. Rev. A **97**, 062105 (2018).

[155] S. Belan and V. Parfenyev, New J. Phys. **22**, 073065 (2020).

[156] W. Magnus, Communications on pure and applied mathematics **7**, 649 (1954).

[157] A. Kofman and G. Kurizki, Phys. Rev. Lett. **87**, 270405 (2001).

[158] A. Kofman and G. Kurizki, Phys. Rev. Lett. **93**, 130406 (2004).

[159] G. Gordon, N. Erez, and G. Kurizki, J. Phys. B **40**, S75 (2007).

[160] G. Gordon, G. Kurizki, and D. A. Lidar, Phys. Rev. Lett. **101**, 010403 (2008).

[161] M. W. Noel, W. Griffith, and T. Gallagher, Phys. Rev. A **58**, 2265 (1998).

[162] F. Grossmann, T. Dittrich, P. Jung, and P. Hänggi, Phys. Rev. lett. **67**, 516 (1991).

[163] J. Shao and P. Hänggi, Phys. Rev. A **56**, R4397 (1997).

[164] L. Viola and S. Lloyd, Phys. Rev. A **58**, 2733 (1998).

[165] H.-V. Do, C. Lovecchio, I. Mastroserio, N. Fabbri, F. S. Cataliotti, S. Gherardini, M. M. Müller, N. Dalla Pozza, and F. Caruso, New J. Phys. **21**, 113056 (2019).

[166] T. Vorrath and T. Brandes, Phys. Rev. Lett. **95**, 070402 (2005).

[167] R. Silbey and R. A. Harris, J. Chem. Phys. **80**, 2615 (1984).

[168] C. K. Lee, J. Moix, and J. Cao, J. Chem. Phys. **136**, 204120 (2012).

[169] H.-T. Chang, P.-P. Zhang, and Y.-C. Cheng, J. of Chem. Phys. **139**, 224112 (2013).

[170] S. Jang, Y.-C. Cheng, D. R. Reichman, and J. D. Eaves, J. Chem. Phys. **129**, 101104 (2008).

[171] A. W. Chin, J. Prior, S. F. Huelga, and M. B. Plenio, Phys. Rev. Lett. **107**, 160601 (2011).

[172] D. Gelbwaser-Klimovsky and A. Aspuru-Guzik, J. Chem. Phys. Lett. **6**, 3477 (2015).

[173] A. Z. Chaudhry and J. Gong, Phys. Rev. A **89**, 014104 (2014).

[174] B. Militello, Phys. Rev. A **99**, 033415 (2019).

[175] B. Militello, Phys. Rev. A **99**, 063412 (2019).

[176] D. Georgiev and E. Cohen, Phys Rev A **97**, 052102 (2018).

[177] P. Facchi, H. Nakazato, and S. Pascazio, Phys. Rev. Lett. **86**, 2699 (2001).

[178] J. Prior, I. de Vega, A. W. Chin, S. F. Huelga, and M. B. Plenio, Phys. Rev. A **87**, 013428 (2013).

[179] B. Peropadre, D. Zueco, D. Porras, and J. J. García-Ripoll, Phys. Rev. Lett **111**, 243602 (2013).

[180] I. M. Gradshteyn and I. S. Ryzhik, *Table of Integrals, Series, and Products* (Academic Press, San Diego, 1994).

[181] R. H. Dicke, Phys. Rev. **93**, 99 (1954).

[182] G. Kurizki, E. Shahmoon, and A. Zwick, Physica Scripta **90**, 128002 (2015).

[183] L. Tian, S. Lloyd, and T. Orlando, Phys. Rev. B **65**, 144516 (2002).

[184] I. Chiorescu, Y. Nakamura, C. M. Harmans, and J. Mooij, Science **299**, 1869 (2003).

[185] E. Paladino, M. Sassetti, G. Falci, and U. Weiss, Phys. Rev. B **77**, 041303 (2008).

[186] A. Lupaşcu, P. Bertet, E. F. C. Driessen, C. J. P. M. Harmans, and J. E. Mooij, Phys. Rev. B **80**, 172506 (2009).

[187] N. P. Oxtoby, A. Rivas, S. F. Huelga, and R. Fazio, New J. Phys. **11**, 063028 (2009).

[188] L. Faoro and L. Viola, Phys. Rev Lett. **92**, 117905 (2004).

[189] C. Vierheilig, D. Bercioux, and M. Grifoni, Phys. Rev. A **83**, 012106 (2011).

[190] H. Moreno, T. Gorin, and T. Seligman, Phys. Rev. A **92**, 030104 (2015).

[191] Z.-X. Man, Y.-J. Xia, and R. L. Franco, Sci. Rep. **5**, 13843 (2015).

[192] J. M. Torres and T. H. Seligman, New J. Phys. **19**, 113016 (2017).

[193] P. Huang and H. Zheng, Chem. Phys. Lett. **500**, 256 (2010).

[194] D. Zueco, G. M. Reuther, S. Kohler, and P. Hänggi, Phys. Rev. A **80**, 033846 (2009).